12-1-2012

Volcanic Evolution Of The Southern Quinn Canyon Range: Implications For Regional Correlation Of Volcanic Units

Christina Emery
University of Nevada, Las Vegas, emeryc2@unlv.nevada.edu

VOLCANIC EVOLUTION OF THE SOUTHERN QUINN CANYON RANGE:

IMPLICATIONS FOR REGIONAL CORRELATION OF VOLCANIC UNITS

By

Christina Ann Emery

Bachelor of Science in Geology
University of Tennessee at Chattanooga
2005

A thesis submitted in partial fulfillment
of the requirements for the

Master of Science in Geoscience

Department of Geoscience
College of Science
The Graduate College

University of Nevada, Las Vegas
December 2012

THE GRADUATE COLLEGE

We recommend the thesis prepared under our supervision by

Christina Emery

entitled

Volcanic Evolution of the Southern Quinn Canyon Range: Implications for Regional Correlation of Volcanic Units

be accepted in partial fulfillment of the requirements for the degree of

Master of Science in Geoscience
Department of Geoscience

Eugene I. Smith, Ph.D., Committee Chair

Terry L. Spell, Ph.D., Committee Member

Wanda T. Taylor, Ph.D., Committee Member

Chih-Hsiang Ho, Ph.D., Graduate College Representative

Tom Piechota, Ph.D., Interim Vice President for Research &
Dean of the Graduate College

December 2012

ABSTRACT

Volcanic Evolution Of The Southern Quinn Canyon Range: Implications For Regional Correlation Of Volcanic Units

By

Christina Emery

Dr. Eugene Smith, Committee Chair
Professor of Geoscience
University of Nevada, Las Vegas

The southern Quinn Canyon Range lies in an area of the Great Basin subjected to large-volume Oligocene-Miocene silicic volcanism and smaller volume basaltic volcanism during the Pliocene. Three major ash-flow tuff units were correlated in the southern Quinn Canyon Range (the Pahranagat Tuff, Clifford Spring Tuff, and the Cow Canyon Tuff) with regional units by utilizing U/Pb and $^{40}Ar/^{39}Ar$ geochronology, geochemical correlation, and field mapping. Isotopic analysis suggests that basalt in the southern Quinn Canyon Range is part of the Death Valley-Pancake Range Basalt Zone and is similar to Reveille Range Episode 1 and 2 basalts. Further comparison of geochemical data from samples within the Death Valley-Pancake Range Basalt Zone show isotopic differences between the northern and southern end of the Death Valley-Pancake Range Basalt Zone with the northern end having an asthenospheric derived signature. Depth of melting calculations of basalt samples also suggest an asthenospheric source.

ACKNOWLEDGEMENTS

I am most grateful for my advisor Dr. Eugene Smith for seeing my potential and taking me as a student and for his patience, encouragement, and guidance. I would like to thank my advising committee including: Dr. Wanda Taylor, Dr. Terry Spell, and Dr. Chih-Hsiang Ho for their support and suggestions. I would also like to thank Dr. Mike Nicholl for his advisement and support for entering the graduate program. I am indebted to Keith Cooper for his assistance in the field but most of all his never ending support on my journey. My family and friends for their support, and lastly, I would like to acknowledge the individuals that aided in analysis work including: Dr. Denise Honn, Dr. Axel Schmitt, Dr. Al Dieno, and Racheal Johnsen.

TABLE OF CONTENTS

LIST OF TABLES

LIST OF FIGURES

CHAPTER 1

INTRODUCTION

The stratigraphy, source and evolution of volcanic rocks in the southern Quinn Canyon Range (SQCR) have not been studied in great detail. Knowledge of the petrogenesis of these rocks is important for understanding the nature of volcanism during a period of intense upper crustal extension in the Great Basin (Best and Christiansen, 1991). The SQCR (Figure 1) is located to the east of the Reveille Range, which is the site of three calderas (Martin and Naumann, 1995). Outflow ash-flow tuff from these calderas has not been identified. Best et al. (1989) described the Shingle Pass Tuff and suggested that it erupted from a source in the northern Quinn Canyon Range. Little is known about the Quinn Canyon caldera; therefore, if the tuffs are correlated to the Shingle Pass Tuff then their study will provide information about the age and history of this caldera. If the tuffs in the SQCR are the outflow units from the Reveille Range calderas then their study can provide important age and petrologic information about the Reveille Range calderas that cannot be obtained by studying the calderas themselves. Recently, Ekren et al. (2012) described the geology of the Quinn Canyon Range but did not concentrate on the SQCR in detail.

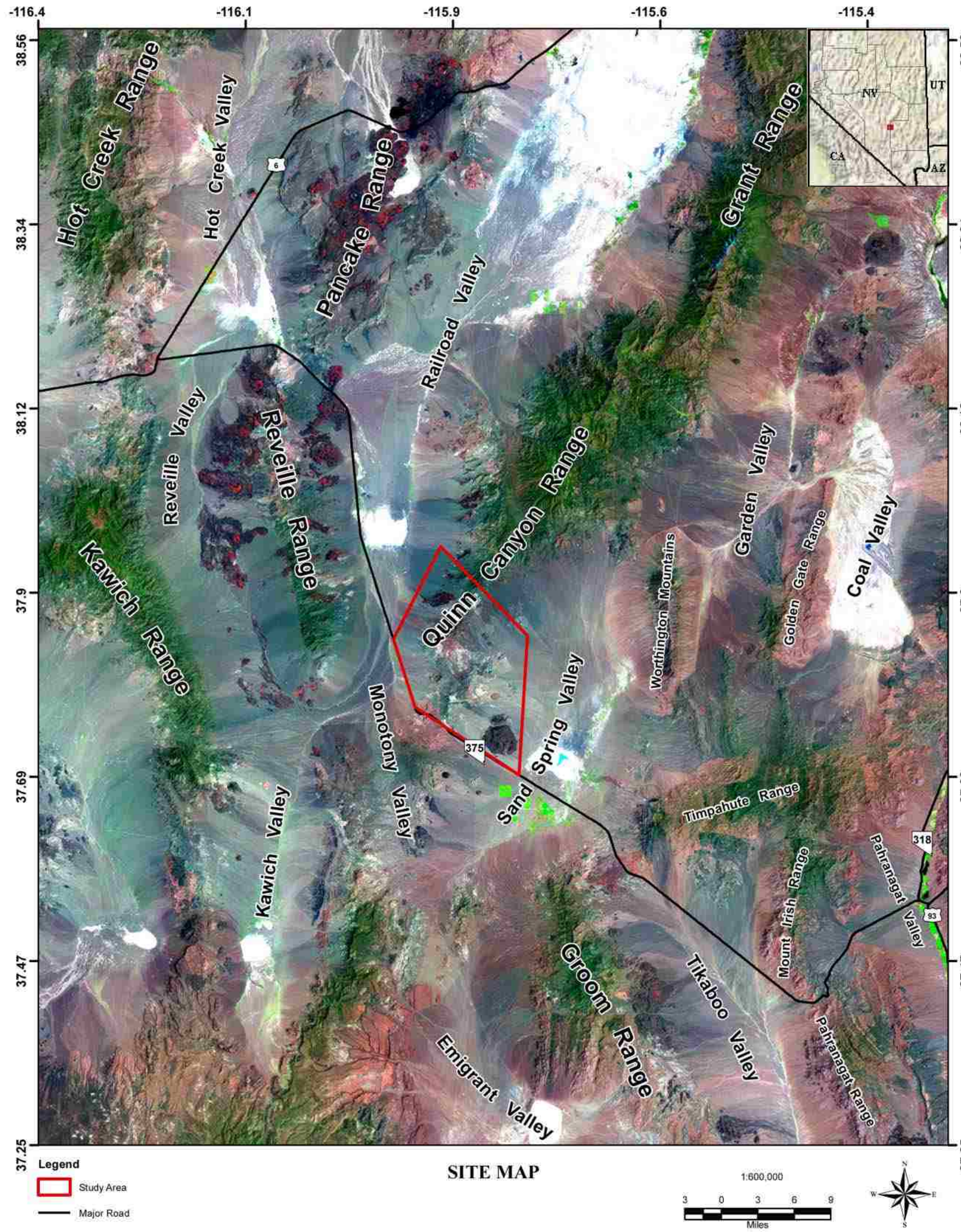

Figure 1: Satellite image of Central Nevada with the red line outlining the field area for this study in the southern Quinn Canyon Range.

Basalt of the SQCR may be similar to basalt in the Death Valley-Pancake Range Basalt Zone; herein called the Basalt Zone (Figure 2). This zone extends across central Nevada and includes basalt fields near Yucca Mountain, the site of a proposed high-level nuclear waste repository. The Basalt Zone contains Pliocene basalts that show isotopic differences trending from north to south (Farmer et al., 1989). In the south, the basalts have isotopic ratios characteristic of an enriched mantle or a lithospheric mantle source, but to the north isotopic ratios are more similar to ocean island basalt originating from an asthenospheric mantle source (Yogodzinski et al., 1996).

The objectives of this research are to determine whether the basalts of the SQCR are similar to those in the Reveille Range and the Basalt Zone, and to also determine whether the volcanic section in the SQCR represents the eruptive products of the Reveille Range calderas, the Quinn Canyon Range caldera or some other source area. Hypotheses to be tested are: (1) Outflow ash-flow tuffs of the SQCR represent eruptive products of the Reveille Range calderas, (2) The tuffs are similar to the Shingle Pass Tuff, which may have erupted from the Quinn Canyon Range caldera, (3) Basalts of the SQCR are similar to those in the Reveille Range and the Basalt Zone, and (4) Basalts do not correlate to the Basalt Zone and thus originated from a different source.

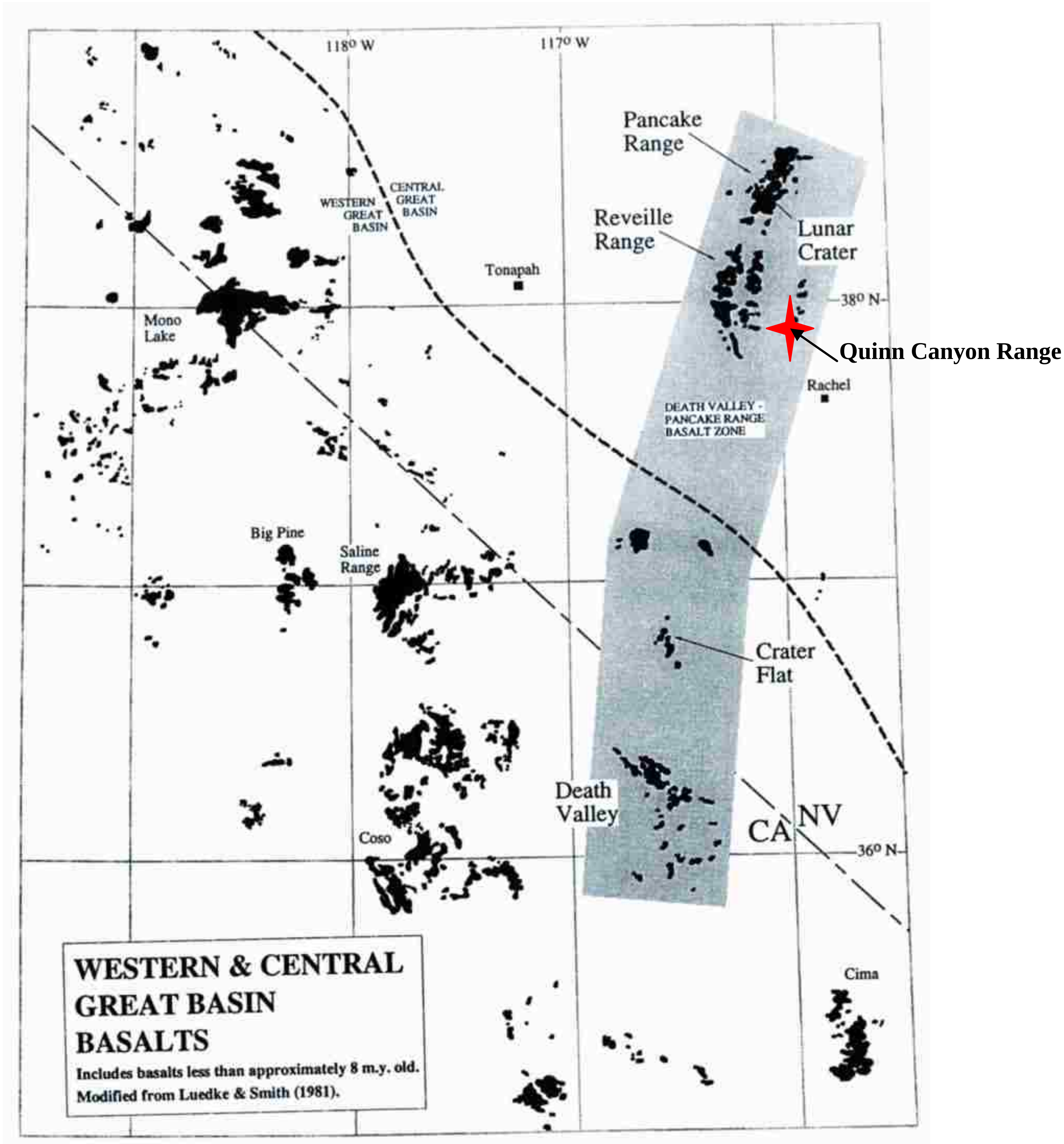

Figure 2: Map showing the location of the Quinn Canyon Range (red star) within the Death Valley-Pancake Range Basalt Zone (shaded area). Diagram taken from Yogodzinski et al. (1996).

CHAPTER 2

BACKGROUND

Regional Geology

The SQCR lies in the eastern part of the Great Basin. Volcanism swept through the northern part of the Great Basin in the Eocene starting at 43 Ma and continued southward into southern Nevada by the Miocene (14-12 Ma) (Cross and Pilger, 1978; Best et al., 1991). Two north-northeast oriented extensional belts were formed during late Paleogene extension. The Quinn Canyon Range lies in the western extensional belt and contains late Oligocene-early Miocene extensional structures. In both belts, magmatism post-dated or was synchronous with extension in the north, however, extension predated magmatism in the southern part of the belts. Thus, volcanism and extension only coincided for a short period of time (Best et al., 1991; Axen et al., 1993). Until the early Miocene, volcanism in the Great Basin was dominated by andesite to dacite lava flows, and ash-flow tuffs of dacite to rhyolite composition (McKee et al., 1970; McKee and Siberman, 1975). Basalt volcanism began in the middle Miocene (17 Ma) and continued to the present (20 ka in the Lunar Crater field). Volcanism during the Pliocene in the Great Basin occurred in small volume monogenetic basalt fields like those at Crater Flat and Lunar Crater (Best and Hamblin, 1978; McKee and Noble, 1986).

Ash-flow Tuff Stratigraphy

Silicic calderas form by eruptions of substantial amounts of magma which is emplaced as ash-flow tuff (Lipman, 1997; Druit and Sparks, 1984). It is unusual, therefore, for a caldera not to be associated with outflow tuffs. Oligocene-Miocene ash-flow tuff stratigraphy in the SQCR is poorly known, and knowledge of the regional ash-flow stratigraphy of the nearby ranges is important for correlation of any outflow tuffs that crop out in the SCQR. A table of Oligocene-Miocene ash-flow tuff units that may be present in the SQCR is provided in Chapter 6 and also described below. Ekren et al. (2012) described the geology of the Quinn Canyon Range but did not concentrate on the SQCR in detail. Although some interpretations may differ, Ekren's overall geological interpretations are beneficial to this project and help solidify stratigraphic conclusions.

Kawich Range and Pahranagat Formation

The northern Kawich Range, which lies two ranges to the west of the Quinn Canyon Range, contains five calderas with associated intracaldera tuffs (Honn, 2005). Intracaldera tuffs associated with the five calderas described in Honn (2005) are: Warm Springs Tuff (23.59 ± 0.07 Ma), Bellehelen Tuff (22.87 ± 0.16 Ma), Cow Canyon Tuff (22.78 ± 0.07 Ma), Tobe Spring Tuff (22.77 ± 0.07 Ma), and the Clifford Spring Tuff (23.67 ± 0.09 Ma). Best et al. (1995) suggested that the Kawich Caldera is the source for the Pahranagat Formation that covers an area of 33,000 km^2 and extends into the southern Reveille Range. Figure 3 shows the location of the Kawich Caldera and the Pahranagat Formation in relation to the Quinn Canyon Range. The Pahranagat Formation (22.636 ± 0.009 Ma) is an ash-flow tuff sheet with intracaldera and outflow facies (Best et al., 1995). Outflow units of the Pahranagat Formation were divided into the Salisbury and the overlying Alamo petrographic type tuffs. Scott et al. (1992) described the individual tuffs that were combined by Best et al. (1995) into the Pahranagat Formation.

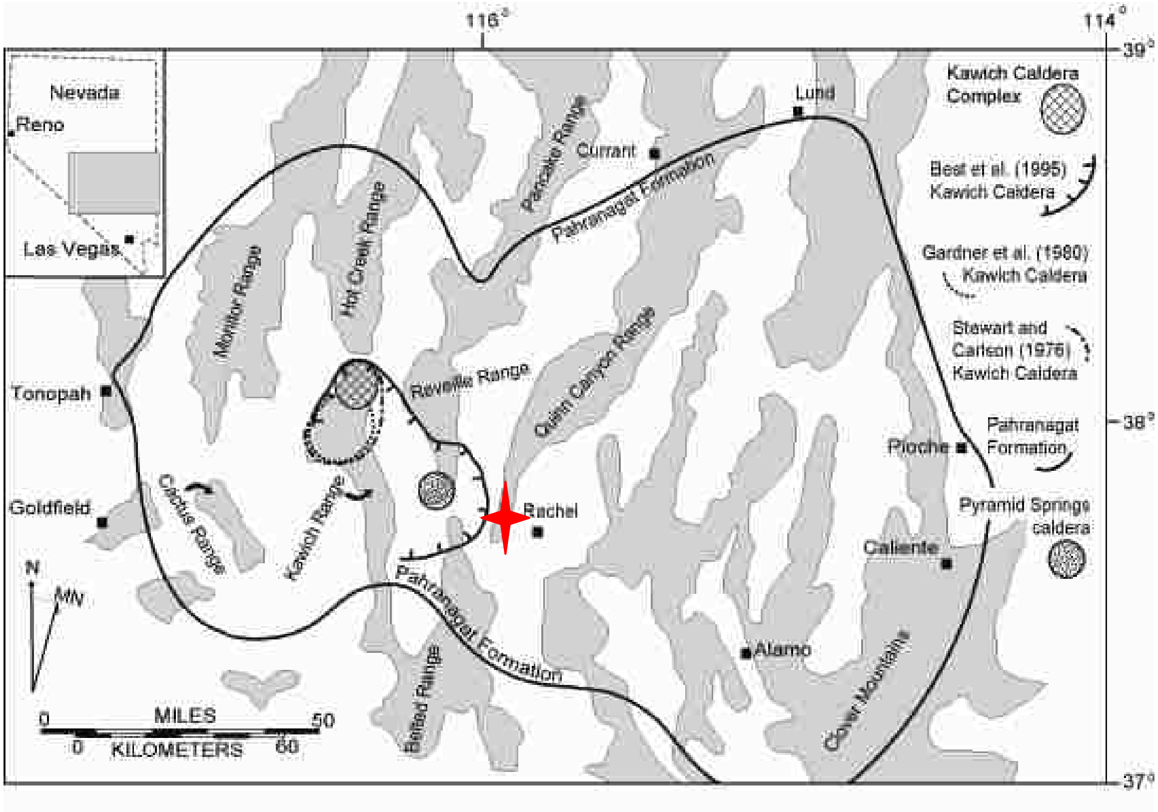

Figure 3: The extent of the Pahranagat Formation. Note interpretations of the location of the Kawich caldera. Approximate location of the study area in the SQCR is represented by the red star. Map from Honn (2005).

Reveille Range

The Reveille Range lies directly to the west of the Quinn Canyon Range and contains three calderas: Goblin Knobs, northern Reveille Range, and Pyramid Springs (Martin and Naumann, 1995; McKelvey, 2008). Ages of intracaldera ash-flow tuff in each caldera are tightly constrained by sanidine and biotite $^{40}Ar/^{39}Ar$ geochronology (Appendix B). The caldera of Goblin Knobs, in the eastern Reveille Range, contains an intracaldera tuff known as the Tuff of Goblin Knobs (25.64 ± 0.53 Ma) (Ekren et al., 1973; Martin and Naumann, 1995; Rash, 1995; McKelvey, 2008). The caldera of the northern Reveille Range contains the Tuff of northern Reveille Range (25.27 ± 0.86 Ma) and the outflow facies of the Tuff of Streuben Knobs (absolute age unknown) (Ekren et al., 1973; Martin and Naumann, 1995; Rash, 1995). Stratigraphic information for the southern Pancake Range and northern Reveille Range are given in Rash (1995).

In the southern Reveille Range, the Pyramid Spring caldera contains the Pyramid Spring Tuff (22.89 ± 0.15 Ma and 22.86 ± 0.15 Ma) which consists of three cooling units: the lower Pyramid Springs, middle Pyramid Springs, and upper Pyramid Springs ash-flow tuffs. These units are primarily distinguished by the increase in pumice clast size from the lower to upper ash-flow sheet (McKelvey, 2008).

The Monotony Tuff found in the northern Reveille Range is a crystal rich dacite ash-flow tuff with an estimated volume of more than 2,900 km^3 that may have erupted from a caldera in the Pancake Range (Ekren et al., 1971). Rash (1995) dated the Monotony Tuff at 27.64 ± 0.34 Ma. Overlying the Monotony Tuff at the southern tip of the Pancake Range is the Tuff of Bald Mountain dated at 26.46 ± 0.42 Ma (Rash, 1995).

<u>Quinn Canyon Range</u>

The Shingle Pass Tuff lies stratigraphically above the Monotony Tuff and may have erupted from a caldera in the Quinn Canyon Range (Best et al., 1989). Distinctive upper and lower cooling units comprise the Shingle Pass Tuff. The lower unit contains an unusual mafic phenocryst assemblage of pyroxene, olivine, amphibole, magnetite, ilmenite, allanite, and biotite (Scott et al., 1992). Sanidine is also more abundant than plagioclase and quartz in the lower unit. In contrast, the upper unit contains greater amounts of plagioclase than sanidine, biotite phenocrysts, but little quartz, and no olivine or ilmenite (Scott et al., 1992). Described by Rash (1995) in the Reveille Range, the Shingle Pass Tuff contains four cooling units (A-D) with the Tuff of Arrowhead (25.78 ± 0.39 Ma) lying between Shingle Pass Tuff cooling units B and C (Rash, 1995). Ekren et al., (1971) gives dates for the Shingle Pass Tuff in the southern Pancake Range as 25.4 ± 0.8 Ma and in the Belted Range as 25.3 ± 0.68 Ma.

Ekren et al. (2012) identifies the Quinn Canyon Range as part of the "Monotony Cauldron Complex" which he relates to the eruptions of the Monotony Tuff and the Shingle Pass Tuff. Major ash-flow units identified by Ekren et al. (2012) in the Quinn Canyon Range are: the Pahranagat Tuff, Tuff of Goblin Knobs, Shingle Pass Tuff, and the Monotony Tuff.

Basalt Volcanism

Pliocene basalts in the Reveille Range lie in the Basalt Zone that extends from Lunar Crater to Death Valley (Figure 2). The northern end of the zone, represented by the Reveille Range, Pancake Range, and Lunar Crater volcanic fields, are isotopically distinctive ($\varepsilon_{Nd} > +3$, $^{87}Sr/^{86}Sr \sim 0.7035$) and have major and trace element signatures similar to ocean island basalts (Yogodzinski et al., 1996). In contrast, Crater Flat basalts, located in the central part of the zone, have $\varepsilon_{Nd} < -8.5$ and $^{87}Sr/^{86}Sr \sim 0.707$ with major and trace element signatures that suggest a lithospheric mantle source (Farmer et al., 1989; Foland and Bergman, 1992; Yogodzinski et al., 1996). Yogodzinski et al. (1996) separated Pliocene volcanism in the Reveille Range into three episodes: (1) Episode 1 basalts (alkali) are most abundant and erupted between 5.9-5.1 Ma. They are characterized by phenocrysts of olivine and plagioclase, while some may also contain phenocryts of clinopyroxene, Fe-Ti oxide, and biotite. Large phenocrysts or glomercrysts of calcic feldspar are also present. (2) Trachyte flows (4.3 Ma) with associated pyroclastic surge deposits overlie Episode 1 basalts. These flows are mostly free of alteration and contain phenocrysts of sanidine, plagioclase, clinopyroxene, Fe-Ti oxides, and apatite. (3) Episode 2 basalts (alkali) are the youngest (4.6-3.0 Ma) and contain large phenocrysts of plagioclase and clinopyroxene, and smaller olivine and Fe-Ti oxides. Episode 2 basalts lacking plagioclase phenocrysts are classified as basanites (Naumann et al., 1991; Yogodzinski et al., 1996). Geochemical evidence suggests that Episode 1 basalts were contaminated by the addition of carbonate material from the underlying Paleozoic basement, while younger Episode 2 basalts were not. Because Episode 2 basalts are isotopically distinct and overlie trachyte and Episode 1 basalts, it was suggested that they represent the beginning of a new episode of basaltic volcanism (Naumann et al., 1991;Yogodzinski et al., 1996). Ekren et al. (2012) references Ekren et al. (1973) and reports a K/Ar date of 5.9 ± 0.2 Ma for a basalt in the Reveille Range. He further suggests that this basalt is related to the basalt on the western edge of the Quinn Canyon Range.

Mining in the Southern Quinn Canyon Range

Mining in the Quinn Canyon Range was concentrated in two main areas. In the northern part of the range, the Quinn Canyon mining district was mainly a fluorite district, but was also prospected for lead, silver and zinc (Tingley, 1991). Approximately 29,500 tons of fluorspar was produced from the mining district (Tingley, 1991). In the southern part of the range, part of my study area, the Queen City mining district is located near Queen City Summit to the north and south of State Highway 375 and was prospected for mercury and gold, with mercury being the only mineral produced (Tingley, 1991).

The primary mine from the Queen City mining district, Black Hawk mine, is located in the SQCR at 37° 46' 13.928 "N, 115° 57' 55.386 "W. This mine was one of the main producers of 80 flasks of mercury between the 1930's and 1960's after being discovered in 1929 (Tingley, 1991). Black Hawk mine geology consists of limestone of the Cambrian Windfall/Nopah Formation with silicified quartz breccia/jasperoid deposits that form along northeast-trending structures. Cinnabar mineralization is associated with the jasperoid bodies (Tingley, 1991). Lovering (1962) defines a jasperoid as an "epigenetic siliceous body formed largely by replacement" and describes the replacement of limestone by silica as being "favored by low temperature, acid solutions, the presence of CO_2."

The Fallini property (37° 46' 35.924"N, 115° 57' 47.721"W) and the Red Wing prospect (37° 45' 18.149"N, 115° 56' 45.464"W) are also located in the SQCR and prospected for mercury in the same time frame as activity at the Black Hawk mine. At the Fallini property, breccia masses within fractures in the limestone host cinnabar and jarosite (Tingley, 1991). Red Wing prospect mine workings are associated with an east-west shear zone that intersects a north south silicified section of ash-flow tuff. Cinnabar is located on quartz crystals in vugs of breccia (Tingley, 1991). Other Queen City mining district claims on the south side of State Highway 375 in the Belted Range occur in limestone of the Cambrian Nopah Formation, and were prospected for mercury, gold, and manganese (Tingley, 1991).

In the SQCR, the Cambrian Nopah Formation contains a thinly bedded gray limestone section that Palmer (written communication to Cornwall, 1963) states to be the Cambrian Windfall Formation because of identified trilobite species, but since the area of exposure is small, the section is included into the upper member of the Nopah Formation (Cornwall, 1972). Kleinhampl and Ziony (1985) suggest that some outcrops in the Quinn

Canyon Range identified as Windfall Formation could be undifferentiated Pogonip Group, which is "an applied name given to Ordovician strata between the Cambrian Windfall Formation and the Ordovician Eureka Quartzite." Ekren et al. (2012) follows descriptions taken from Kleinhampl and Ziony (1985) and places the SQCR mining areas of the Black Hawk and Fallini Mines in the Pogonip Group and Cambrian undivided shale and limestone.

Mercury/cinnabar mineralization in the SQCR may have formed in a similar way to the classic hot-spring mercury deposit (Sherlock et al., 1996). Hot-spring mercury deposits typically form in siliceous sinter with cinnabar coating or dissemination in fractured sinter (Rytuba and Heropoulos, 1992; Sherlock et al., 1996). Mercury and other metals may represent concentrations of minerals from tuffs, rhyolite domes and flows, and intracaldera sedimentary rocks caused by near surface hydrothermal systems active during late stage caldera-forming eruptions (Sherlock et al., 1996). This is not the case in the SQCR where cinnabar deposits are fault related in sedimentary rocks of Cambrian age (Tingley, 1991).

The Quinn Canyon Range lies in a north-northeast oriented extensional belt formed during Paleogene extension and contains late Oligocene-early Miocene extensional structures (Best et al., 1991; Axen et al., 1993). Although the geometry of these faults explains the presence of cinnabar in northeast-trending structures, the relative age of faulting mineralization and volcanism in this area is unclear. If faulting is younger or coeval with volcanism then mineralization may relate to volcanism. Conversely, if faulting in the sedimentary section is older than volcanism then mineralization may not be related to volcanism.

CHAPTER 3

ANALYTICAL TECHNIQUES AND METHODOLOGY

This study utilized geologic mapping, geochemistry, Pb, Nd, and Sr isotopes, petrographic analysis, and $^{40}Ar/^{39}Ar$ and U/Pb dating to determine the volcanic stratigraphy and evolution of the SQCR. Mapping was completed at a scale of 1:50,000 (Appendix J).

Major, Trace, and Rare-Earth Geochemistry

Forty-three whole rock samples were crushed in the Rock Chemistry Laboratory at the University of Nevada Las Vegas (UNLV) using the badger rock crusher, sieved to remove weathered pieces that may add contamination to the sample, and further ground to fine power using the shatter box. Samples were then sent to Activation Laboratories Ltd. in Toronto, Canada to be analyzed using Inductively-Coupled Plasma Mass Spectrometry (ICP-MS). Six of the forty-three samples were analyzed at UNLV by X-ray fluorescence spectrometry (XRF) for quality control and to obtain immediate results. Chemistry is reported in weight percent for major elements and Loss on Ignition (LOI) and parts per million (ppm) for trace and rare-earth elements (REE) (Appendix C). Precision and accuracy of geochemical analyses are presented in Appendix D.

Isotope Analysis

Four mafic samples were prepared at UNLV using the same crushing techniques as the geochemical samples. One andesite and three basalt samples were analyzed for Pb, Nd, and Sr isotopes by fully automated VG sector 6 collector system with an ion-counting thermal ionization mass spectrometry (TIMS at the University of Kansas). Procedures for laboratory analysis are listed on the Kansas University Department of

Geology Tectonics and Geochronology webpage:

(http://www.geo.ku.edu/programs/tectonics/tims.shtml). Rb-Sr and Sm-Nd techniques follow those of Krogh (1973), Richard et al. (1976), and Patchett and Ruiz (1987). Rb-Sr techniques utilize dissolution with HF-HNO_3 in sealed Teflon vessels along with elemental separations using HCL elution on cation exchange columns. U-Pb techniques follow Krogh (1973), Krogh (1982), and Parrish (1987). Isotopic analysis data from the SQCR and additional information used for regional comparison of mafic samples are in Appendix E.

Petrographic Analysis

Thirty-six samples were cut into billets in the UNLV rock preparation lab and sent to Quality Thin sections in Tucson, Arizona for thin section preparation. Mineralogy and visually estimated phenocryst percentages are presented in Appendix F.

$^{40}Ar/^{39}Ar$ Geochronology

Ten ash-flow tuff samples were crushed and sieved to 0.5 mm - 1.5 mm. Dating was done on 20-30 handpicked grains of sanidine per sample. Grains were washed with HCL before being sent for irradiation. Samples were irradiated for seven hours at the USGS Triga Reactor in Denver, Colorado. $^{40}Ar/^{39}Ar$ analyses were conducted at the University of California at Berkeley. Procedures for laboratory analysis are listed on the Berkeley Geochronology Center webpage http://www.bgc.org/facilities/argon_lab.html. Personal communication with Dr. Al Dieno from the University of Berkeley Geochronology lab details $^{40}Ar/^{39}Ar$ sanidine analysis results for SQCR samples. “Results show only those analyses with Ca/K < 5 (to ensure no plagioclase), %$^{40}Ar^*$ >97 (to ensure sample is not altered or low radiogenic), and trimmed for outliers using 1.5

normalized deviations from the median. Ca/K was fixed to zero since ^{37}Ar had decayed because of the long time between irradiation and analyses. Ca/K was also fixed to zero in the Fish Canyon sanidine standard (dated at 28.201 Ma) for uniformity in analysis" (A. Dieno, personal communication, 2010). Analysis results are given in Appendix B.

In order to compare SQCR age results to other analyses for correlation, an Excel spreadsheet written by Dr. Terry Spell was utilized. $^{40}Ar/^{39}Ar$ results for SQCR samples analyzed at the University of California at Berkeley and adjusted ages for comparison to the University of Nevada Las Vegas lab and to dates from Best et al. (1995) are given in Chapters 5 and 6.

U/Pb geochronology

Six ash-flow tuff samples were crushed and sieved to <0.417 mm. Powdered samples were sorted by utilizing heavy liquids and then processed in a Frantz Magnetic Separator to separate magnetic grains from nonmagnetic. Zircons were sorted microscopically yielding 20-30 grains per sample and were mounted in epoxy and gold coated. Catholuminesence (CL) images of individual grains were taken to aide in identification of analysis spots for the SIMS analysis. Analyses were done using the IMS 1270 SIMS at the University of California, Los Angeles under the supervision of Dr. Axel Schmitt. An explanation of operational steps for the SIMS is listed on the UCLA U-Pb geochronology website: http://sims.ess.ucla.edu/Tutorial/UPbtutorial.php. Further analysis of the samples was done utilizing the UCLA in-house software ZIPS v3.04 (courtesy of Chris Coath). Zircon results were processed using ISOPLOT (Ludwig, 2000), an Excel Macro, which calculates a weighted average age for each sample, and regresses the data using weighted residuals and mean squared weighted deviation (MSWD) values (Wendt and Carl, 1991). All analyses and plots are given in Appendix A.

Depth of Melting

Two SQCR basalt samples collected from the western side of the range were used in depth of melting analysis. The Lee et al. (2009) barometer was calibrated using 433 basalt compositions in equilibrium with olivine and orthopyroxene over a range of temperatures from 1110 to 1800 ˚C and pressures of 1 atmosphere to 7GPa. Barometer calibration yielded an uncertainty of +/- 0.20 GPa (Lee et al., 2009). The thermometer generated is consistent with the barometer and has an uncertainty of +/- 3% (Lee et al., 2009). This technique uses an Excel macro provided by Cin-Ty-Lee (Lee personal communication, 2009). After inserting primitive basalt major element compositions, the Excel macro adds olivine to calculate a primary magma in equilibrium with mantle peridotite and calculates the pressure and temperature using equations in Lee et al. (2009). Only two SQCR samples were used in the analysis because the model requires a minimum of at least 97 wt% total for major element analysis for samples being input into the Excel macro.

Co-crystallization of plagioclase or clinopyroxene with olivine is identified by Lee et al. (2009) as a complication with the model calculations. Plagioclase causes a slight overestimate of SiO_2 and MgO yielding a higher temperature and pressure, while clinopyroxene causes a slight underestimate in SiO_2 and overestimate of MgO yielding higher temperature and lower pressure (Lee et al., 2009). Both samples from the SQCR contain plagioclase and clinopyroxene. Lee suggests that by using the most primitive magmas these effects are minimized (Lee et al., 2009). Other guidelines for using this model are: the primary magma must contain olivine and pyroxene, the barometer is not calibrated for silica-undersaturated rocks with < 40 wt.% SiO_2, and it is best to choose the most primitive magma with MgO > 8.0 wt.%. SQCR samples have MgO wt.% values of 4.15 and 4.66, which could complicate the fractionation correction and result in shallower calculated melting depths.

CHAPTER 4

GEOCHEMICAL DATA RESULTS

Geochemistry was conducted on SQCR samples by analyzing whole rock samples. Samples for geochemical analysis were chosen by field observations of major stratigraphic units. Geochemical analysis was performed by ICP-MS and XRF. Geochemical analysis and accuracy results are shown in Appendix C and D with complete methods description given in Chapter 3. Figure 4 shows SQCR samples plotted on the LeBas et al. (1986) classification diagram in wt%, and the range of compositions present in the study area. In addition, seen in Appendix I, is an independent study that displays the capability of correlating ash-flow tuff units by major and trace element geochemistry.

Basalts

Basalts in the SQCR are present on the western side of the range. Based on whole rock analysis, SiO_2 content ranges from 47.87 wt. % to 49.75 wt. %. Figure 5 plots trace element geochemical data on a Sun and McDonough (1989) primitive mantle normalized spider diagram in ppm, and shows a lack of Nb anomaly along with enrichment in P and Ti. Further analysis of southern Quinn Canyon basalts in comparison to regional basalts is given in Chapter 7.

Andesites

Andesites in the SQCR are present along the western and eastern part of the range with whole rock analysis, SiO_2 contents ranging from 58.33 wt. % to 61.99 wt. %. Figure 6 plots trace element geochemical data on the Sun and McDonough (1989) primitive mantle normalized spider diagram and shows anomalies in Nb, P, and Ti. Andesite and basalt from the study area have different trace element and isotopic geochemical signatures; a topic which is discussed further in Chapter 7.

<u>Dacites</u>

Figure 7 plots trace element geochemical data on the Sun and McDonough (1989) primitive mantle normalized spider diagram. Five samples taken from the SQCR were identified as dacite with SiO_2 contents ranging from 63.34 to 69.31 wt. %. Figure 7 shows two trends in dacite sample geochemistry with trend one having P and Ti anomalies (filled diamond symbols) and trend two lacking these anomalies (open diamond symbols).

<u>Rhyolites</u>

Rhyolite tuffs in the SQCR are the most abundant rock type with SiO_2 contents ranging from 71.04 to 78.48 wt. %. Figure 8 plots trace element geochemical data on the Sun and McDonough (1989) primitive mantle normalized spider diagram and displays a trend showing a large range in the composition of Ba, Pb, Sr, and P. $^{40}Ar/^{39}Ar$ and U/Pb geochronology was performed on eight rhyolite tuff samples (Table 1) for correlation to regional tuffs (see Chapter 6 for details).

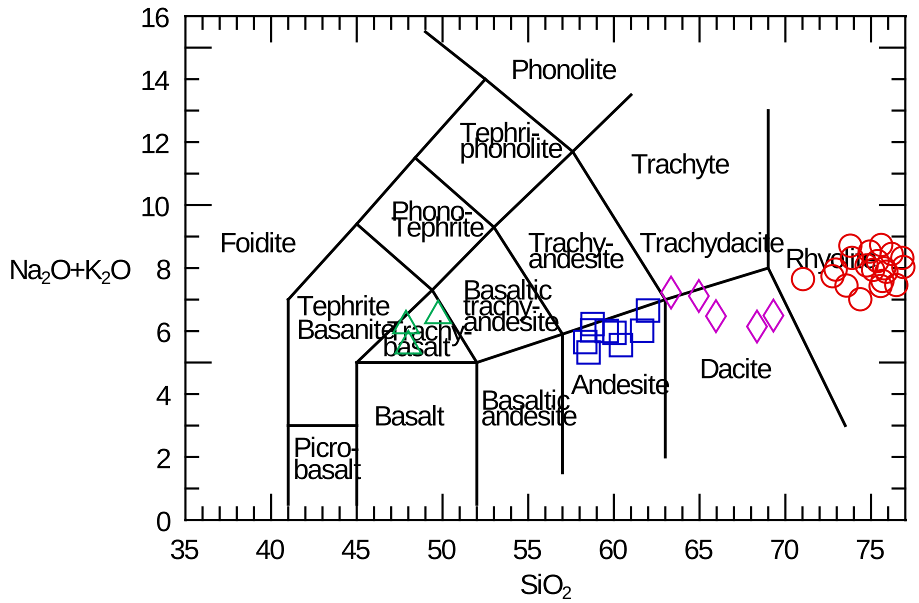

Figure 4: SQCR samples plotted on the LeBas et al. (1986) diagram. Open triangles are basalts, andesites (boxes), dacite (diamonds), and rhyolite (circles).

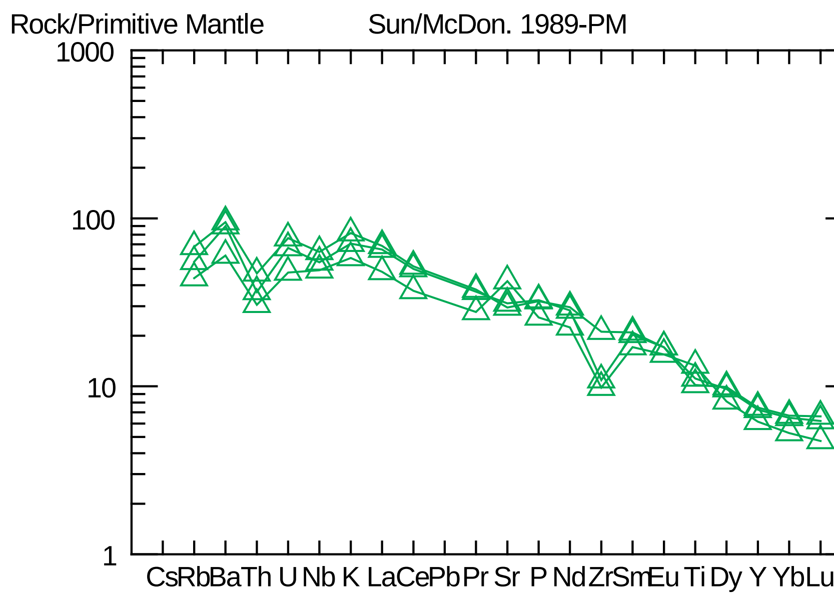

Figure 5: SQCR basalts showing a lack of Nb anomaly along with enrichment in P and Ti compared to andesites (see Figure 6).

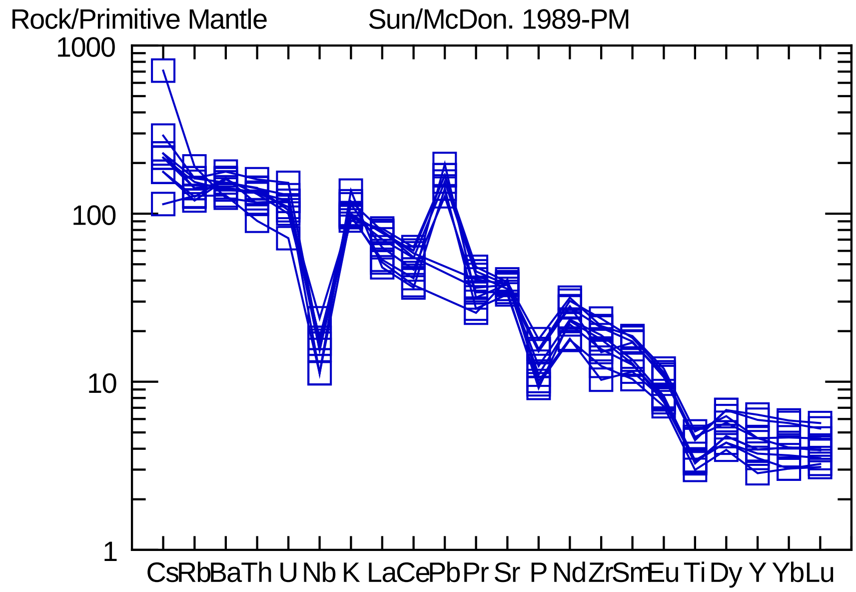

Figure 6: SQCR andesites showing negative anomalies in Nb, P, and Ti.

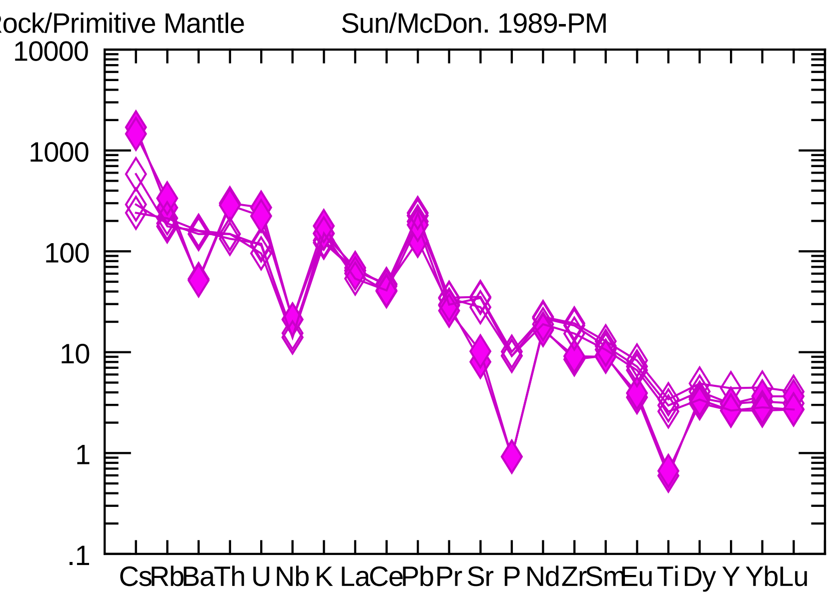

Figure 7: SQCR dacites showing two trends (filled diamond symbols and unfilled diamond symbols).

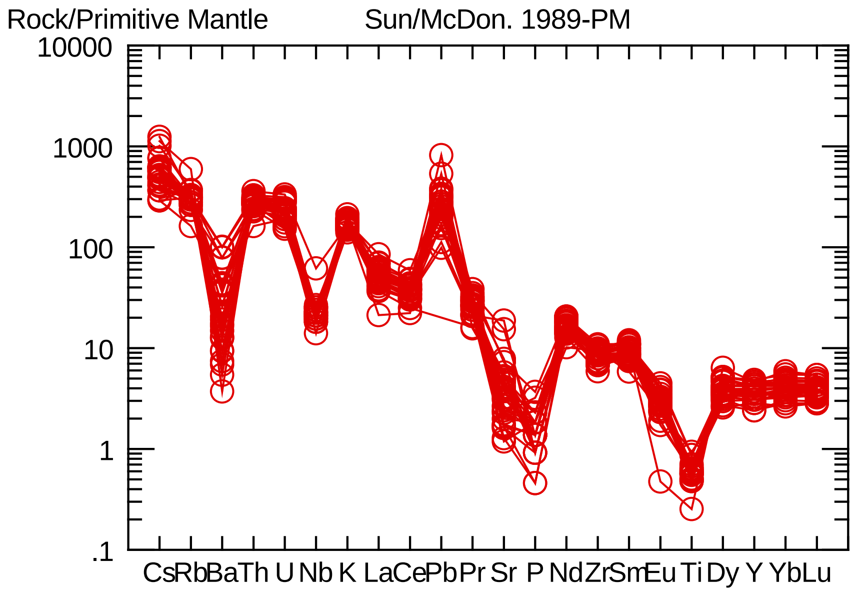

Figure 8: SQCR rhyolites display large variations in Ba, Pb, Sr, and P.

CHAPTER 5

GEOCHRONOLOGY RESULTS

$^{40}Ar/^{39}Ar$ single sanidine crystal analysis performed at the University of California, Berkeley along with U/Pb spot zircon analysis by SIMS at the University of California, Los Angeles, yielded dates for nine major stratigraphic units, see Apendix G for sample locations, in the SQCR. $^{40}Ar/^{39}Ar$ and U/Pb dates are weighted means with outliers removed.

Ages and one sigma errors for $^{40}Ar/^{39}Ar$ results and two sigma errors for U/Pb are shown in Table 1 with detailed information from specific crystal and spot analyses given in Appendix A and B. Also shown in Table 1 are adjustments made to SQCR $^{40}Ar/^{39}Ar$ ages results for comparison with previously analyzed samples that used a different age for the Fish Canyon standard in analysis.

Samples Q18, Q23, Q24, Q50 have $^{40}Ar/^{39}Ar$ sanidine ages of 22.88 ± 0.02, 22.92 ± 0.02, 22.95 ± 0.03, and 22.94 ± 0.02 Ma. U/Pb zircon analyses yielded ages of 24.00 ± 1.8 (Q18), 24.42 ± 0.98 (Q23), and 26.72 ±0.92 (Q24) Ma. $^{40}Ar/^{39}Ar$ geochronology yielded ages of 20.09 ± 0.03 (Q38), 23.01 ± 0.04 (Q9), and 23.03 ± 0.03 (Q59) Ma. No U/Pb analysis was done on these samples. Sample Q13 was dated at 23.72 ± 0.03 Ma by $^{40}Ar/^{39}Ar$ sanidine and 23.49 ±0.73 Ma by U/Pb zircon analysis, whereas Q61 was dated at 23.77 ± 0.03 Ma ($^{40}Ar/^{39}Ar$ sanidine) and 25.2 ± 2.3 Ma by U/Pb zircon.

Table 1: Geochronology weighted mean ages and associated uncertainties.

Method	40Ar/39Ar Date Using Fish Canyon Standard of 28.201 Ma*		40Ar/39Ar Date Adjusted to Fish Canyon Standard of 27.90 Ma **		40Ar/39Ar Date Adjusted to Fish Canyon Standard of 27.84 Ma ***		U/Pb	
Sample ID	Age (Ma)	+/- 1σ	Age (Ma)	+/- 1σ	Age (Ma)	+/- 1σ	Age (Ma)	+/- 2σ
Q9	23.01	0.04	22.76	0.04	22.72	0.04	Not Analyzed	
Q59	23.03	0.03	22.78	0.03	22.74	0.03	Not Analyzed	
Q18	22.88	0.02	22.64	0.02	22.59	0.02	24.00	1.8
Q23	22.924	0.019	22.679	0.019	22.630	0.019	24.42	0.98
Q24	22.95	0.03	22.71	0.03	22.66	0.03	26.72	0.92
Q50	22.938	0.019	22.693	0.019	22.644	0.019	Not Analyzed	
Q13	23.72	0.03	23.47	0.03	23.42	0.03	23.49	0.73
Q61	23.77	0.03	23.52	0.03	23.47	0.03	25.2	2.3
Q38	20.09	0.03	19.88	0.03	19.83	0.03	Not Analyzed	

* Southern Quinn Canyon Range results analyzed by UC Berkeley.

** Adjustment required to compare southern Quinn Canyon Range results to dates analyzed at the UNLV Geochronology Lab.

*** Adjustment required to compare southern Quinn Canyon Range results to dates of the Pahranagat Tuff from Best et al., 1995.

CHAPTER 6

MIOCENE STRATIGRAPHY AND CORRELATION TO REGIONAL UNITS

A prime objective of this work is to correlate ash-flow tuffs in the southern Quinn Canyon range with well-recognized tuff units in central Nevada (Table 2). Nine SQCR samples dated for regional correlation where further discriminated using geochemical plots. Unfortunately all analyzed rhyolites have very similar geochemical trends (Figure 9), consequently geochronology, petrography and field descriptions must be used in addition to geochemistry for correlation of these rhyolites to regional units. Table 3 shows correlated units for SQCR dated samples and the date used for correlation. SQCR correlated ages are adjusted to the same Fish Canyon standard that was used in the date of the correlated unit.

Petrographic and field descriptions of units within the SQCR were completed as part of this thesis unless otherwise specified. Unit descriptions from Ekren et al. (2012) were compared to this study and incorporated to benefit the overall description of SQCR stratigraphy. Petrographic descriptions are presented in Appendix F with phenocrysts given as the volume percent of total phenocrysts. Abbreviations for the phenocrysts are: q (quartz), af (alkali feldspar; sanidine, unless otherwise noted), pf (plagioclase), b (biotite), hb (hornblende), cpx (clinopyroxene), opx (orthopyroxene), and px (pyroxene).

Based on geochronology alone, several regional ash-flow tuffs including The Tuff of Goblin Knobs, Tuff of Northern Reveille Range, Shingle Pass Tuff, and the Monotony Tuff are significantly older than SQCR rhyolites (Table 2) and can be eliminated as candidates for correlation to SQCR units. The data indicate, however, that there are three major ash-flow tuff units in the SQCR that correlate with the Pahranagat Tuff (Best et al. (1995), Clifford Spring Tuff, and Cow Canyon Tuff (Honn, 2005).

Pahranagat Tuff

Samples Q18, Q23, Q24, and Q50 adjusted $^{40}Ar/^{39}Ar$ sanidine ages correlate with the Pahranagat Tuff dated at 22.636 ± 0.009 Ma (Best et al., 1995) shown in Table 3. U/Pb zircon ages are older and may suggest that some of the zircon crystals are antecrysts or xenocrysts, but this topic is not considered in this thesis.

The Pahranagat Tuff is a multi-flow cooling unit (Scott et al., 1992; Best et al., 1995) and according to mapping for this thesis is the youngest ash-flow tuff in the Quinn Canyon Range. The Pahranagat Tuff in the SQCR is densely welded thick pale-red to buff color in outcrop.

Thin section identification yielded the following range of percentages: q (35-10), af (60-30), pf (30-10), b (30-5), hb (10) with pumice and lithic fragments in multiple samples. Best et al. (1995) separated the Pahranagat outflow facies into the following four groups based on the abundance of pumice and TiO_2 concentration: (1) quartz-rich high silica rhyolite, (2) quartz-poor high silica rhyolite, (3) low silica rhyolite, and (4) trachydacite. SQCR samples Q18, Q23, and Q50 correlate to either high silica rhyolite group 1 or 2 (Figure 10). According to Best et al., (1995) tuffs in this group should contain TiO_2 concentrations between 0.10-0.21 wt.% and phenocrysts of quartz, sanidine, plagioclase, biotite, Fe-Ti oxides +/- amphibole. This compares closely to the petrographic analysis and TiO_2 values of samples Q18, Q23 and Q50 ranging from 0.055-0.153 wt. %. Sample Q24 is dacite (Figure 10) with a TiO_2 concentration of 0.643 wt % and a phenocryst assemblage which may correlate to group 4 of Best et al. (1995). See

Appendix C and F for additional petrographic and geochemical information for SQCR samples.

Eric Christiansen (personal communication, 2010) gave coordinates of a dated Pahranagat Tuff sample within the Quinn Canyon Range (Figure 11) and further divided the Pahranagat Tuff based on trace-element geochemistry (Figure 12 and Appendix H). His data identified two trends represented by green triangles (trend 1) and blue squares (trend 2) on Figure 12, and These same two trends are shown in Figure 13 plotting the SQCR samples that correlate to the Pahranagat Tuff. Comparing Christiansen's Pahranagat Tuff trends with SQCR samples suggest that Q24 correlates to trend 2 of the Pahranagat Tuff (Figure 14) and Q18, Q23, and Q50 to trend 1 (Figure 15).

Younger Pahranagat Tuff

An ash-flow tuff (Q38) lying stratigraphically above the Pahranagat Tuff yielded a $^{40}Ar/^{39}Ar$ sanidine age of 20.09 ± 0.03 Ma. Although this date is younger than normally associated with the Pahranagat Formation, Best et al. (1995) and Scott et al. (1992) indentified 20 Ma old tuffs associated with the Pahranagat Tuff. Best et al. (1995) dated post-caldera lava capping the Pahranagat Formation in the Kawich Range by $^{40}Ar/^{39}Ar$ sanidine at 20.58 ± 0.07 Ma. Scott et al. (1992) referenced a K/Ar biotite date of 20.0 ± 0.6 Ma from McKee and John (1987) as part of the Pahranagat Formation. Based on this information, this tuff is correlated with the younger member of the Pahranagat Tuff.

In outcrop the unit is more resistant to erosion than the underlying Pahranagat Tuff and has a larger amount of quartz and pumice. It is densely welded, thick pale-red to buff color in outcrop with fine to medium grained phenocrysts within a highly devitrified pumiceous matrix containing spherulites. Thin section analysis yielded the following percentages: q (35), af (30), pf (30), b (5). See Appendix C and F for additional information.

Cow Canyon Tuff

Several units in the SQCR are slightly but significantly older than the Pahranagat Tuff. Honn (2005) based on work in the Kawich Range identified five calderas containing five intracaldera tuffs. These tuffs were originally correlated to the Pahranagat Tuff (Best et al., 1995) but reinterpreted by Honn (2005) as five separate units older than the Pahranagat Tuff.

One of these units, the Cow Canyon Tuff, was dated at 22.78 ± 0.07 Ma (Honn, 2005). Based on nearly identical ages with SQCR adjusted ages of 22.76 Ma ± 0.04 and 22.78 ± 0.03 Ma, samples Q9 and Q59 are correlated with the Cow Canyon Tuff (Table 3) The Cow Canyon Tuff as described by Honn (2005) is a vitric rhyolite tuff that is greater than 500 meters thick. In the SQCR the Cow Canyon Tuff is not widespread and is similar geochemically (Figure 16) to the Clifford and Pahranagat Tuffs but is older.

Thin section analysis of Q9 and Q59 yielded the following phenocryst percentages: af (60), q (20), b (20) in a glassy matrix sometimes showing fine grained devitrification. This compares well to the mode of the Cow Canyon tuff in the Kawich Range of af (50), q (20), pf (15), b (15) (Honn, 2005). Other possible candidates for correlation are the Bellehelen and Tobe Spring tuffs originally described by Honn (2005) in the Kawich Range. The Bellehelen tuff does not contain biotite, which is not true for samples Q9 and Q59. Samples Q9 and Q59 are similar in age and trace element signature to the Tobe Spring, Cow Canyon, and Bellehelen tuffs from the northern Kawich Range (Figure 16), but based on a combination of mineralogy, chemistry and age the best candidate for correlation with samples Q9 and Q59 is the Cow Canyon tuff (Figure 17).

Clifford Spring Tuff

The Clifford Spring Tuff was identified by Honn (2005) as a vitric rhyolite intracaldera tuff that erupted from the Clifford Spring caldera at 23.67 ± 0.09 Ma. ago. Honn (2005) describes the Clifford Spring Tuff as a rhyolite with pumice and lithic fragments. Intracaldera units contain large (up to 1 km) megabreccia blocks. The tuff in the Kawich Range contains phenocryst of af (55), q (25), pf (10), and b (10) with abundant iron oxide alteration (Honn, 2005). Thin section analysis of the samples Q13 and Q61 yielded a similar rock mode: af (60), q(35), b (5).

Ages of SQCR samples Q13 and Q61 were compared to the Clifford Spring Tuff, Tuff of White Blotch Spring, and the Warm Springs Tuff (Honn, 2005), but Q13 adjusted age of 23.47 ± 0.03 Ma and Q61 adjusted age of 23.52 ± 0.03 Ma correlate with the Clifford Spring Tuff (Table3). Geochemical comparisons in Figure 18 show similar trace element patterns when comparing the Clifford Spring tuff and SQCR samples Q13 and Q61. The Tuff of White Blotch Spring and the Warm Springs Tuff can be eliminated from consideration for the following reasons. The Tuff of White Blotch Spring has a wide range of dates (Table 2) and was later incorporated as part of the Pahranagat Formation by Scott et al. (1992). The Warm Springs Tuff was incorrectly sampled as stated on page 43 of Honn (2005) and is actually equivalent to the Clifford Spring Tuff.

Based on petrography, geochemistry and geochronology, samples Q13 and Q61 are correlated to the Clifford Spring Tuff.

Table 2: Regional ash-flow tuff geochronology.

Outflow Sheet	Associated Range	Age	Method	Reference
Shingle Pass Tuff	Southern Pancake Range	25.78 ± 0.39 Ma	sanidine 40Ar/ 39Ar	Rash (1995)
	Southern Pancake Range	25.4 ± 0.8 Ma	sanidine K/Ar	Ekren et al. (1971)
	Belted Range	25.3 ± 0.68 Ma	sanidine K/Ar	Ekren et al. (1971)
Tuff of Arrowhead	Reveille Range	26.56 ± 0.59 Ma	biotite 40Ar/ 39Ar	Rash (1995)
Monotony Tuff	Pancake Range	27.64 ± 0.34 Ma	sanidine 40Ar/ 39Ar	Rash (1995)
Tuff of Bald Mountain	Pancake Range	26.46 ± 0.42 Ma	sanidine 40Ar/ 39Ar	Rash (1995)
Northern Reveille Range	Reveille Range	25.27 ± 0.86 Ma	biotite 40Ar/ 39Ar	Rash (1995)
Tuff of Goblin Knobs	Reveille Range	25.64 ± 0.53 Ma	sanidine 40Ar/ 39Ar	Rash (1995) and McKelvey (2008)
Pyramind Spring Tuff	Reveille Range	22.89 ± 0.15 Ma	sanidine 40Ar/ 39Ar	McKelvey (2008)
Pyramind Spring Tuff	Reveille Range	22.86 ± 0.15 Ma	sanidine 40Ar/ 39Ar	McKelvey (2008)
Pahranagat Formation	Kawich Range	22.636 ± 0.009 Ma	sanidine 40Ar/ 39Ar	Best et al. (1995)
Warm Springs Tuff	Northern Kawich Range	23.59 ± 0.07 Ma	sanidine 40Ar/ 39Ar	Honn (2005)
Bellehelen Tuff	Northern Kawich Range	22.87 ± 0.16 Ma	sanidine 40Ar/ 39Ar	Honn (2005)
Cow Canyon Tuff	Northern Kawich Range	22.78 ± 0.07 Ma	sanidine 40Ar/ 39Ar	Honn (2005)
Tobe Spring Tuff	Northern Kawich Range	22.77 ± 0.07 Ma	sanidine 40Ar/ 39Ar	Honn (2005)
Clifford Spring Tuff	Northern Kawich Range	23.67 ± 0.09 Ma	sanidine 40Ar/ 39Ar	Honn (2005)
Belted Range Tuff	Belted Range	13.8 ± 0.6 Ma	Nonhydrated Glass K/Ar	Ekren et al. (1971)
Fraction Tuff	Northern Kawich Range	19.7 ± 0.6 Ma 20.4 ± 0.6 Ma	alkali feldspar K/Ar	Silberman et al. (1978)
	Cactus Range	15.7 ± 0.5 Ma	sanidine K/Ar	Ekren et al. (1971)
	Cactus Range	16.4 ± 0.5 Ma	sanidine K/Ar	Ekren et al. (1971)
Tuff of White Blotch Spring	Monotony Valley	24.4 ± 0.7 Ma	sanidine K/Ar	Ekren et al. (1971)
	Kawich Range	23.4 ± 0.7 Ma	sanidine K/Ar	Ekren et al. (1971)
	Northern Cactus Range	22.9 ± 0.7 Ma	sanidine K/Ar	Ekren et al. (1971)
	Northern Cactus Range	21.8 ± 0.7 Ma	sanidine K/Ar	Ekren et al. (1971)

Table 3: SQCR correlated units.

Sample	40Ar/39Ar Date Used in Correlation	Correlated Unit	Date of Correlated Unit
Q38	20.09 +/- 0.03 Ma	younger Pahranagat Tuff	20.58 +/- 0.07 Ma
Q18	22.59 +/- 0.02 Ma	Pahranagat Tuff	22.636 +/- 0.009 Ma
Q23	22.62 +/- 0.019 Ma	Pahranagat Tuff	22.636 +/- 0.009 Ma
Q24	22.66 +/- 0.03 Ma	Pahranagat Tuff	22.636 +/- 0.009 Ma
Q50	22.64 +/- 0.019 Ma	Pahranagat Tuff	22.636 +/- 0.009 Ma
Q9	22.76 +/- 0.04 Ma	Cow Canyon Tuff	22.78 +/- 0.07 Ma
Q59	22.78 +/- 0.03 Ma	Cow Canyon Tuff	22.78 +/- 0.07 Ma
Q13	23.47 +/- 0.03 Ma	Clifford Spring Tuff	23.67 +/- 0.09 Ma
Q61	23.52 +/- 0.03 Ma	Clifford Spring Tuff	23.67 +/- 0.09 Ma

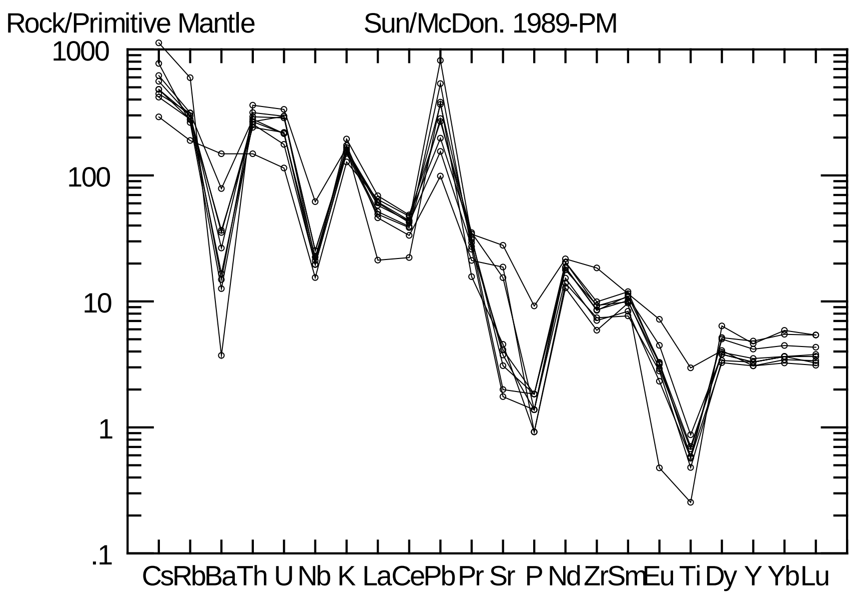

Figure 9: Dated SQCR samples showing similarity in trace-element patterns.

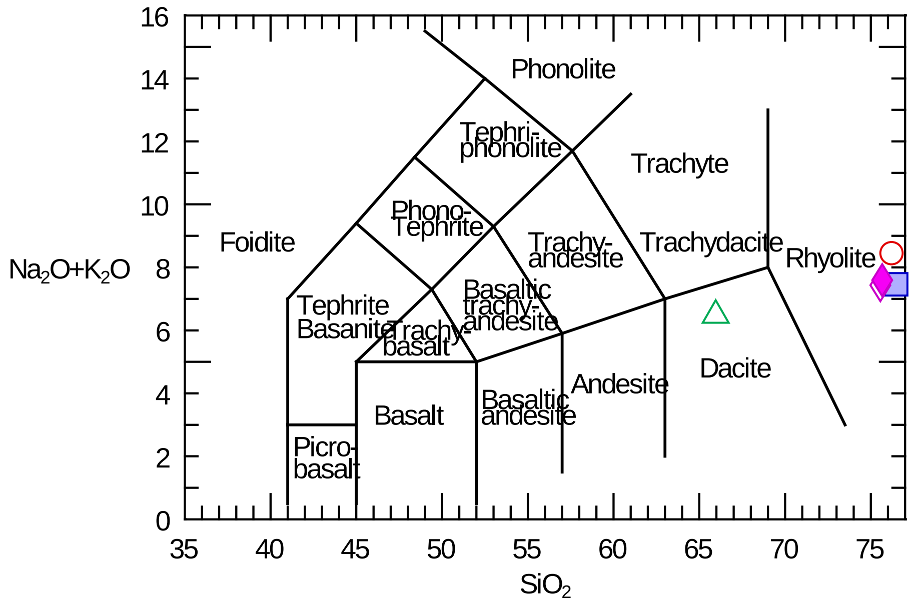

Figure 10: Composition of SQCR samples correlated to the Pahranagat Tuff with Q24 (green triangle) and Q18, Q23, Q50,and Q38 (other symbols).

Figure 11: Location of the Pahranagat Tuff sample dated by Eric Christiansen in the Quinn Canyon Range with coordinates based on data provided by Eric Christiansen. Study area from this thesis outlined in red.

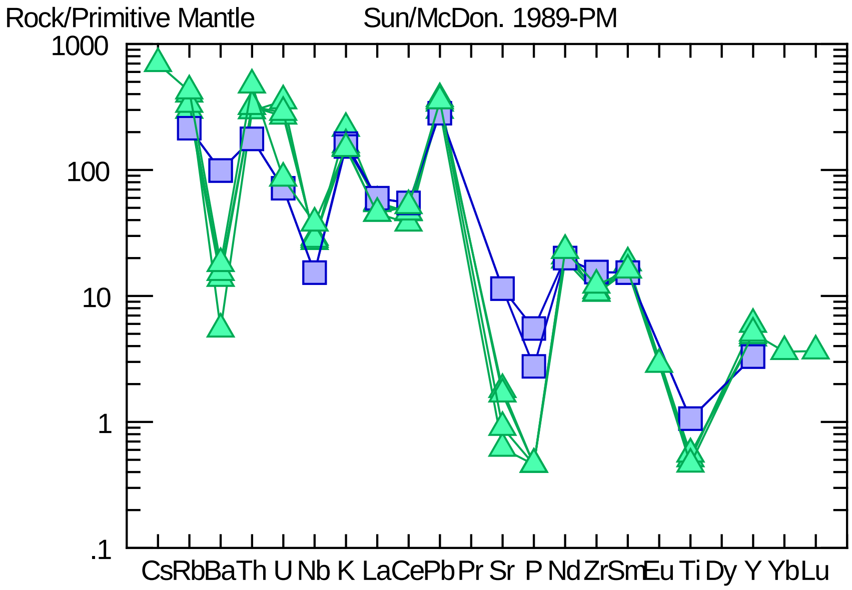

Figure 12: Based on data provided by Eric Christiansen, the Pahrangat Tuff has two trends represented by green triangles (trend 1) and blue squares (trend 2).

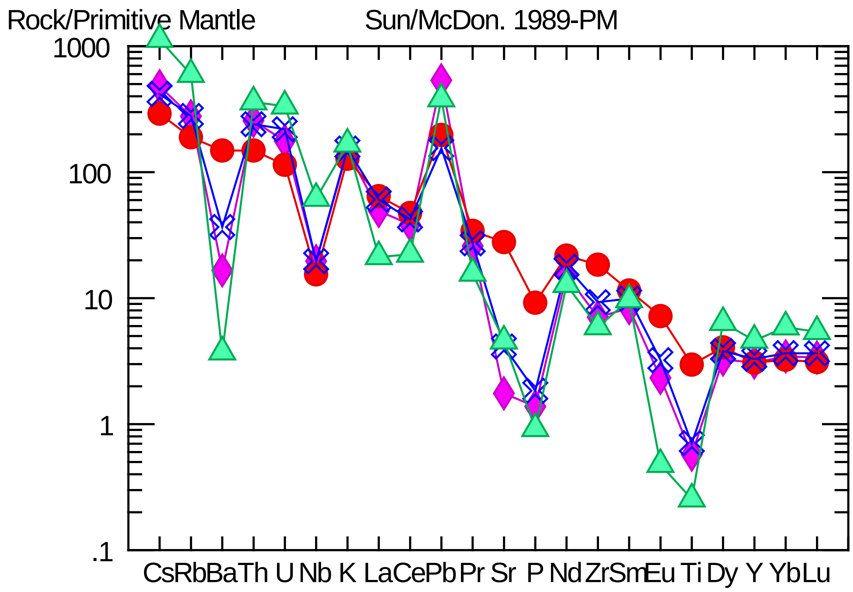

Figure 13: Dated SQCR samples correlated to the Pahranagat Tuff show two different trends with Q24 (red circles) different from Q18, Q23, and Q50.

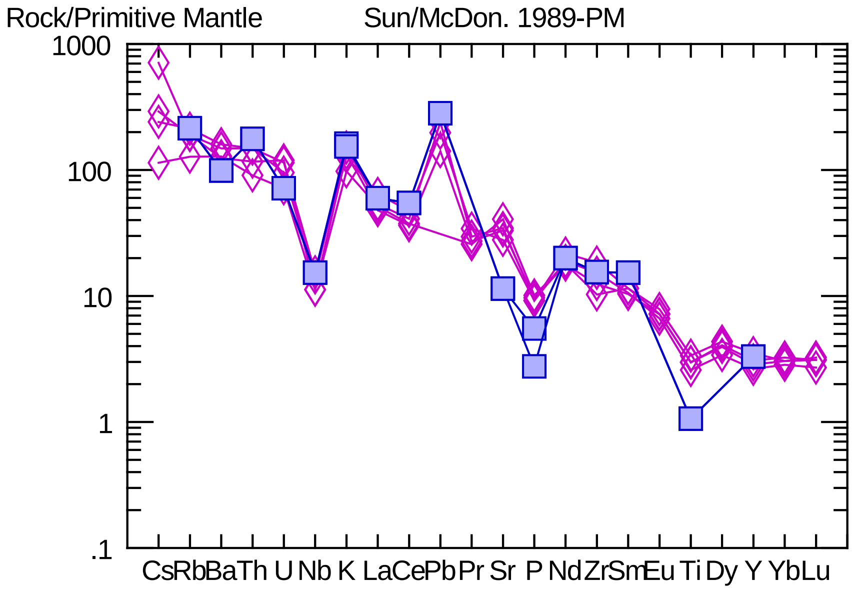

Figure 14: Sample Q24 and other correlated SQCR samples (diamonds) with Pahranagat Tuff trend 2 (squares).

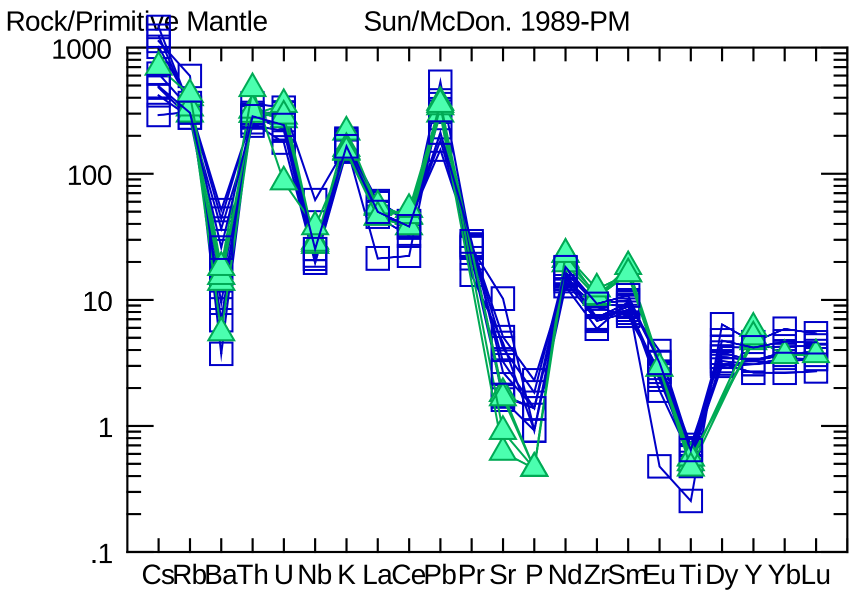

Figure 15: SQCR samples Q18, Q23, Q50 (blue squares) are similar to Pahranagat Tuff trend 1 (green triangles).

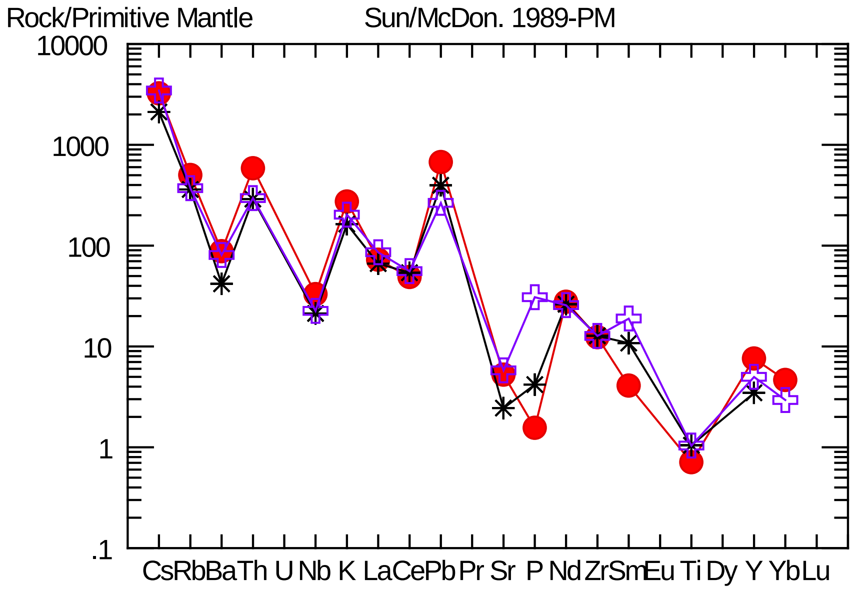

Figure 16: Similarity of geochemical signatures between the Bellehelen, Cow Canyon, and Tobe Spring tuffs from data in Honn (2005).

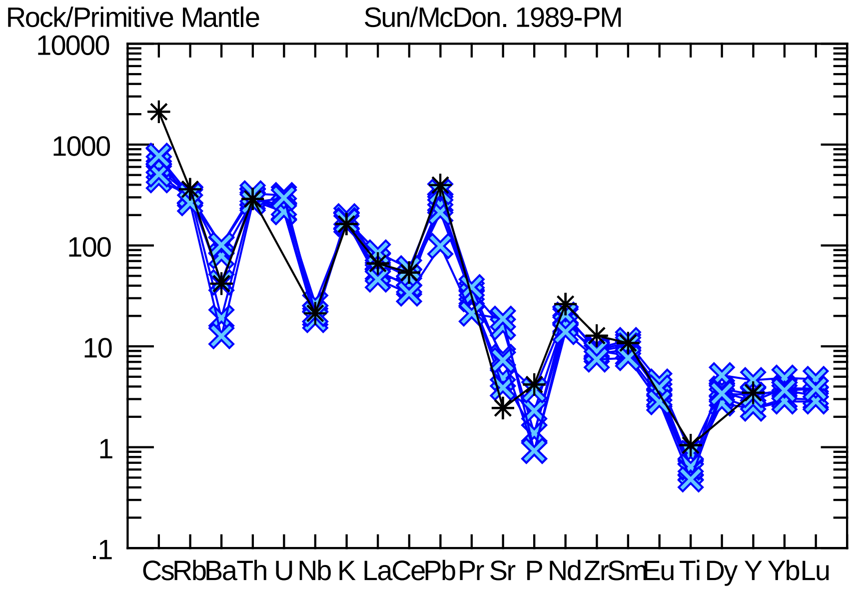

Figure 17: SQCR Samples (Q59 & Q9-blue X's) correlate to the Cow Canyon Tuff from the Kawich Range (black asterisk).

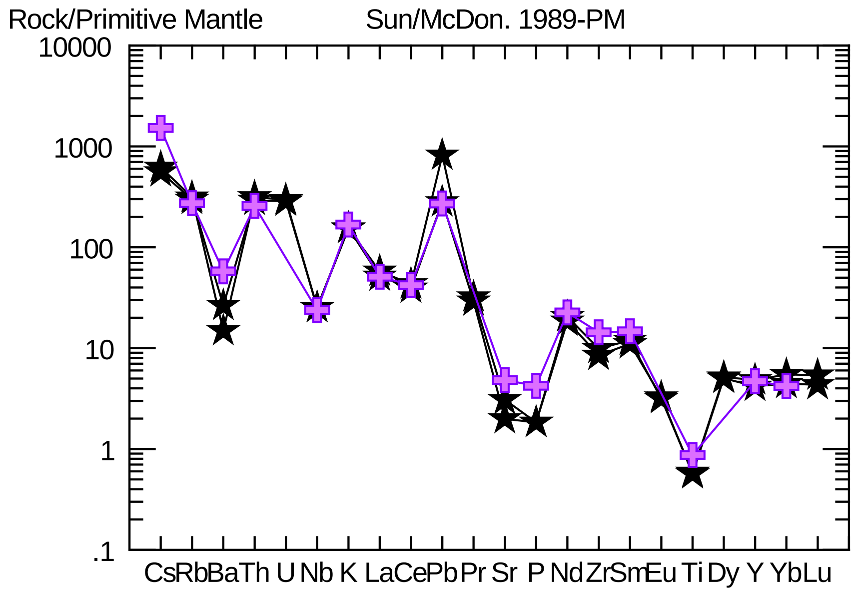

Figure 18: Correlation between SQCR samples Q13 and Q61 (black) and Clifford Spring Tuff (pink).

CHAPTER 7

MAFIC COMPOSITIONAL COMPARISON

Pliocene basalt occurs along the western flank of the SQCR but is not abundant, whereas Miocene andesite crops out on both sides of the range. Three basalt samples and one andesite sample (eastern part of the range) that were the least weathered were analyzed for isotopic analysis. Comparison of these samples to data from a regional database of mafic rocks Pliocene in age or younger (this thesis) including the Cima Domes, Reveille Range, Lunar Crater, Nevada Test Site, Crater Flat, and Death Valley was completed to determine the relationship of SQCR basalt to the Basalt Zone (Figure 19) and to characterize source areas.

A compilation of geochemical data for mafic volcanic rocks of the Basalt Zone for this thesis defines three distinct regional groups (Figure 20): (1) Crater Flat and Death Valley, (2) SQCR basalt and Reveille Range Episode 1, and (3) Lunar Crater, Reveille Range Episode 2, and Pliocene basalt of the Nevada Test Site. Group 1 (Crater Flat and Death Valley) has initial Sr values between 0.706 - 0.710 and Epsilon Nd values between -15 to -5. Group 2 (SQCR basalts and Reveille Range Episode 1) has initial Sr values between 0.704 - 0.706 and Epsilon Nd between 0 - 5. Group 3 (LC, RR Episode 2, and NTS) has initial Sr values between 0.702 - 0.704 and Epsilon Nd between 3 and 7.

Plotting an incompatible element (Th or La) vs. an index of differentiation (MgO) is a good way to model a differentiation process. If fractional crystallization is an important process, the incompatible element should increase and MgO decrease during magma evolution. If magma mixing or assimilation is important, then the incompatible element concentration may increase without any change in the index of differentiation.

Plotting the regional data set on element variation diagrams (Figures 21 and 22) with an incompatible element on the Y-axis and the index of differentiation on the X, shows fractional crystallization trends for SQCR, Reveille Range Episode 1 and Reveille Range Episode 2. Death Valley and Crater Flat basalts display a large increase in both La and Th without much change in MgO suggesting that contamination may have been important in their evolution.

Lead comparison diagrams (Figures 23 and 24) show that samples from the southern end of the Basalt Zone (Death Valley, Crater Flat, and Nevada Test Site) are low in $^{206}Pb/^{204}Pb$, while samples from the northern end of the Basalt Zone (SQCR, Reveille Range, and Crater Flat) are high in $^{206}Pb/^{204}Pb$ and lie closer to the Northern Hemisphere Reference Line (NHRL). Since low Pb indicates low Uranium in the source, it is probable that both Crater Flat and Death Valley basalts have a component of depleted Uranium lower crust in their source area.

Trace element geochemistry for the three SQCR basalts were plotted on the Sun and McDonough (1989) primitive mantle normalized spider diagram and compared to Reveille Range Episode 1 and Episode 2 basalts from Yogodzinski et al. (1996) (Figure 25). SQCR basalts and Reveille Range Episode 1 and 2 basalts follow the same trend with a lack of Nb anomaly and enrichment in P and Ti with the exception of two SQCR samples having a slight negative Zr anomaly. This similarity is additional support for SQCR basalt as part of the Basalt Zone and provides additional data for a direct correlation of SQCR basalt to basalt in the Reveille Range and an asthenospheric source.

Conclusions

Isotopes (Figures 19, 23 and 24) reveal that samples from the northern and southern end of the Basalt Zone separate into at least two populations. Northern Basalt Zone samples have low initial Sr, high Epsilon Nd, and high $^{206}Pb/^{204}Pb$. These differences were also observed by Yogodzinski et al. (1996). Figures 20-22 also show the same separation of populations on element variation diagrams between three major groups of data: (1) Crater Flat and Death Valley, (2) SQCR basalt and Reveille Range Episode 1, and (3) Lunar Crater, Reveille Range Episode 2, and Pliocene basalt of the Nevada Test Site. The Miocene-aged SQCR andesite Q1 is geochemically different from other mafic samples in the SQCR. It is higher in initial Sr and is similar to the Death Valley basalts. This andesite is interbedded with tuffs and is therefore older than other mafic rocks in the SQCR. The overall grouping of the northern Basalt Zone versus the southern Basalt Zone suggests different melt sources, with northern Basalt Zone (SQCR, Reveille Range, and Lunar Crater) samples being derived from asthenospheric mantle.

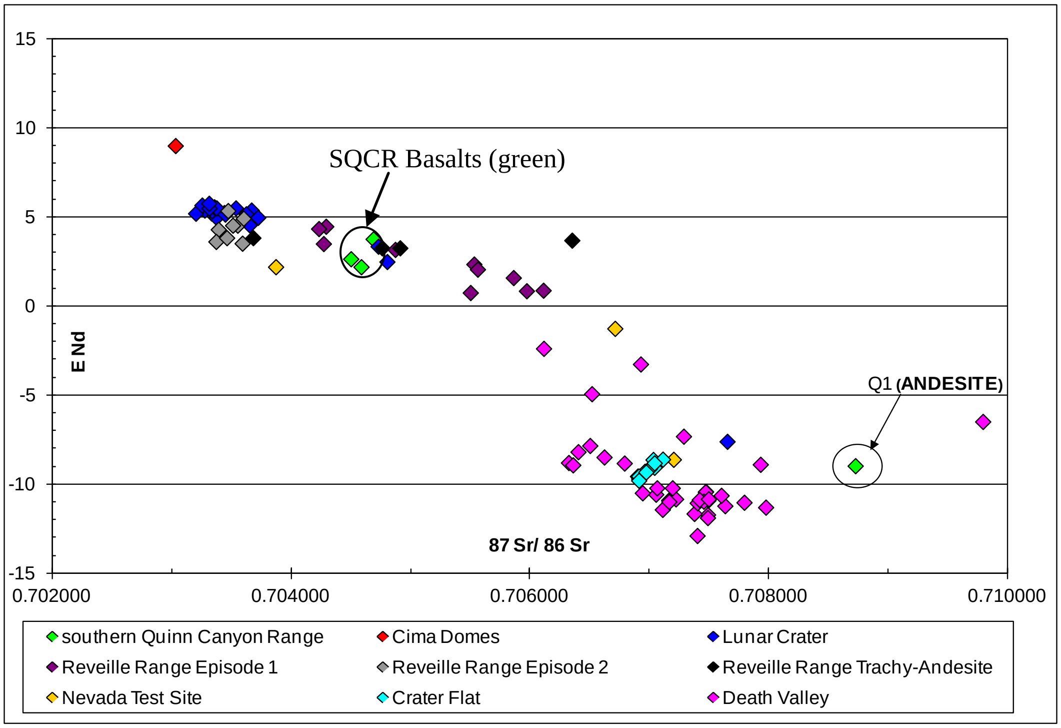

Figure 19: Epsilon Nd vs. initial Sr for mafic volcanic rocks of the Basalt Zone.

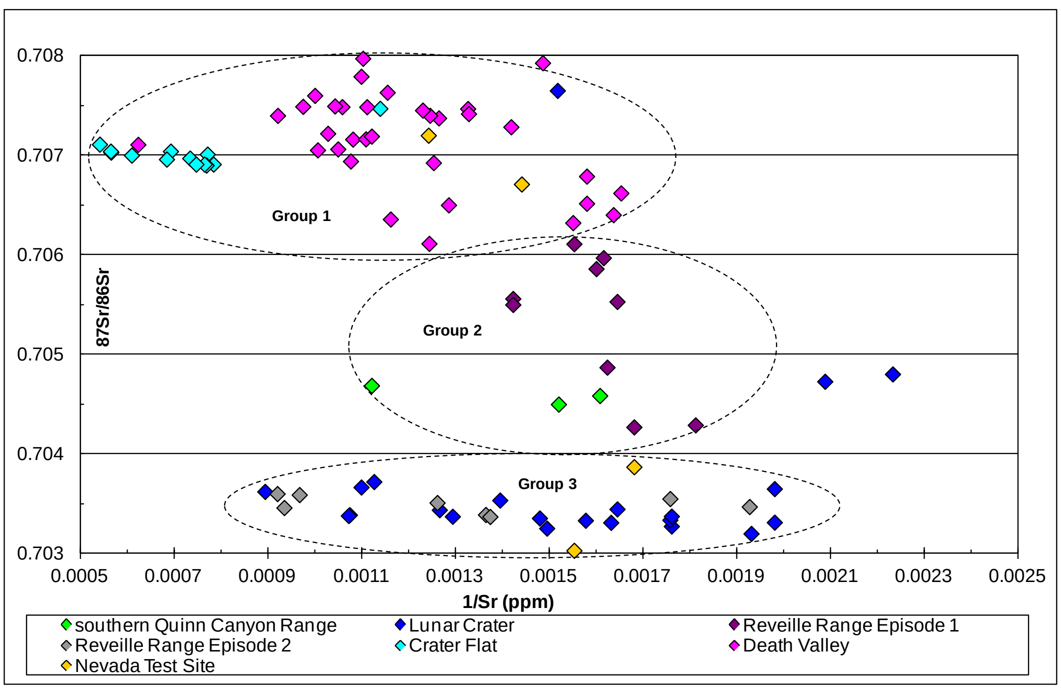

Figure 20: Initial Sr vs. 1/Sr for basalts of the Basalt Zone. Basalt in the SQCR is similar to Reveille Range episode 1 basalt.

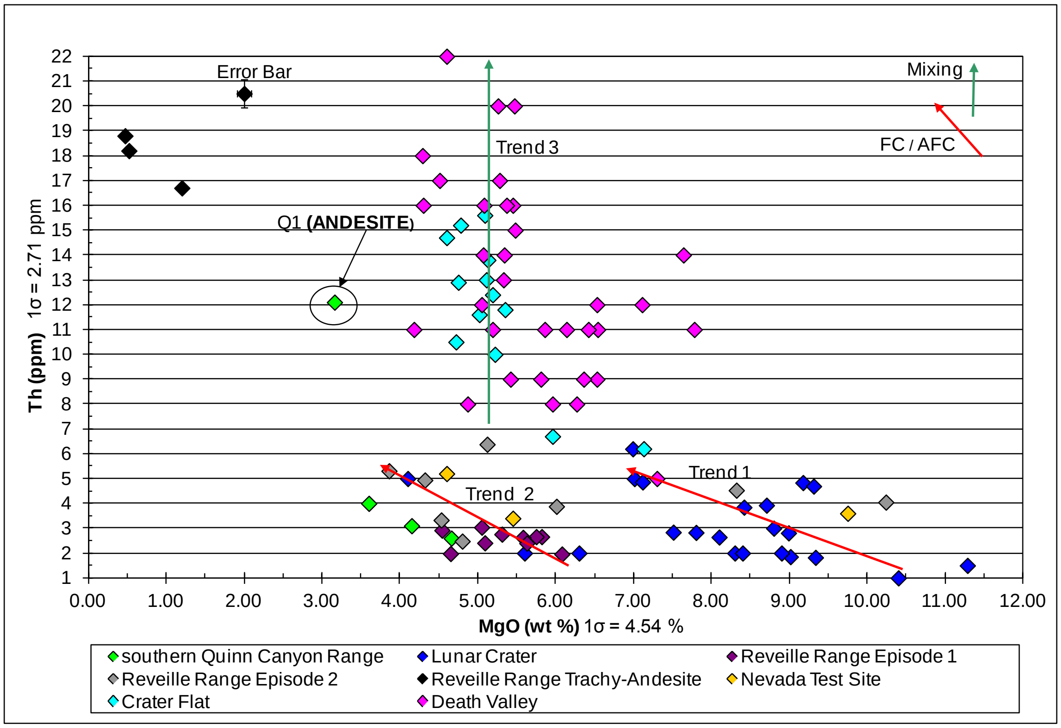

Figure 21: Element variation diagram showing that SQCR basalt is similar to Reveille Range Episode 1& 2.

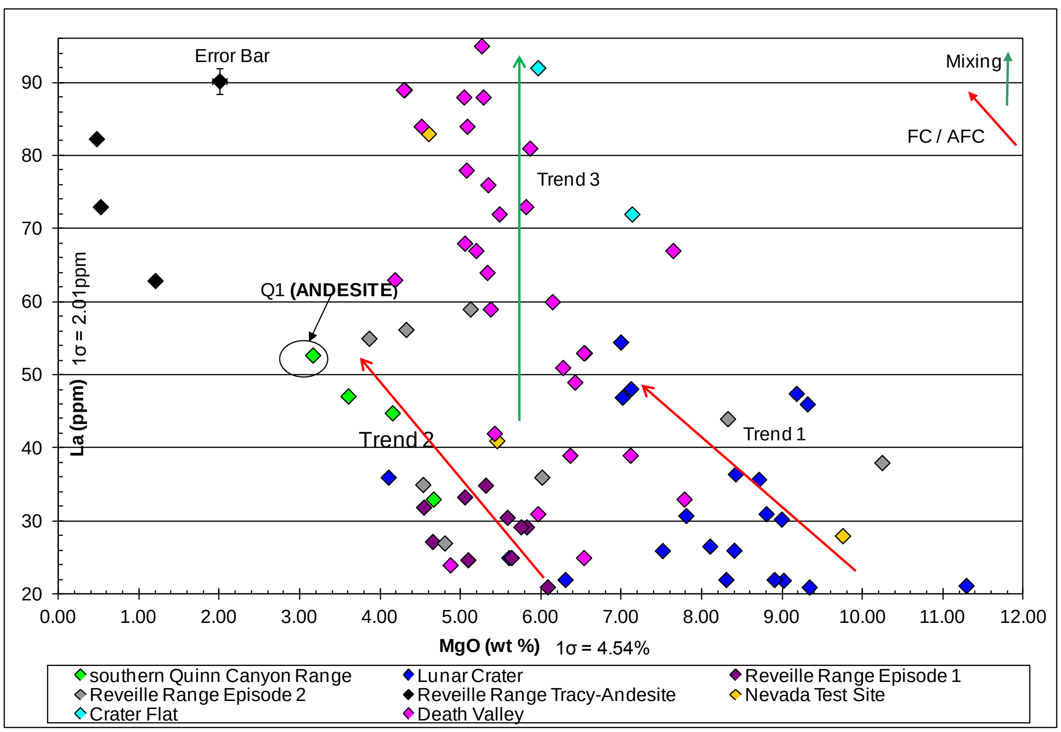

Figure 22: Element variation diagram showing SQCR basalt is similar to Reveille Range Episode 1& 2.

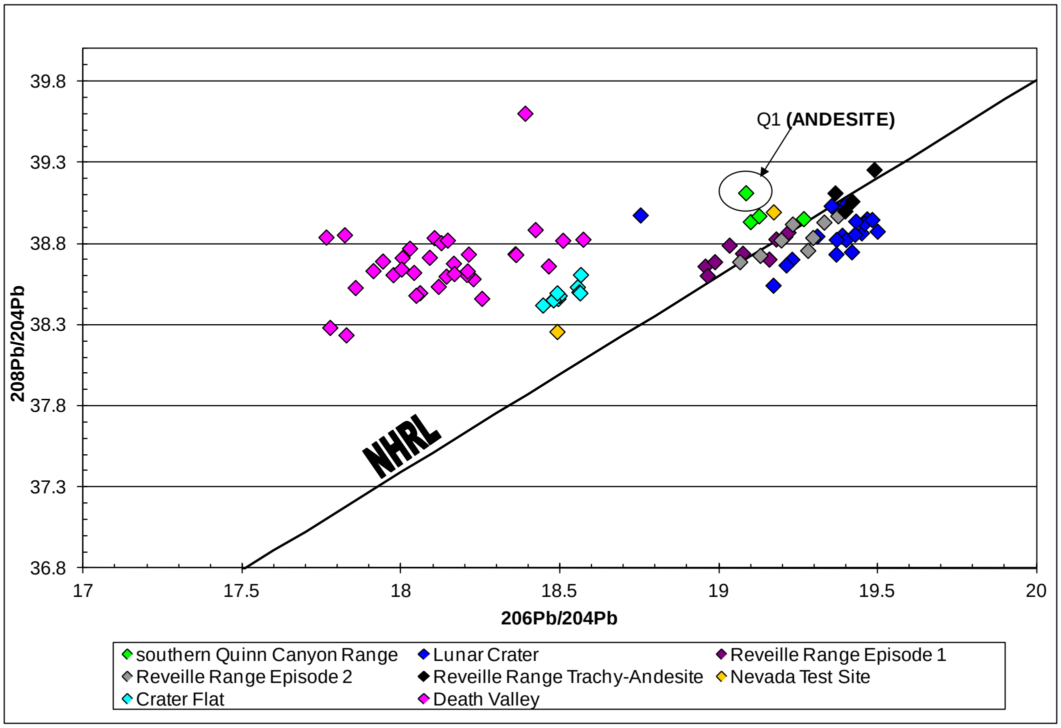

Figure 23: SQCR basalt plots just above the Northern Hemisphere Reference Line (NHRL) on a Pb isotope diagram.

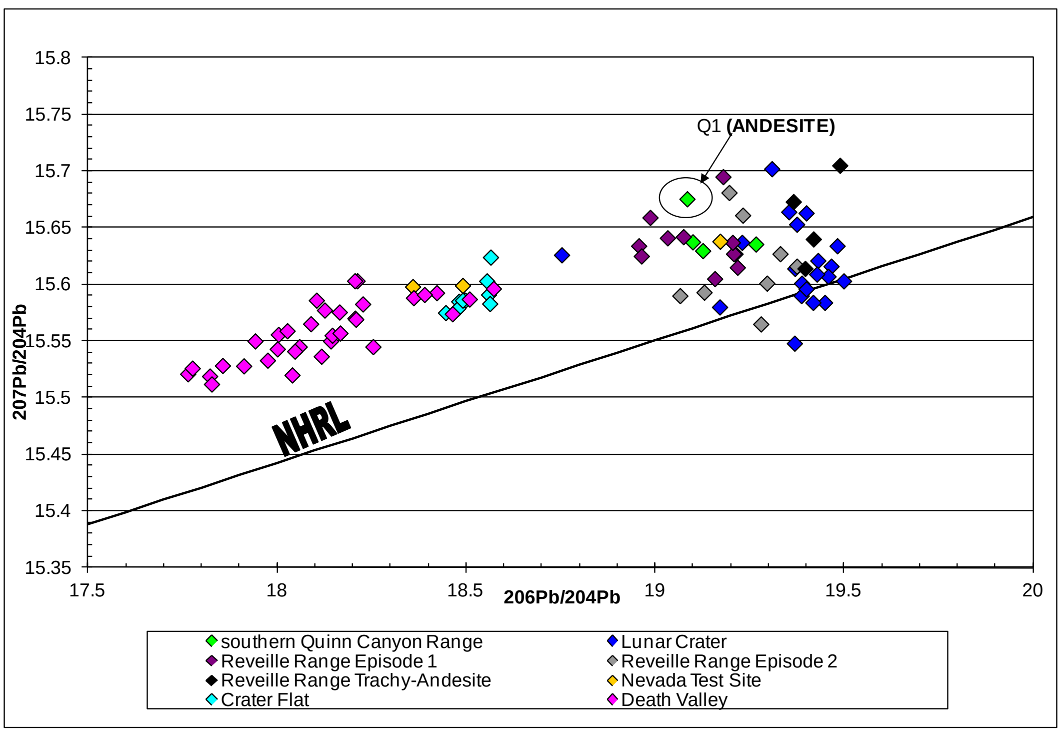

Figure 24: SQCR basalt plots just above the Northern Hemisphere Reference Line on a Pb isotope diagram.

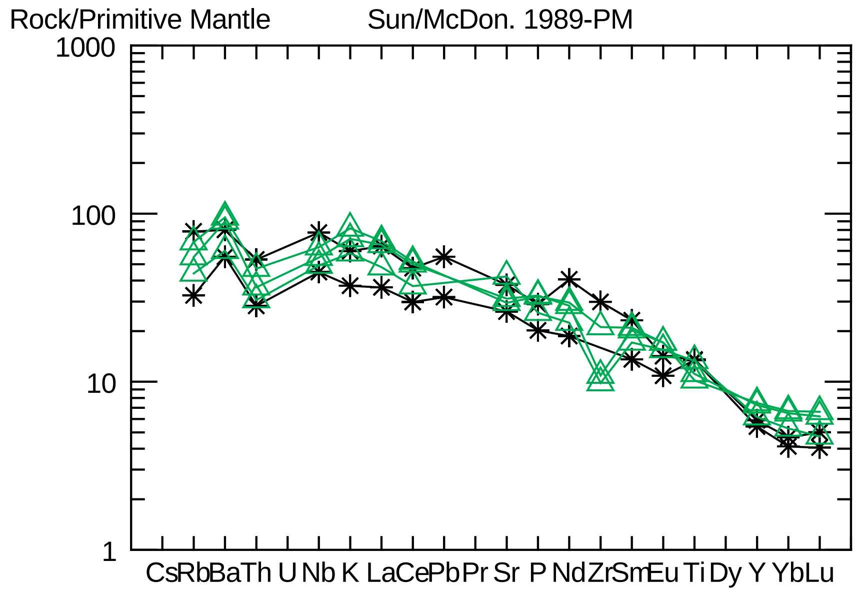

Figure 25: SQCR basalts (green triangle) compared Reveille Range Episode 1 & 2 basalts (black asterisk).

CHAPTER 8

DEPTH OF MELTING

Estimating pressures and temperatures of melting and inferring depth of melting is important for assessing the role of mantle in the generation of basaltic magma. Depth of melting calculations for two SQCR basalts collected along the western side of the Range were performed by utilizing the Lee et al. (2009) silica-liquid barometer. Only two basalt samples were analyzed due to the requirement that major element analyses have totals of at least 97 wt.%. The Lee et al. (2009) technique applies a silica-based barometer that is less sensitive to variations in mantle composition because it is based solely on the activity of silica. As a result, it is more reliable, and less sensitive to incompatible element variability and mantle composition in comparison to other models (Lee et al., 2009).

Depth of melting and temperatures calculated using the silica-activity barometer are listed in Table 4. Although Lee uses 37 km/GPa in his depth calculations, Table 4 shows a range of km/GPa for comparison based on rock density at different depths. Accordingly, basalt sample Q2 was generated at a temperature of 1449 ˚C at 2.50 GPa, and Q91 formed at a temperature of 1469 ˚C at 2.66 GPa, which corresponds to depths of 98.40 km and 92.39 km (using 37 km/GPa). Table 4 also shows calculated uncertainties for both samples based on a +/- 0.20 GPa uncertainty for the barometer and a +/- 3% uncertainty for temperature.

Wernicke and Spencer (1999) indicate that basalts in the Great Basin are generated at temperatures of 1350-1450 ˚C and pressures between 2-3 GPa (60-90km). These results are consistent with the depths and temperatures calculated by Wang et al.

(2002) in their survey of mantle temperatures and melting depths across the Great Basin. Shallow P-S conversion results in the same region by Li et al. (2007) give melting depths of 60-80 km. From these and other results, Lee et al. (2009), calculates a lithospheric thickness in the western Basin and Range of ~ 70km, which is thin compared to the estimate of 120-150 km for the Colorado Plateau (West et al., 2007).

Temperatures calculated for SQCR samples may be higher due to the presence of plagioclase and clinopyroxene, as discussed earlier in the chapter, but depth of melting indicates an asthenospheric melt source. When plotted on a P-T diagram (Figure 26) with the range of lithosphere-asthenosphere boundary (LAB) depths depicted for the Basin and Range (Lee et al., 2009), SQCR sample Q2 with a minimum depth of 74.40 km and Q91 with a minimum depth of 79.20 km (Table 4) was produced in the uppermost asthenosphere.

An orthopyroxene-liquid barometer from Putirka (2008) was used as a comparison to results from the Lee et al., (2009) barometer. The Putirka (2008) opx-barometer is calibrated for basalts with SiO_2 contents as low as 35 wt.%, will work for basalt with olivine and both cpx and opx, and is independent of source composition (as long as pyroxene and olivine are in equilibrium with the source at the time of melting). Using cpx + olivine results in almost no increased error relative to ol + opx (Putirka, written communication, 2011). The major drawback of the Putirka (2008) model is that it is much more dependent on the MgO content compared to Lee et al. (2009). The low MgO wt.% values in the SQCR samples indicate that the samples are evolved because primitive MgO wt.% values are usually greater than 8 wt.%. Thus, the Putirka barometer provides shallower depths of melting at 45.14 km (Q2) and 47.73 km (Q91) with temperatures of 1449 ˚C (Q2) and 1145 ˚C (Q91). These depths should be regarded as a minimum value and are perhaps recording a part of the magma ascent history in the lithosphere.

Calculated depths of melting are plotted on an ambient noise tomographic profile from Death Valley to Lunar Crater (Yang, personal communication, 2010) (Figure 27). This diagram illustrates the seismically slow (either hot or wet) area in which the SQCR basalts originated from within the asthenosphere. This seismically slow area is considered by Conrad et al., (2010) to represent an area of the mantle where shear-driven upwelling and partial melting could occur.

Table 4: SQCR basaltic samples depth to melting and temperature results based on Lee et al., (2009).

Model Lee et al. (2009)	*Sample*			
	Q91	**Q91 Uncertainty**	**Q2**	**Q2 Uncertainty**
Temperature (°C)	1468.50	1424.44-1512.56	1449.33	1405.85-1492.81
Pressure (GPa)	2.66	2.64-2.68	2.50	2.48-2.52
Depth (km) using (37km/GPa)	98.40	97.68-99.16	92.39	91.76-93.24
Depth (km) using (33km/GPa)	87.77	87.12-88.44	82.40	81.84-83.16
Depth (km) using (30km/GPa)	79.79	79.20-80.40	74.91	74.40-75.60

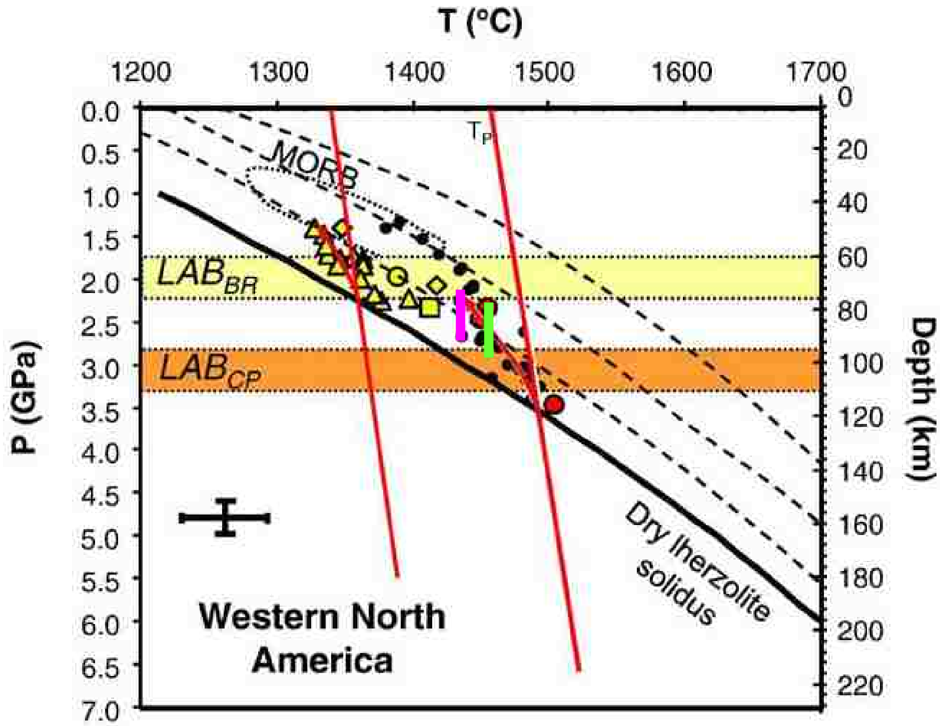

Figure 26: Graph taken from Lee et al., (2009) with SQCR basaltic samples plotted in pink and green. Basaltic samples include: Q2 (pink), Q91 (green), western Basin and Range (yellow), Rio Grange Rift (black dots), Colorado Plateau (red dots). Showing SQCR samples plotting below the lithosphere-asthenosphere boundary.

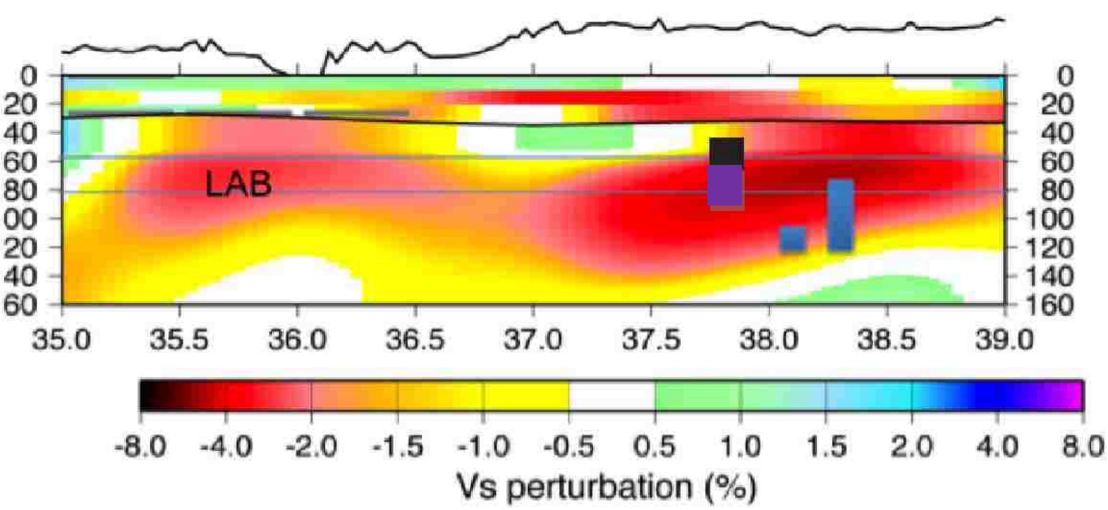

Figure 27: Ambient noise tomographic profile with red patterns indicating seismically slow (either hot or wet) areas, and colder colors are seismically fast. Boxes indicate depths of melting calculated using Putirka (2008) for SQCR (black box) and Lunar Crater (blue boxes). Lee et al., (2009) depths of melting for the SQCR are represented by the purple box. X-axis represents latitude values, Y-axis represents depth (km), LAB represents lithosphere-asthenosphere boundary.

CHAPTER 9

CONCLUSIONS

The SQCR contains three major ash-flow tuff units: the Pahranagat Tuff, Clifford Spring Tuff, and the Cow Canyon Tuff (Chapter 6). These tuffs were identified by utilizing U/Pb and ^{40}Ar/^{39}Ar geochronology, geochemical correlation, and field mapping, thus, showing that the ash-flow units identified in this study represent eruptive products from the Kawich Range and not the Reveille Range calderas or the Shingle Pass Tuff.

Pb, Nd, and Sr isotopic analysis suggests that the SQCR lies within the Death Valley-Pancake Range Basalt Zone and is similar to basalts from the Reveille Range. Further comparison of geochemical data from samples within the Death Valley-Pancake Range Basalt Zone show isotopic difference between the northern and southern end of the Death Valley-Pancake Range Basalt Zone with the northern end having an asthenospheric derived signature (Chapter 7). Depth to melting calculations performed by using a silica based barometer developed by Lee et al. (2009) on two basalt samples from the western part of the SQCR yield an asthenospheric melt source, which confirms the isotopic and geochemical analyses made (Chapter 8).

APPENDIX A

SIMS U/Pb Zircon Analysis Results

Sample	Grain	Age (Ma) 206Pb/ 238U	Age (Ma) 206Pb/ 238U 1 s.e.	Age (Ma) 207Pb/ 235U	Age (Ma) 207Pb/ 235U 1 s.e.	Age (Ma) 207Pb/ 206Pb	Age (Ma) 207Pb/ 206Pb 1 s.e.	U O/ U	Common 206Pb/ 204Pb	Common 207Pb/ 204Pb	Common 208Pb/ 204Pb	Pb corr.
Q13	9	26.25	1.06	33.46	2.16	587.4	115	8.33	18.86	15.62	38.34	(None)
Q13	2	22.70	0.607	45.04	2.38	1493	92.2	8.55	18.86	15.62	38.34	(None)
Q13	3	26.40	0.788	37.7	2.23	833.2	103	8.11	18.86	15.62	38.34	(None)
Q13	14	25.65	0.657	29.61	1.82	364	109	8.57	18.86	15.62	38.34	(None)
Q13	19	24.03	0.63	29.47	2.04	498.8	147	8.4	18.86	15.62	38.34	(None)
Q13	18	22.26	0.594	24.66	1.73	265.5	136	8.58	18.86	15.62	38.34	(None)
Q13	19	24.03	0.63	29.47	2.04	498.8	147	8.4	18.86	15.62	38.34	(None)
Q13	14	22.68	0.622	31.61	1.61	776.2	84.8	8.33	18.86	15.62	38.34	(None)
Q13	13	24.55	0.631	29.47	1.45	451.3	93.3	8.36	18.86	15.62	38.34	(None)
Q13	11	24.03	0.784	40	3.11	1148	134	8.05	18.86	15.62	38.34	(None)
Q13	8	24.09	0.652	26.92	1.22	287.2	77.1	8.37	18.86	15.62	38.34	(None)
Q18	1	22.12	0.903	94.56	9.53	2514	92.6	7.39	18.86	15.62	38.34	(None)
Q18	2	24.05	1.19	71.85	9.01	2120	200	7.72	18.86	15.62	38.34	(None)
Q18	3	24.2	0.916	70.81	11	2142	212	8.06	18.86	15.62	38.34	(None)
Q18	4	25.28	1.72	43.4	3.98	855.8	148	7.95	18.86	15.62	38.34	(None)
Q18	5	25.98	1.78	27.41	1.29	519.8	64.9	8	18.86	15.62	38.34	(None)
Q18	6	27.49	1.81	59.92	4.27	1914	125	8.12	18.86	15.62	38.34	(None)
Q18	7	30.14	1.27	45.27	4.72	1392	181	7.96	18.86	15.62	38.34	(None)
Q23	1	26.18	1.4	90.54	16.3	2520.00	265	7.91	18.86	15.62	38.34	(None)
Q23	4	25.65	1.61	92.7	11	2595.00	231	8.15	18.86	15.62	38.34	(None)
Q23	5	24.21	0.794	36.1	3.79	921.10	216	8.17	18.86	15.62	38.34	(None)
Q23	6	36.58	1.64	134.7	8.3	2660.00	58.8	7.93	18.86	15.62	38.34	(None)
Q23	12	28.06	0.934	121.6	8.7	2917.00	92.4	8.08	18.86	15.62	38.34	(None)
Q23	13	22.56	0.844	35.54	3.61	1033.00	185	8.27	18.86	15.62	38.34	(None)
Q23	13	23.31	0.814	37.95	2.67	1102.00	130	8.24	18.86	15.62	38.34	(None)
Q23	14	28.37	0.851	31.5	1.49	277.30	77.8	8.06	18.86	15.62	38.34	(None)
Q23	15	25.77	0.96	53.65	4.44	1591.00	126	8.4	18.86	15.62	38.34	(None)
Q23	17	26.29	1.05	52.31	3.65	1505.00	121	8.13	18.86	15.62	38.34	(None)
Q23	20	29.03	0.987	43.94	3.6	959.10	141	8.17	18.86	15.62	38.34	(None)
Q23	21	24.36	1.1	72.53	9.71	2250.00	215	8.61	18.86	15.62	38.34	(None)
Q23	23	24.52	0.794	32.79	2.5	690.50	158	8.2	18.86	15.62	38.34	(None)
Q24	2	28.8	1.62	53.96	4.58	1391	131	7.52	18.86	15.62	38.34	(None)
Q24	3	29.61	1.2	41.71	3.88	808	177	7.8	18.86	15.62	38.34	(None)
Q24	4	24.73	0.95	27.13	1.86	244.8	119	8.04	18.86	15.62	38.34	(None)
Q24	6	27.73	1.35	81.89	9.39	2243	143	7.97	18.86	15.62	38.34	(None)
Q24	8	27.38	1.2	38.31	2.63	791	110	7.93	18.86	15.62	38.34	(None)
Q24	10	25.28	1.05	34.59	3.06	741	145	8.13	18.86	15.62	38.34	(None)
Q24	9	28.27	1.65	63.05	7.7	1727	187	7.57	18.86	15.62	38.34	(None)
Q24	12	27.36	1.18	58.59	7.15	1648	210	8.21	18.86	15.62	38.34	(None)
Q24	17	25.63	0.94	38.62	4.52	944.9	249	8.12	18.86	15.62	38.34	(None)
Q24	19	27.37	0.967	47.35	3.49	1230	114	7.97	18.86	15.62	38.34	(None)
Q24	20	35.96	1.51	225.7	12.2	3583	64.1	8.82	18.86	15.62	38.34	(None)
Q24	21	28.43	1.54	57.45	6.36	1538	162	8.1	18.86	15.62	38.34	(None)
Q24	26	26.96	1.22	42.58	4.31	1044	153	8.12	18.86	15.62	38.34	(None)
Q24	26	25.36	0.907	33.35	2.69	654.4	153	7.96	18.86	15.62	38.34	(None)
Q61	1	23.19	0.828	26.96	1.73	377.7	128	8.04	18.86	15.62	38.34	(None)
Q61	2	26.01	1.06	31.84	2.42	496.7	151	7.59	18.86	15.62	38.34	(None)
Q61	3	26.06	0.848	31.36	1.76	459.1	101	8.08	18.86	15.62	38.34	(None)
Q61	4	25.97	0.787	28.7	1.1	263.6	54.9	8.39	18.86	15.62	38.34	(None)

Q13

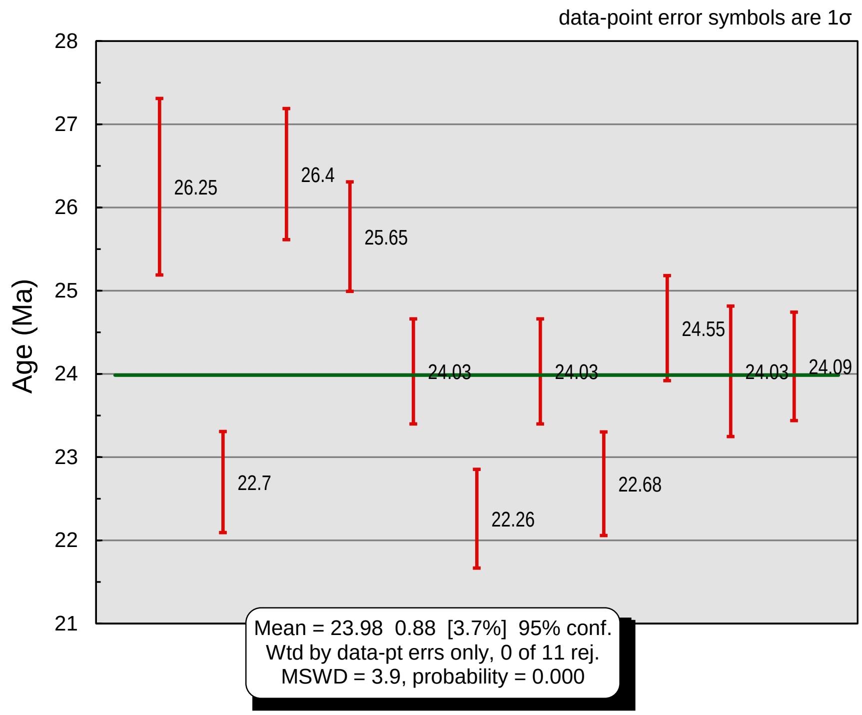
data-point error symbols are 1σ
Age (Ma)
28
27
26
25
24
23
22
21
26.25
22.7
26.4
25.65
24.03
22.26
24.03
22.68
24.55
24.03
24.09
Mean = 23.98 0.88 [3.7%] 95% conf.
Wtd by data-pt errs only, 0 of 11 rej.
MSWD = 3.9, probability = 0.000

Q18

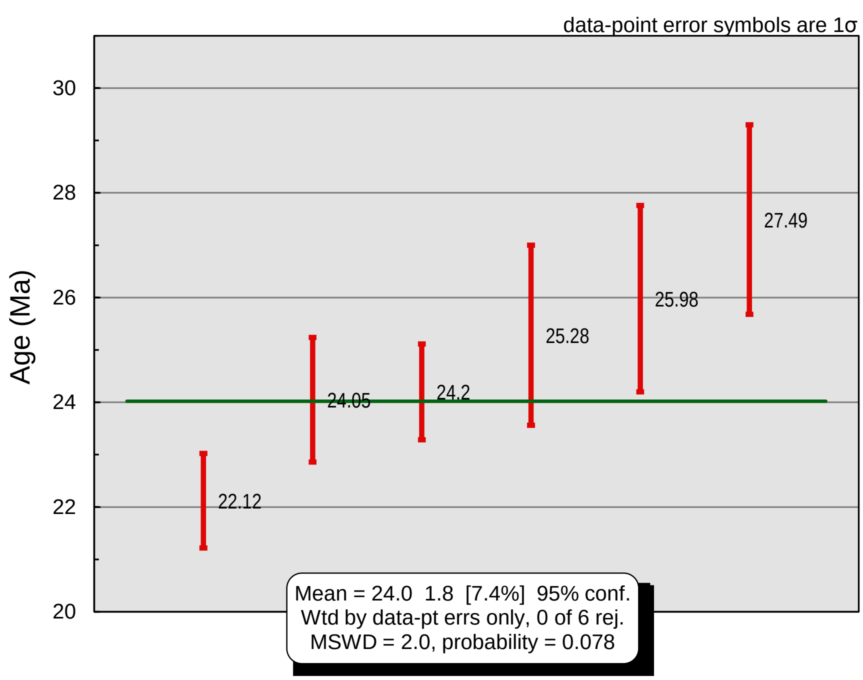
data-point error symbols are 1σ
Age (Ma)
30
28
26
24
22
20
22.12
24.05
24.2
25.28
25.98
27.49
Mean = 24.0 1.8 [7.4%] 95% conf.
Wtd by data-pt errs only, 0 of 6 rej.
MSWD = 2.0, probability = 0.078

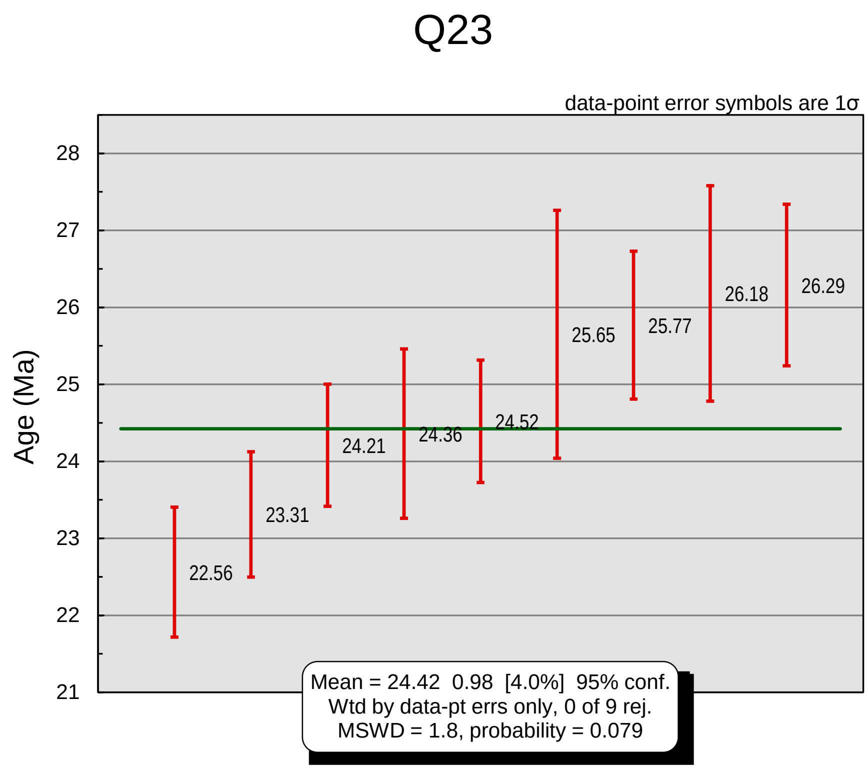
Q23
data-point error symbols are 1σ
Age (Ma)
28
27
26
25
24
23
22
21
22.56
23.31
24.21
24.36
24.52
25.65
25.77
26.18
26.29
Mean = 24.42 0.98 [4.0%] 95% conf.
Wtd by data-pt errs only, 0 of 9 rej.
MSWD = 1.8, probability = 0.079

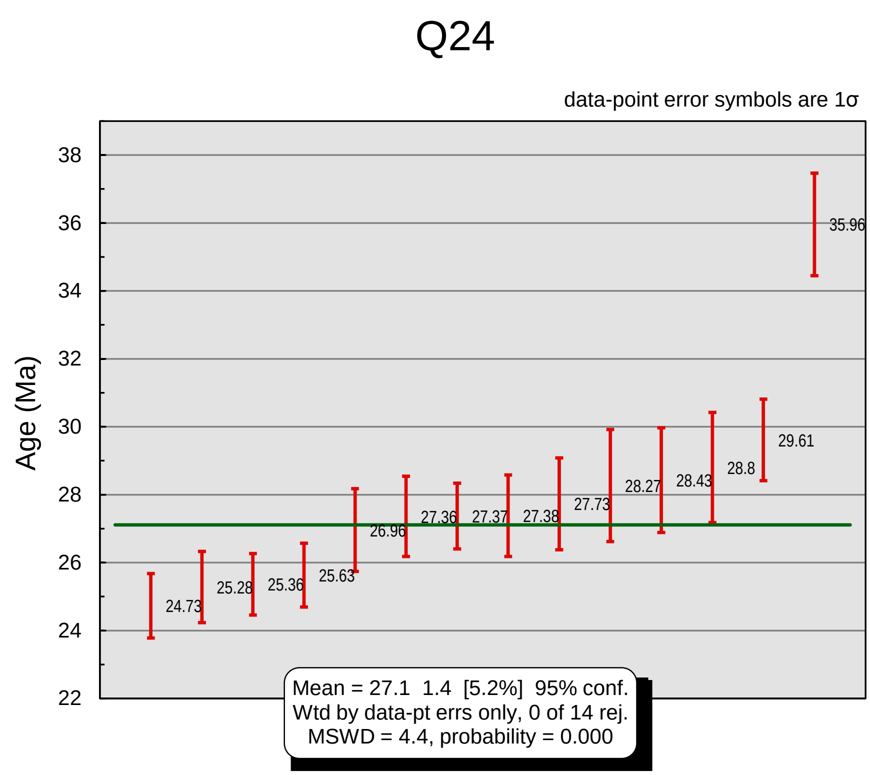
Q24
data-point error symbols are 1σ
Age (Ma)
38
36
34
32
30
28
26
24
22
24.73
25.28
25.36
25.63
26.96
27.36
27.37
27.38
27.73
28.27
28.43
28.8
29.61
35.96
Mean = 27.1 1.4 [5.2%] 95% conf.
Wtd by data-pt errs only, 0 of 14 rej.
MSWD = 4.4, probability = 0.000

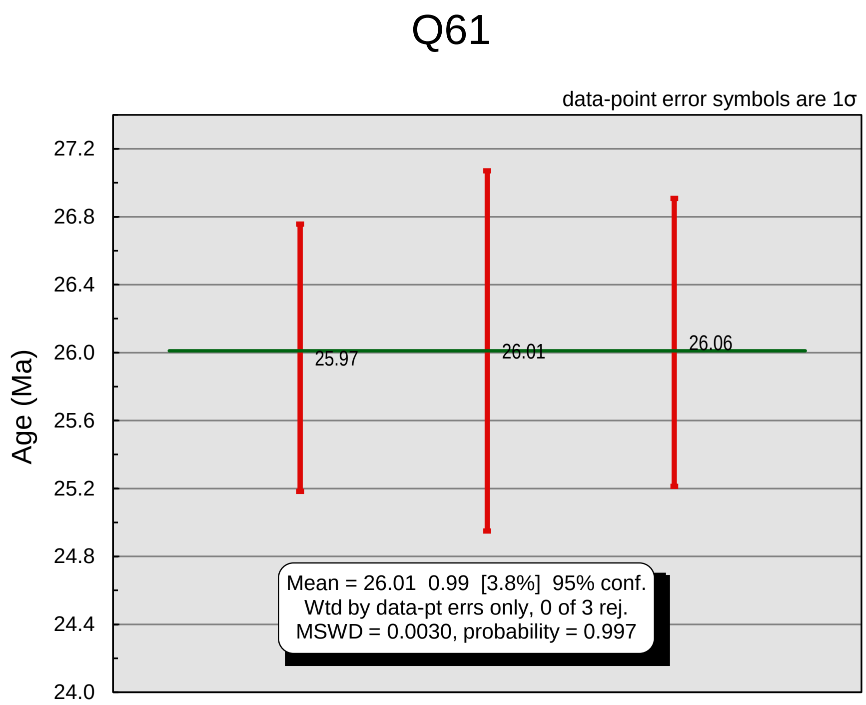
Q61
data-point error symbols are 1σ
Age (Ma)
27.2
26.8
26.4
26.0
25.6
25.2
24.8
24.4
24.0
25.97
26.01
26.06
Mean = 26.01 0.99 [3.8%] 95% conf.
Wtd by data-pt errs only, 0 of 3 rej.
MSWD = 0.0030, probability = 0.997

APPENDIX B

^{40}Ar/^{39}Ar Sanidine Analysis Results

Summary Table

Sample	Lab ID#	Material	Irrad.	J (∞ 10^{-3}) ± 1σ		Age (Ma) ±1s		(with ±*J*) ±1s	MSWD	Prob.	n/n_{total}
Q9	25295	sanidine	UNLV653	1.647	0.005	23.01	0.04	0.08	1.38	0.24	6/6
Q13	25296	sanidine	UNLV653	1.636	0.005	23.72	0.03	0.08	0.30	0.98	11/11
Q18	25298	sanidine	UNLV653	1.603	0.005	22.88	0.02	0.07	0.58	0.81	10/10
Q23	25299	sanidine	UNLV653	1.587	0.005	22.924	0.019	0.07	1.08	0.37	12/12
Q38	25302	sanidine	UNLV654	1.703	0.005	20.09	0.03	0.07	1.99	0.05	8/8
Q50	25303	sanidine	UNLV654	1.699	0.005	22.938	0.019	0.07	0.44	0.94	12/12
Q59	25305	sanidine	UNLV654	1.684	0.005	23.03	0.03	0.07	2.21	0.03	8/8
Q61	25306	sanidine	UNLV654	1.676	0.005	23.77	0.03	0.08	0.49	0.81	7/7
Q24	25317	sanidine	UNLV655	1.588	0.008	22.95	0.03	0.12	0.66	0.65	6/6

Detailed Analysis Data

Lab ID#	Relative Isotopic Abundances									
	^{40}Ar	±1σ	^{39}Ar	±1σ	^{38}Ar	±1σ	^{37}Ar	±1σ	^{36}Ar	±1σ
Q9										
25295-04	517.6	0.9	65.90	0.13	0.76	0.02		12	0.0211	0.0018
25295-06	269.5	0.5	34.36	0.10	0.342	0.018		12	0.0050	0.0015
25295-08	628.8	0.7	79.64	0.16	0.82	0.02		12	0.032	0.002
25295-10	114.6	0.2	14.44	0.04	0.154	0.008		12	0.0032	0.0014
25295-12	388.3	0.7	49.72	0.12	0.44	0.02		12	0.0083	0.0017
Q13										
25296-01	230.6	0.5	28.59	0.09	0.271	0.011		12	0.0003	0.0014
25296-03	386.0	0.7	47.48	0.12	0.477	0.018		12	0.0067	0.0017
25296-04	275.6	0.5	33.67	0.10	0.372	0.013		12	0.0090	0.0018
25296-05	73.2	0.2	8.94	0.04	0.097	0.013	1	13	0.0006	0.0015
25296-06	476.6	0.7	58.70	0.13	0.54	0.02		12	0.0082	0.0018
25296-08	94.66	0.18	11.45	0.04	0.099	0.007		12	0.0062	0.0015
25296-10	346.5	0.7	42.86	0.12	0.429	0.013	2	12	0.0013	0.0014
25296-11	702.2	0.8	86.06	0.15	0.92	0.04		12	0.0243	0.0018
25296-12	549.4	0.8	67.51	0.16	0.760	0.018		12	0.0120	0.0017
25296-13	233.7	0.4	28.59	0.10	0.312	0.010		12	0.0076	0.0014
25296-14	3861	3	471.0	0.5	4.09	0.16		12	0.140	0.005
Q18										
25298-01	5382	2	670.3	0.7	7.32	0.17		12	0.143	0.005
25298-02	5858	4	732.5	0.7	8.6	0.2		12	0.096	0.005
25298-03	3341	2	414.0	0.5	4.91	0.06		12	0.156	0.004
25298-04	3820	2	475.5	0.6	4.92	0.18		12	0.093	0.004
25298-05	3594	3	448.5	0.5	4.99	0.09		12	0.055	0.004
25298-06	5059	4	632.6	0.7	7.30	0.14		12	0.096	0.004
25298-07	5059	4	633.0	0.7	5.6	0.2		13	0.056	0.005
25298-08	7360	6	916.9	0.8	10.15	0.19		12	0.126	0.006
25298-09	5920	4	736.5	0.7	9.26	0.09		12	0.121	0.005
25298-12	5160	4	645.5	0.7	7.34	0.14		12	0.136	0.006

Lab ID#	Relative Isotopic Abundances									
	^{40}Ar ±1σ		^{39}Ar ±1σ		^{38}Ar ±1σ		^{37}Ar ±1σ		^{36}Ar ±1σ	
Q23										
25299-01	6805	4	835.6	0.9	9.93	0.09		12	0.154	0.006
25299-02	5677	4	693.0	0.7	6.3	0.2		12	0.342	0.006
25299-03	6373	4	782.8	0.7	8.28	0.13	3	12	0.116	0.005
25299-04	4688	3	575.1	0.7	6.11	0.19		13	0.174	0.005
25299-05	5967	5	719.1	0.7	6.52	0.19		12	0.543	0.008
25299-06	4788	2	592.1	0.6	5.65	0.18	2	12	0.082	0.004
25299-07	2746	2	338.8	0.5	3.37	0.10		12	0.096	0.004
25299-08	7495	5	923.9	0.8	10.22	0.18	4	13	0.096	0.006
25299-09	5444	4	671.1	0.8	8.17	0.14		12	0.152	0.006
25299-10	4576	3	566.2	0.7	4.54	0.15	5	12	0.097	0.005
25299-11	3344	2	413.1	0.6	4.58	0.10		12	0.072	0.004
25299-13	4519	3	550.2	0.6	6.48	0.11		12	0.293	0.005
Q38										
25302-02	588.7	0.9	87.13	0.16	0.88	0.04		12	0.052	0.002
25302-03	305.4	0.5	45.43	0.09	0.473	0.017		12	0.0194	0.0019
25302-04	223.8	0.5	33.38	0.12	0.366	0.011		12	0.0166	0.0018
25302-06	615.3	0.8	90.82	0.19	0.94	0.03		13	0.054	0.003
25302-07	309.8	0.6	46.06	0.11	0.42	0.02	5	12	0.0229	0.0017
25302-09	399.4	0.5	60.30	0.13	0.62	0.02		12	0.0157	0.0017
25302-11	173.9	0.3	25.99	0.09	0.272	0.015		13	0.0175	0.0016
25302-13	317.6	0.6	47.51	0.12	0.504	0.018		12	0.0063	0.0017
Q50										
25303-01	7028	6	918.5	0.8	7.99	0.10	3	13	0.277	0.006
25303-02	7445	5	982.1	0.9	7.1	0.3	21	13	0.141	0.006
25303-03	3751	2	494.2	0.6	5.68	0.06		12	0.082	0.004
25303-04	4008	2	529.0	0.5	5.76	0.11		12	0.088	0.004
25303-05	4647	4	614.1	0.7	5.12	0.17	14	12	0.097	0.005
25303-06	4466	3	589.7	0.6	6.4	0.3		13	0.120	0.005
25303-08	6958	5	911.4	0.8	9.8	0.2		13	0.279	0.006
25303-09	2764.8	1.9	362.3	0.6	4.11	0.09		12	0.135	0.004
25303-10	5455	4	715.5	0.7	6.0	0.3	8	13	0.257	0.005
25303-11	3862	3	506.8	0.6	5.0	0.2		13	0.161	0.004
25303-12	2673	2	350.9	0.5	3.18	0.12	7	13	0.082	0.004
25303-13	5915	4	781.6	0.7	9.05	0.10		12	0.091	0.006

Lab ID#	Relative Isotopic Abundances									
	^{40}Ar ±1σ		^{39}Ar ±1σ		^{38}Ar ±1σ		^{37}Ar ±1σ		^{36}Ar ±1σ	
Q59										
25305-02	557.8	0.8	71.74	0.13	0.58	0.03	4	12	0.037	0.002
25305-03	349.4	0.7	45.51	0.12	0.49	0.02		13	0.0000	0.0018
25305-05	612.5	0.8	79.70	0.15	0.68	0.03		13	0.033	0.002
25305-06	711.9	1.0	92.0	0.2	1.09	0.03		12	0.021	0.002
25305-07	490.6	0.8	63.51	0.14	0.559	0.016		12	0.0149	0.0019
25305-08	398.4	0.7	51.95	0.13	0.58	0.03		12	0.0147	0.0019
25305-12	758.3	1.0	96.15	0.16	0.89	0.04		13	0.074	0.003
25305-13	873.6	0.9	114.13	0.19	1.20	0.02		13	0.019	0.002
Q61										
25306-02	716.4	0.9	89.13	0.18	0.969	0.018		13	0.043	0.002
25306-03	1147.7	1.0	143.72	0.17	1.69	0.04		13	0.033	0.002
25306-04	785.8	0.9	98.85	0.15	0.96	0.03		13	0.016	0.002
25306-07	902.1	1.0	112.53	0.19	1.34	0.04		12	0.044	0.002
25306-08	341.6	0.6	42.47	0.11	0.506	0.015		13	0.0119	0.0018
25306-09	486.7	0.8	61.29	0.12	0.68	0.02		13	0.0067	0.0019
25306-11	1002.6	1.0	124.8	0.2	1.45	0.05		13	0.048	0.003
Q24										
25317-01	406.6	0.8	50.24	0.15	0.54	0.02		13	0.0100	0.0019
25317-03	824.8	0.8	101.4	0.2	0.99	0.04		13	0.014	0.002
25317-04	628.0	0.8	77.07	0.15	0.854	0.020		13	0.021	0.002
25317-05	376.6	0.6	45.95	0.12	0.449	0.013		13	0.0220	0.0018
25317-06	591.7	0.8	73.40	0.16	0.81	0.02		13	0.0057	0.0017
25317-11	872.5	1.0	105.89	0.16	1.13	0.05		13	0.056	0.002

Lab ID#	Derived Results							Inverse Isochron Data				
	^{39}Ar Mol ∞ 10^{-14}	Ca/K ±1σ		$\%^{40}Ar^{*}$	Age (Ma) ±1σ		w/±*J* ±1σ	$^{36}Ar/^{40}Ar$ ±%1σ		$^{39}Ar/^{40}Ar$ ±%1σ		$^{36}Ar/^{39}Ar$ Er. Corr.
	Q9											
25295-04	0.88	0	0	98.8	22.91	0.09	0.11	0.00004	8.41	0.12733	0.37	0.0970
25295-06	0.46	0	0	99.4	23.03	0.10	0.12	0.00002	30.51	0.12749	0.41	0.0264
25295-08	1.06	0	0	98.5	22.96	0.08	0.11	0.00005	6.89	0.12667	0.34	0.1169
25295-10	0.19	0	0	99.2	23.24	0.13	0.15	0.00003	43.56	0.12600	0.45	0.0184
25295-12	0.66	0	0	99.4	22.91	0.09	0.12	0.00002	20.77	0.12804	0.39	0.0390
	Q13											
25296-01	0.38	0	0	100.0	23.63	0.12	0.14	0.00000	397.98	0.12397	0.47	0.0020
25296-03	0.63	0	0	99.5	23.71	0.10	0.12	0.00002	25.27	0.12300	0.40	0.0321
25296-04	0.45	0	0	99.0	23.76	0.11	0.13	0.00003	19.84	0.12218	0.42	0.0407
25296-05	0.12	0	0	99.8	23.9	0.2	0.22	0.00001	261.10	0.12222	0.60	0.0031
25296-06	0.78	0	0	99.5	23.67	0.09	0.12	0.00002	21.93	0.12317	0.37	0.0369
25296-08	0.15	0	0	98.1	23.76	0.16	0.17	0.00007	24.33	0.12098	0.46	0.0330
25296-10	0.57	0	0	99.9	23.67	0.10	0.13	0.00000	100.67	0.12369	0.42	0.0080
25296-11	1.14	0	0	99.0	23.67	0.08	0.11	0.00003	7.46	0.12256	0.32	0.1083
25296-12	0.90	0	0	99.4	23.70	0.09	0.12	0.00002	14.29	0.12289	0.38	0.0565
25296-13	0.38	0	0	99.0	23.73	0.12	0.14	0.00003	18.20	0.12235	0.46	0.0438
25296-14	6.26	0	0	98.9	23.77	0.07	0.10	0.00004	3.72	0.12198	0.29	0.2176
	Q18											
25298-01	8.91	0	0	99.2	22.88	0.06	0.10	0.00003	3.51	0.12454	0.27	0.2296
25298-02	9.74	0	0	99.5	22.86	0.06	0.10	0.00002	5.06	0.12506	0.28	0.1599
25298-03	5.50	0	0	98.6	22.86	0.07	0.10	0.00005	2.91	0.12393	0.29	0.2775
25298-04	6.32	0	0	99.3	22.91	0.07	0.10	0.00002	4.75	0.12450	0.29	0.1700
25298-05	5.96	0	0	99.5	22.91	0.07	0.10	0.00002	7.02	0.12480	0.29	0.1152
25298-06	8.41	0	0	99.4	22.84	0.07	0.10	0.00002	4.63	0.12506	0.29	0.1748
25298-07	8.42	0	0	99.7	22.88	0.06	0.10	0.00001	9.17	0.12513	0.28	0.0882
25298-08	12.19	0	0	99.5	22.94	0.06	0.10	0.00002	5.24	0.12458	0.28	0.1546
25298-09	9.79	0	0	99.4	22.95	0.06	0.10	0.00002	4.47	0.12441	0.28	0.1808
25298-12	8.58	0	0	99.2	22.78	0.07	0.10	0.00003	4.48	0.12510	0.28	0.1807

Lab ID#	^{39}Ar Mol ∞ 10^{-14}	Ca/K	±1σ	%^{40}Ar*	Age (Ma)	±1σ	w/±*J* ±1σ	^{36}Ar/^{40}Ar	±%1σ	^{39}Ar/^{40}Ar	±%1σ	^{36}Ar/^{39}Ar Er. Corr.
	Derived Results							**Inverse Isochron Data**				
	Q23											
25299-01	11.11	0	0	99.3	23.01	0.06	0.10	0.00002	4.23	0.12280	0.28	0.1910
25299-02	9.22	0	0	98.2	22.89	0.07	0.10	0.00006	2.10	0.12208	0.28	0.3839
25299-03	10.41	0	0	99.5	23.04	0.06	0.10	0.00002	4.55	0.12283	0.27	0.1780
25299-04	7.65	0	0	98.9	22.94	0.07	0.10	0.00004	3.12	0.12266	0.28	0.2585
25299-05	9.56	0	0	97.3	22.97	0.07	0.10	0.00009	1.71	0.12052	0.28	0.4724
25299-06	7.87	0	0	99.5	22.89	0.06	0.10	0.00002	5.23	0.12366	0.28	0.1546
25299-07	4.51	0	0	99.0	22.82	0.07	0.10	0.00004	3.98	0.12337	0.30	0.2028
25299-08	12.28	0	0	99.6	22.99	0.06	0.10	0.00001	5.97	0.12327	0.27	0.1358
25299-09	8.92	0	0	99.2	22.89	0.07	0.10	0.00003	4.43	0.12329	0.29	0.1828
25299-10	7.53	0	0	99.4	22.85	0.07	0.10	0.00002	5.22	0.12374	0.29	0.1547
25299-11	5.49	0	0	99.4	22.88	0.07	0.10	0.00002	4.91	0.12353	0.29	0.1644
25299-13	7.31	0	0	98.1	22.92	0.07	0.10	0.00006	2.03	0.12176	0.28	0.3979
	Q38											
25302-02	1.16	0	0	97.4	20.11	0.08	0.10	0.00009	4.83	0.14800	0.35	0.1685
25302-03	0.60	0	0	98.1	20.15	0.08	0.10	0.00006	9.73	0.14875	0.37	0.0838
25302-04	0.44	0	0	97.8	20.03	0.11	0.13	0.00007	10.76	0.14919	0.50	0.0750
25302-06	1.21	0	0	97.4	20.16	0.08	0.10	0.00009	5.31	0.14762	0.36	0.1525
25302-07	0.61	0	0	97.8	20.10	0.09	0.11	0.00007	7.29	0.14867	0.40	0.1119
25302-09	0.80	0	0	98.8	20.00	0.08	0.10	0.00004	11.13	0.15099	0.36	0.0727
25302-11	0.35	0	0	97.0	19.83	0.11	0.13	0.00010	9.05	0.14946	0.47	0.0878
25302-13	0.63	0	0	99.4	20.30	0.09	0.11	0.00002	26.38	0.14958	0.41	0.0309
	Q50											
25303-01	12.21	0	0	98.8	23.03	0.07	0.09	0.00004	2.41	0.13069	0.28	0.3355
25303-02	13.06	0	0	99.4	22.95	0.06	0.09	0.00002	4.04	0.13192	0.28	0.2005
25303-03	6.57	0	0	99.4	22.96	0.07	0.10	0.00002	5.29	0.13176	0.29	0.1530
25303-04	7.03	0	0	99.3	22.92	0.06	0.09	0.00002	4.50	0.13198	0.28	0.1797
25303-05	8.16	0	0	99.4	22.90	0.07	0.09	0.00002	4.93	0.13214	0.29	0.1643
25303-06	7.84	0	0	99.2	22.88	0.06	0.09	0.00003	4.10	0.13205	0.28	0.1976
25303-08	12.12	0	0	98.8	22.97	0.06	0.09	0.00004	2.32	0.13099	0.28	0.3486
25303-09	4.82	0	0	98.6	22.90	0.07	0.10	0.00005	3.33	0.13106	0.30	0.2420
25303-10	9.51	0	0	98.6	22.89	0.07	0.09	0.00005	2.23	0.13117	0.28	0.3624
25303-11	6.74	0	0	98.8	22.92	0.07	0.10	0.00004	2.83	0.13124	0.29	0.2857
25303-12	4.66	0	0	99.1	22.99	0.07	0.10	0.00003	4.83	0.13125	0.31	0.1674
25303-13	10.39	0	0	99.5	22.94	0.06	0.09	0.00002	6.25	0.13215	0.28	0.1298

Lab ID#	^{39}Ar Mol ∞ 10^{-14}	Ca/K	±1σ	%^{40}Ar*	Age (Ma)	±1σ	w/±*J* ±1σ	^{36}Ar/^{40}Ar	±%1σ	^{39}Ar/^{40}Ar	±%1σ	^{36}Ar/^{39}Ar Er. Corr.
	Derived Results							**Inverse Isochron Data**				
	Q59											
25305-02	0.95	0	0	98.0	23.00	0.09	0.11	0.00007	5.86	0.12862	0.34	0.1387
25305-03	0.61	0	0	100.0	23.18	0.10	0.12	0.00000	0.00	0.13023	0.42	0.0009
25305-05	1.06	0	0	98.4	22.82	0.08	0.11	0.00005	6.17	0.13013	0.34	0.1315
25305-06	1.22	0	0	99.1	23.15	0.09	0.11	0.00003	10.57	0.12926	0.36	0.0766
25305-07	0.84	0	0	99.1	23.11	0.09	0.11	0.00003	12.39	0.12945	0.37	0.0656
25305-08	0.69	0	0	98.9	22.90	0.10	0.12	0.00004	12.60	0.13039	0.40	0.0646
25305-12	1.28	0	0	97.1	23.12	0.08	0.11	0.00010	3.68	0.12680	0.33	0.2212
25305-13	1.52	0	0	99.3	22.96	0.08	0.10	0.00002	12.12	0.13063	0.32	0.0669
	Q61											
25306-02	1.18	0	0	98.2	23.71	0.09	0.11	0.00006	5.51	0.12442	0.35	0.1472
25306-03	1.91	0	0	99.1	23.78	0.07	0.10	0.00003	7.11	0.12522	0.29	0.1142
25306-04	1.31	0	0	99.4	23.73	0.08	0.11	0.00002	14.36	0.12579	0.32	0.0566
25306-07	1.50	0	0	98.6	23.73	0.08	0.11	0.00005	5.22	0.12473	0.32	0.1554
25306-08	0.56	0	0	99.0	23.91	0.10	0.13	0.00003	14.87	0.12431	0.40	0.0544
25306-09	0.81	0	0	99.6	23.75	0.09	0.11	0.00001	27.79	0.12594	0.36	0.0295
25306-11	1.66	0	0	98.6	23.78	0.08	0.11	0.00005	6.38	0.12450	0.32	0.1271
	Q24											
25317-01	0.67	0	0	99.3	22.87	0.10	0.16	0.00002	18.63	0.12357	0.44	0.0435
25317-03	1.35	0	0	99.5	23.04	0.08	0.14	0.00002	15.66	0.12291	0.34	0.0516
25317-04	1.02	0	0	99.0	22.97	0.08	0.14	0.00003	10.31	0.12274	0.35	0.0788
25317-05	0.61	0	0	98.3	22.93	0.10	0.15	0.00006	8.10	0.12200	0.40	0.1000
25317-06	0.98	0	0	99.7	22.88	0.08	0.14	0.00001	29.13	0.12405	0.36	0.0278
25317-11	1.41	0	0	98.1	23.01	0.08	0.14	0.00006	4.21	0.12136	0.31	0.1929

APPENDIX C

Southern Quinn Canyon Range Geochemical Data

Sample Number	SiO2 %	Al2O3 %	Fe2O3(T) %	MnO %	MgO %	CaO %	Na2O %	K2O %	TiO2 %	P2O5 %	LOI %	Total %
Q1	59.58*	16.41*	6.9*	0.11*	3.16*	6.48*	3.00*	3.00*	0.99*	0.34*	1.04*	99.96*
Q2	47.87	15.54	11.85	0.166	4.15	6.98	4.03	2.13	2.415	0.71	0.85	96.69
Q90	49.75	15.21	11.06	0.157	3.6	6.54	4.02	2.46	2.209	0.7	1.17	96.88
Q91	48.01	16.89	12.21	0.159	4.66	7.88	3.77	1.75	2.885	0.56	0.21	98.98
Q22	58.52	15.38	6.98	0.124	3.52	6.74	2.37	2.95	0.974	0.33	0.66	98.54
Q68	58.33	15.59	6.22	0.102	2.54	5.8	2.71	2.94	0.729	0.22	1.67	96.83
Q78	58.76	14.6	5.21	0.098	1.45	5.49	2.1	4.12	0.648	0.21	7.15	99.84
Q82	61.65	15.12	4.94	0.098	2.14	5.58	2.59	3.42	0.715	0.2	2.4	98.85
Q84	60.41	15.66	5.53	0.101	2.73	5.63	2.66	2.89	0.709	0.24	2.12	98.68
Q92	61.99	14.95	4.95	0.086	1.83	4.49	3.09	3.56	0.74	0.27	1.53	97.47
Q94	58.73	15.16	6.41	0.096	2.48	5.7	3.15	2.87	1.018	0.34	1.1	97.06
Q95	60.04	15.85	6.54	0.101	2.78	6.07	3.2	2.74	1.098	0.39	0.74	99.55
Q4	63.34*	16.14*	6.00*	0.08*	1.69*	5.53*	3.56*	3.66*	0.74*	0.22*	1.97*	100.96*
Q24	65.96	15.43	4.79	0.027	0.95	3.44	2.62	3.85	0.643	0.2	2.97	100.9
Q29	69.31	12.75	0.88	0.064	0.7	1.24	1.99	4.5	0.129	0.02	6.56	98.13
Q55	68.35	12.55	1.1	0.019	0.4	2.29	0.78	5.36	0.144	0.02	8.88	99.88
Q75	64.96	15.11	4.36	0.082	1.29	3.76	2.57	4.54	0.56	0.2	1.92	99.35
Q6	77.58*	12.17*	0.71*	0.04*	0.09*	0.84*	3.53*	5.05*	0.11*	0.01*	0.61*	100.13*
Q7	77.40*	12.85*	0.74*	0.08*	0.06*	1.37*	3.62*	5.05*	0.12*	0.01*	0.97*	101.30*
Q9	71.04	11.72	0.86	0.071	0.2	1.08	2.44	5.21	0.104	0.02	5.23	97.97
Q10	76.89	11.71	0.95	0.085	0.17	0.7	3.22	4.81	0.131	0.03	0.7	99.39
Q13	75.13	12.05	0.96	0.107	0.18	0.9	3.31	4.63	0.127	0.04	1.33	98.77
Q14	73.8	12.04	0.99	0.096	0.17	0.85	3.07	5.64	0.132	0.04	1.02	97.83
Q18	76.48	11.64	1.11	0.054	0.22	0.63	2.97	4.49	0.124	0.03	0.91	98.65
Q23	75.56	11.99	1.06	0.042	0.26	0.82	2.8	4.63	0.153	0.04	1.45	98.79
Q25	75.39	11.9	0.71	0.046	0.18	0.7	3.02	5.2	0.104	0.03	1.25	98.53
Q30	77.06	12.99	1.14	0.008	0.19	0.25	0.16	4.22	0.189	0.05	3.31	99.58
Q34	72.76	12.61	0.98	0.07	0.29	0.87	2.16	5.58	0.127	0.05	4.25	99.74
Q33	72.94	12.38	0.78	0.067	0.23	1.64	2.25	5.7	0.11	0.03	4.31	100.4
Q38	75.67	12.08	1.09	0.019	0.25	0.76	2.78	4.81	0.146	0.03	1.76	99.4
Q42	76.83	12.09	1.14	0.04	0.21	0.36	1.94	6.38	0.131	0.04	1.3	100.5
Q44	74.38	11.68	1.11	0.028	0.38	0.88	2.21	4.8	0.203	0.04	2.6	98.31
Q46	78.48	11.8	0.87	0.044	0.19	0.56	2.5	4.85	0.122	0.02	1.3	100.7
Q50	76.21	12.78	0.71	0.108	0.18	0.8	3.44	5.01	0.055	0.02	1.21	100.5
Q56	75.9	11.91	0.88	0.043	0.19	0.7	2.95	4.93	0.122	0.05	1.68	99.36
Q57	74.75	12.33	0.66	0.016	0.24	0.88	2.82	5.26	0.124	0.03	1.4	98.51
Q59	73.57	12.52	1.18	0.041	0.67	1.04	1.59	5.85	0.189	0.03	3.48	100.2
Q61	77.59	11.69	0.77	0.035	0.14	0.68	3.27	4.67	0.123	0.04	1.06	100.1
Q65	73.89	12.4	1	0.033	0.21	1.46	2.97	5.35	0.136	0.02	0.98	98.45
Q66	74.93	12.57	0.95	0.047	0.09	0.89	3.19	5.33	0.139	0.08	0.62	98.85
Q70	75.77	11.88	0.93	0.046	0.19	0.75	3.03	4.96	0.139	0.03	1.29	99.02
Q83	75.6	12.42	0.79	0.076	0.07	0.89	3.48	5.25	0.109	0.07	0.66	99.4
Q85	77.96	9.57	0.76	0.076	0.16	0.84	2.13	4.55	0.105	0.02	2.38	98.56

Analyses from ACT labs by FUS-ICP and FUS-MS
*Analyses from UNLV lab by XRF

Sample Number	Sc ppm	Be ppm	V ppm	Cr ppm	Co ppm	Ni ppm	Cu ppm	Zn ppm	Ga ppm	Ge ppm	As ppm	Rb ppm	Sr ppm	Y ppm	Zr ppm	Nb ppm	Mo ppm	Ag ppm	In ppm	Sn ppm	Sb ppm	Cs ppm
Q1	16*	…..	140	60	274	< 20	< 10	80	20	2	< 5	90	797	29	266	13	< 2	< 0.5	< 0.2	2	3.9	1.8
Q2	15	3	151	30	221	< 20	30	100	23	1	< 5	35	658	33	122	39	4	< 0.5	< 0.2	2	< 0.5	< 0.5
Q90	14	3	152	40	43	< 20	< 10	140	24	1	< 5	43	622	34	237	45	4	0.8	< 0.2	6	< 0.5	< 0.5
Q91	16	2	197	20	50	< 20	40	150	23	1	161	28	892	28	110	35	2	< 0.5	< 0.2	2	3.1	< 0.5
Q22	17	2	168	110	37	< 20	30	60	19	2	< 5	90	752	27	235	17	< 2	< 0.5	< 0.2	1	5.4	1.7
Q68	12	2	88	40	273	< 20	< 10	40	20	1	5	81	856	16	115	8	< 2	< 0.5	< 0.2	1	< 0.5	0.9
Q78	11	2	105	20	32	< 20	10	80	18	3	< 5	121	698	13	139	8	< 2	< 0.5	< 0.2	2	2.5	5.6
Q82	13	2	114	30	17	< 20	< 10	40	17	1	< 5	103	722	18	200	11	< 2	< 0.5	< 0.2	1	2.2	2.3
Q84	12	3	104	< 20	232	< 20	< 10	80	20	1	6	98	804	18	175	11	< 2	< 0.5	< 0.2	1	2.7	1.7
Q92	10	2	112	< 20	132	< 20	< 10	60	19	1	6	103	795	17	212	12	< 2	< 0.5	< 0.2	1	< 0.5	1.8
Q94	13	2	143	< 20	30	< 20	10	30	20	1	< 5	80	802	21	168	12	< 2	1.2	< 0.2	1	< 0.5	1.4
Q95	16	2	155	< 20	197	< 20	10	80	20	2	< 5	76	825	21	240	13	< 2	< 0.5	< 0.2	1	3.7	1.4
Q4	16*	….	97	< 20	31	< 20	< 10	80	20	1	6	112	745	20	216	10	< 2	< 0.5	< 0.2	2	2.8	4.6
Q24	10	2	93	< 20	27	< 20	< 10	50	19	1	13	120	588	14	206	11	< 2	< 0.5	< 0.2	1	5.6	2.3
Q29	2	3	< 5	< 20	20	< 20	< 10	< 30	16	1	7	172	169	14	95	15	2	< 0.5	< 0.2	2	< 0.5	13.4
Q55	2	2	8	< 20	4	< 20	< 10	40	16	1	< 5	213	215	12	102	15	< 2	< 0.5	< 0.2	2	1.4	11.5
Q75	8	2	55	< 20	31	< 20	< 10	60	19	1	< 5	135	728	12	171	10	< 2	< 0.5	< 0.2	1	2.8	1.9
Q6	1*	….	< 5	< 20	271	< 20	< 10	< 30	15	1	9	200	27	18	82	16	< 2	< 0.5	< 0.2	1	2.6	4.6
Q7	2*	….	< 5	< 20	150	< 20	< 10	30	15	2	6	191	35	17	89	16	< 2	< 0.5	< 0.2	1	2.6	4.1
Q9	3	3	10	< 20	364	< 20	10	< 30	14	1	14	167	395	15	83	15	3	< 0.5	< 0.2	2	1.4	6.1
Q10	2	3	7	< 20	44	< 20	10	< 30	15	1	< 5	193	81	16	82	16	< 2	< 0.5	< 0.2	2	2.3	3.2
Q13	3	3	< 5	< 20	285	< 20	< 10	70	16	1	7	199	65	22	111	18	< 2	< 0.5	< 0.2	2	1.8	4.9
Q14	3	2	9	< 20	28	< 20	< 10	40	16	1	< 5	197	51	20	118	17	< 2	< 0.5	< 0.2	1	< 0.5	2.9
Q18	3	2	< 5	< 20	49	< 20	20	40	15	1	< 5	176	37	14	79	14	< 2	< 0.5	< 0.2	2	0.8	3.8
Q23	3	3	9	< 20	331	< 20	< 10	< 30	16	1	6	177	87	15	104	14	< 2	19.9	< 0.2	2	< 0.5	3.3
Q25	2	3	< 5	< 20	41	< 20	< 10	30	16	2	10	207	36	15	76	15	< 2	< 0.5	< 0.2	2	0.7	4.9
Q30	3	2	10	< 20	33	< 20	< 10	< 30	14	1	15	149	85	15	122	13	< 2	< 0.5	< 0.2	2	6.7	4.8
Q34	2	3	6	< 20	29	< 20	< 10	< 30	14	1	11	209	107	14	98	15	2	< 0.5	< 0.2	2	3.1	9.8
Q33	3	3	< 5	< 20	510	< 20	< 10	30	15	1	10	230	68	15	80	16	< 2	< 0.5	< 0.2	2	2.6	8
Q38	3	3	6	< 20	339	< 20	< 10	100	16	2	11	189	79	16	96	16	< 2	0.7	< 0.2	1	3.5	3.8
Q42	3	3	< 5	< 20	379	< 20	10	< 30	15	2	6	234	25	20	101	17	< 2	< 0.5	< 0.2	< 1	2.4	2.4
Q44	3	2	18	< 20	18	< 20	30	< 30	11	< 1	< 5	103	111	13	105	10	< 2	0.6	< 0.2	4	< 0.5	2.3
Q46	3	3	< 5	< 20	489	< 20	< 10	< 30	14	1	6	197	34	19	81	18	< 2	< 0.5	< 0.2	3	2.7	2.3
Q50	5	7	< 5	< 20	252	< 20	< 10	40	21	2	8	378	96	21	66	44	< 2	1.1	< 0.2	6	8.4	8.9
Q56	3	3	< 5	< 20	30	< 20	< 10	30	16	1	8	202	82	21	107	19	< 2	< 0.5	< 0.2	1	3.9	5
Q57	2	3	< 5	< 20	27	< 20	< 10	< 30	15	1	< 5	200	102	11	95	15	< 2	< 0.5	< 0.2	< 1	2.3	4.5
Q59	3	2	12	< 20	11	< 20	< 10	< 30	14	1	6	198	325	15	103	14	< 2	< 0.5	< 0.2	1	2.6	3.5
Q61	3	3	< 5	< 20	462	< 20	< 10	40	15	2	8	189	42	19	95	18	< 2	< 0.5	< 0.2	2	2.8	4.4
Q65	2	3	5	< 20	21	< 20	< 10	< 30	14	1	8	189	165	11	101	13	< 2	< 0.5	< 0.2	1	2.4	4
Q66	2	3	< 5	< 20	380	< 20	< 10	< 30	15	2	12	198	153	13	100	15	< 2	< 0.5	< 0.2	2	3.8	6
Q70	4	3	5	< 20	176	< 20	< 10	30	15	1	7	193	56	19	104	18	< 2	< 0.5	< 0.2	1	2.7	3.9
Q83	2	3	< 5	< 20	30	< 20	< 10	50	16	1	7	197	48	16	76	14	< 2	< 0.5	< 0.2	2	< 0.5	4.8
Q85	2	2	6	< 20	35	< 20	< 10	80	12	1	< 5	167	121	18	81	13	< 2	1.7	< 0.2	1	< 0.5	2.9

Analyses from ACT labs by FUS-ICP and FUS-MS
*Analyses from UNLV lab by XRF

Sample Number	Ba ppm	La ppm	Ce ppm	Pr ppm	Nd ppm	Sm ppm	Eu ppm	Gd ppm	Tb ppm	Dy ppm	Ho ppm	Er ppm	Tm ppm	Yb ppm	Lu ppm	Hf ppm	Ta ppm	W ppm	Ti ppm	Pb ppm	Bi ppm	Th ppm	U ppm
Q1	1070	52.7	107	12.5	41	8.1	1.91	6.4	0.9	5	1	3	0.46	2.9	0.42	6.8	1.1	714	0.4	12	3.4	12.1	2.2
Q2	628	44.8	88.7	10.1	38.3	9	2.87	8.5	1.3	7.1	1.4	3.9	0.53	3.2	0.46	3.8	3.2	465	< 0.1	< 5	< 0.4	3.1	1.4
Q90	664	47.1	91.9	10.4	40	9.3	2.87	8.6	1.3	7.3	1.4	4	0.55	3.3	0.49	6.8	3.8	103	< 0.1	< 5	< 0.4	4	1.6
Q91	420	33	65.7	7.65	30.4	7.6	2.6	7.4	1.1	6	1.1	3.2	0.43	2.6	0.35	3.3	3.1	85	1.2	< 5	< 0.4	2.6	1
Q22	1001	48.3	96.8	11.9	37.5	7.7	1.79	6.2	0.9	5	1	3	0.44	2.8	0.39	6.3	1.8	142	0.3	11	< 0.4	11.3	2.3
Q68	896	35.2	66.6	7.1	24.4	5.1	1.32	4	0.6	3.2	0.6	1.8	0.25	1.5	0.24	3.6	0.7	671	0.1	< 5	< 0.4	7.7	1.5
Q78	868	32.9	64.5	7.51	24	4.6	1.2	3.7	0.5	2.9	0.6	1.7	0.25	1.5	0.23	4	1.2	130	0.4	10	2.1	9.9	2.5
Q82	1070	43.3	82.5	9.38	31.1	5.7	1.27	4.4	0.6	3.5	0.7	2	0.31	2	0.29	5.4	1.1	55	0.3	9	2.3	12	2.7
Q84	972	36.5	73.3	8.75	29.7	5.6	1.35	4.5	0.6	3.5	0.7	2	0.31	2	0.3	4.9	1	634	0.8	14	4.1	11.3	2.5
Q92	1242	54.1	97.5	10	31.7	6	1.38	4.4	0.6	3.2	0.6	1.9	0.28	1.8	0.26	5.5	1	341	0.7	< 5	< 0.4	13.6	3.2
Q94	1139	54.2	103	11.2	38.1	7.6	1.85	5.8	0.8	4.2	0.8	2.3	0.32	2	0.29	4.9	1.3	87	0.3	< 5	< 0.4	9.7	2.5
Q95	1118	56	112	13.3	42.8	8.3	2.01	6.5	0.9	4.6	0.9	2.5	0.37	2.3	0.34	6.8	0.9	476	0.4	12	6.3	11.1	2.1
Q4	1110	44.1	83.3	9.57	30.3	5.7	1.39	4.5	0.7	3.6	0.7	2.2	0.34	2.2	0.3	5.4	1.4	136	0.4	16	1.9	11.3	2.5
Q24	1037	44.3	84	9.44	29.4	5.1	1.21	3.7	0.5	3	0.6	1.7	0.25	1.6	0.23	5.4	1.3	120	0.5	14	< 0.4	12.6	2.4
Q29	371	47	80.1	8	23.2	4.1	0.6	2.8	0.4	2.6	0.5	1.7	0.26	1.8	0.27	3.6	2.2	127	1.7	9	< 0.4	25.5	5.7
Q55	359	41.5	71.3	7.1	22.4	4	0.66	2.7	0.4	2.3	0.5	1.4	0.21	1.3	0.2	3.6	1.6	23	2.5	13	0.6	24.3	4.7
Q75	1117	36.8	72.7	8.16	25.6	4.7	1.11	3.4	0.5	2.5	0.5	1.5	0.23	1.4	0.2	4.7	1.5	155	0.6	17	1.7	12.6	2
Q6	38	30.9	55.4	6.67	20.1	3.9	0.54	3.2	0.5	2.9	0.6	1.9	0.31	2	0.3	3.4	1.6	745	0.8	17	2	24.1	4
Q7	52	31.3	62.5	7.04	22	4.1	0.52	3.1	0.5	2.8	0.6	1.8	0.3	2	0.29	3.8	1.6	424	0.6	20	6.1	23.7	4.4
Q9	88	31.6	59.2	5.83	18.8	3.4	0.47	2.6	0.4	2.5	0.5	1.7	0.26	1.8	0.28	3.2	1.6	959	1.1	7	< 0.4	22.7	6.2
Q10	91	30.2	60	6.63	20.3	3.8	0.29	2.8	0.4	2.8	0.6	1.8	0.27	1.8	0.26	3.2	2.8	306	0.7	16	7.3	22.8	3.4
Q13	104	39.7	76.8	8.85	27.7	5.3	0.53	4.1	0.6	3.8	0.8	2.6	0.41	2.7	0.4	4.9	2	863	1.1	58	23	26.8	6.2
Q14	265	36.7	66.9	7.28	24.3	4.8	0.64	3.6	0.6	3.4	0.7	2.2	0.34	2.3	0.35	4.1	2.5	197	1	12	< 0.4	22.7	4.9
Q18	116	33.8	68.2	7.15	20.7	3.7	0.39	2.8	0.4	2.4	0.5	1.6	0.25	1.7	0.25	3.8	3	347	0.8	38	15.1	21.7	3.7
Q23	256	41.6	74.8	7.51	24	4.4	0.54	3.2	0.5	2.8	0.6	1.7	0.27	1.8	0.27	3.8	1.5	1020	1.5	11	< 0.4	20.4	4.6
Q25	66	31.2	56.8	5.88	19	3.5	0.45	2.7	0.4	2.6	0.5	1.7	0.27	1.8	0.29	3.2	2.8	256	2.8	23	0.5	23.7	6.4
Q30	553	43.7	84.8	9.16	27.5	4.9	0.69	3.5	0.5	3	0.6	1.8	0.29	2	0.29	4.3	2.3	241	0.5	14	1.7	20.1	3.2
Q34	307	39.9	74.1	7.55	19.8	3.3	0.45	2.1	0.3	2.2	0.5	1.5	0.23	1.6	0.25	3.5	2	130	1.2	22	12	25.8	6.4
Q33	48	33.6	66.4	7.32	21.7	3.9	0.42	2.8	0.4	2.6	0.6	1.7	0.27	1.9	0.27	3.3	1.7	1300	1.1	22	14.2	24.5	6.3
Q38	246	42.2	77.8	8.51	25.2	4.5	0.49	3.3	0.5	2.9	0.6	1.8	0.28	1.8	0.27	3.6	1.6	1020	0.8	26	1.5	22.7	4.5
Q42	122	26.3	53.8	5.92	19.3	3.6	0.54	3	0.5	3.1	0.7	2.2	0.38	2.5	0.37	3.8	1.8	1090	0.5	12	< 0.4	23.1	4.4
Q44	292	25.3	44.3	4.46	13.8	2.6	0.4	2	0.3	1.9	0.4	1.2	0.19	1.3	0.21	2.7	1.5	113	0.6	< 5	< 0.4	13.8	4
Q46	88	33.2	66.5	7.23	21.3	4.2	0.32	3.4	0.5	3.1	0.6	2	0.32	2.1	0.32	3.5	1.8	1450	0.5	15	7.1	24.8	4.8
Q50	26	14.6	39.5	4.33	17.3	4.3	0.08	4.1	0.8	4.7	0.9	2.8	0.44	2.9	0.4	3.8	4.9	693	1.9	27	35.7	30.6	7
Q56	134	36.6	73.4	8.31	26.4	5.1	0.51	3.9	0.6	3.8	0.8	2.3	0.38	2.4	0.35	4.1	2.7	209	0.4	18	< 0.4	25.5	5.1
Q57	301	38.5	69.8	8.1	22.8	4.1	0.59	2.8	0.4	2.3	0.5	1.4	0.22	1.5	0.22	3.5	2.2	169	0.6	19	< 0.4	26	4.6
Q59	548	47.3	86	9.68	27.6	4.8	0.75	3.4	0.5	2.8	0.6	1.7	0.28	1.8	0.24	3.5	1.6	71	0.6	19	2.8	23.7	4.5
Q61	185	35.4	69.7	8.06	25	4.9	0.55	3.8	0.6	3.7	0.7	2.2	0.35	2.2	0.32	3.7	2	1290	0.7	20	2.1	24.8	6
Q65	696	48.3	85.1	8.76	21.9	3.6	0.53	2.4	0.3	2	0.4	1.3	0.21	1.4	0.21	3.5	2	135	0.6	15	< 0.4	25.8	4.5
Q66	705	58.4	105	10.6	27.8	4.5	0.65	3.2	0.4	2.6	0.5	1.7	0.28	1.9	0.28	4	1.8	1080	1	24	14.3	27.8	6.6
Q70	181	34.2	67.6	8	24.6	4.8	0.53	4	0.6	3.5	0.7	2.2	0.35	2.3	0.34	3.9	1.7	545	0.6	15	8.3	24.2	5.1
Q83	65	32.3	61.2	6.1	19.8	3.8	0.47	2.9	0.5	2.8	0.6	1.8	0.28	1.9	0.29	3.2	2.4	190	1.3	8	< 0.4	22.6	5.8
Q85	143	28.3	53.9	5.73	19.7	3.9	0.45	2.9	0.5	2.8	0.6	1.9	0.3	2	0.32	2.9	2.5	222	0.8	17	< 0.4	19.3	4.3

Analyses from ACT labs by FUS-ICP and FUS-MS
*Analyses from UNLV lab by XRF

APPENDIX D

Southern Quinn Canyon Range Geochemical Data Accuracies

Analysis Method	Analyte Symbol	Unit Symbol	Absolute Average % Error	BIR-1a Meas	BIR-1a Cert	% Error	W-2a Meas	W-2a Cert	% Error	WMG-1 Meas	WMG-1 Cert	% Error	DNC-1 Meas	DNC-1 Cert	% Error	GBW 07113 Meas	GBW 07113 Cert	% Error
FUS-MS	V	ppm	3.43	318	313	1.60	268	262	2.29	173	149	16.11	148	148	0.00	……	……	……
FUS-MS	Sr	ppm	3.40	103	108	-4.63	194	190	2.11	39	41	-4.88	140	145	-3.45	……	……	……
FUS-MS	Y	ppm	3.33	16	16	0.00	22	24	-8.33	15	12	25.00	18	18	0.00	……	……	……
FUS-MS	Zr	ppm	9.63	14	16	-12.50	98	94	4.26	59	43	37.21	43	41	4.88	……	……	……
FUS-MS	Ba	ppm	8.98	5	7	-28.57	173	182	-4.95	110	114	-3.51	101	114	-11.40	……	……	……
FUS-ICP	SiO2	wt%	0.71	48.29	47.8	1.03	52.74	52.4	0.65	……	……	……	47.56	47	1.19	72.78	72.8	-0.03
FUS-ICP	Al2O3	wt%	0.50	15.56	15.4	1.04	15.43	15.4	0.19	……	……	……	18.51	18.3	1.15	12.95	13	-0.38
FUS-ICP	Fe2O3(T)	wt%	0.90	11.07	11.3	-2.04	10.89	10.7	1.78	……	……	……	9.66	9.93	-2.72	3.19	3.21	-0.62
FUS-ICP	MnO	wt%	7.20	0.183	0.171	7.02	0.177	0.163	8.59	……	……	……	0.158	0.149	6.04	0.15	0.14	7.14
FUS-ICP	MgO	wt%	4.54	9.41	9.68	-2.79	6.32	6.37	-0.78	……	……	……	9.89	10.1	-2.08	0.14	0.16	-12.50
FUS-ICP	CaO	wt%	2.06	13.46	13.2	1.97	11.1	10.9	1.83	……	……	……	11.42	11.3	1.06	0.61	0.59	3.39
FUS-ICP	Na2O	wt%	0.92	1.8	1.75	2.86	2.19	2.14	2.34	……	……	……	1.9	1.87	1.60	2.49	2.57	-3.11
FUS-ICP	K2O	wt%	4.14	<0.01	0.03	……	0.63	0.626	0.64	……	……	……	0.2	0.234	-14.53	5.51	5.43	1.47
FUS-ICP	TiO2	wt%	0.12	0.966	0.96	0.63	1.071	1.06	1.04	……	……	……	0.489	0.48	1.88	0.288	0.3	-4.00
FUS-ICP	P2O5	wt%	15.85	0.02	0.05	-60.00	0.14	0.13	7.69	……	……	……	0.08	0.09	-11.11	0.05	0.05	0.00
FUS-ICP	Sc	ppm	1.26	43	44	-2.27	35	36	-2.78	……	……	……	31	31	0.00	5	5	0.00
FUS-ICP	Be	ppm	26.92	<1	0.58	……	2	1.3	53.85	……	……	……	<1	1	……	4	4	0.00
FUS-MS	Cr	ppm	1.29	390	382	2.09	90	92	-2.17	810	770	5.19	280	285	-1.75	……	……	……
FUS-MS	Co	ppm	0.16	51	51.4	-0.78	44	43	2.33	205	200	2.50	54	54.7	-1.28	……	……	……
FUS-MS	Ni	ppm	6.98	160	166	-3.61	60	70	-14.29	2870	2700	6.30	250	247	1.21	……	……	……
FUS-MS	Cu	ppm	2.34	120	126	-4.76	110	110	0.00	5860	5900	-0.68	90	96	-6.25	……	……	……
FUS-MS	Zn	ppm	4.04	70	71	-1.41	90	80	12.50	130	110	18.18	60	66	-9.09	……	……	……
FUS-MS	Ga	ppm	0.42	15	16	-6.25	18	17	5.88	10	10.3	-2.91	14	15	-6.67	……	……	……
FUS-MS	Ge	ppm	14.53	1	1.5	-33.33	2	1	100.00	……	……	……	1	1.3	-23.08	……	……	……
FUS-MS	As	ppm	110.09	<5	0.44	……	<5	1.2	……	18	7	157.14	<5	0.2	……	……	……	……
FUS-MS	Rb	ppm	12.25	<2	0.25	……	20	21	-4.76	……	……	……	3	4.5	-33.33	……	……	……
FUS-MS	Nb	ppm	13.26	<1	0.6	……	7	7.9	-11.39	5	6	-16.67	2	3	-33.33	……	……	……
FUS-MS	Mo	ppm	……	<2	0.5	……	<2	0.6	……	<2	1.4	……	<2	0.7	……	……	……	……
FUS-MS	Ag	ppm	0.00	<0.5	0.036	……	<0.5	0.046	……	2.7	2.7	0.00	<0.5	0.027	……	……	……	……
FUS-MS	In	ppm	……	……	……	……	……	……	……	……	……	……	……	……	……	……	……	……
FUS-MS	Sn	ppm	12.88	<1	0.65	……	……	……	……	2	2.2	-9.09	……	……	……	……	……	……
FUS-MS	Sb	ppm	58.30	0.9	0.58	55.17	1	0.79	26.58	4.3	1.8	138.89	1.6	0.96	66.67	……	……	……
FUS-MS	Cs	ppm	4.55	<0.5	0.005	……	0.9	0.99	-9.09	<0.5	0.48	……	<0.5	0.34	……	……	……	……
FUS-MS	La	ppm	2.01	0.5	0.62	-19.35	11.3	10	13.00	8.6	8.2	4.88	3.5	3.8	-7.89	……	……	……
FUS-MS	Ce	ppm	2.18	1.9	1.95	-2.56	24.5	23	6.52	17	16	6.25	8.3	10.6	-21.70	……	……	……
FUS-MS	Pr	ppm	0.41	0.39	0.38	2.63	……	……	……	……	……	……	1.11	1.3	-14.62	……	……	……
FUS-MS	Nd	ppm	7.28	2.1	2.5	-16.00	12.4	13	-4.62	9	9	0.00	4.5	4.9	-8.16	……	……	……
FUS-MS	Sm	ppm	4.92	1	1.1	-9.09	3.2	3.3	-3.03	2.3	2.3	0.00	1.3	1.38	-5.80	……	……	……
FUS-MS	Eu	ppm	0.16	0.53	0.54	-1.85	1.17	1	17.00	0.76	0.82	-7.32	0.6	0.59	1.69	……	……	……
FUS-MS	Gd	ppm	2.70	1.7	1.85	-8.11	……	……	……	……	……	……	2	2	0.00	……	……	……
FUS-MS	Tb	ppm	9.37	0.4	0.36	11.11	0.7	0.63	11.11	0.4	0.3	33.33	0.4	0.41	-2.44	……	……	……
FUS-MS	Dy	ppm	0.83	2.5	2.5	0.00	3.9	3.6	8.33	2.4	2.8	-14.29	2.8	2.7	3.70	……	……	……
FUS-MS	Ho	ppm	1.07	0.6	0.57	5.26	0.8	0.76	5.26	0.5	0.5	0.00	0.6	0.62	-3.23	……	……	……
FUS-MS	Er	ppm	0.36	1.8	1.7	5.88	2.4	2.5	-4.00	……	……	……	2	2	0.00	……	……	……
FUS-MS	Tm	ppm	1.78	0.28	0.26	7.69	0.37	0.38	-2.63	0.23	0.2	15.00	0.32	0.38	-15.79	……	……	……
FUS-MS	Yb	ppm	3.22	1.7	1.65	3.03	2.2	2.1	4.76	1.3	1.3	0.00	2.1	2.01	4.48	……	……	……
FUS-MS	Lu	ppm	5.95	0.24	0.26	-7.69	0.31	0.33	-6.06	0.2	0.21	-4.76	0.3	0.32	-6.25	……	……	……
FUS-MS	Hf	ppm	4.59	0.5	0.6	-16.67	2.6	2.6	0.00	1.5	1.3	15.38	1.2	1.01	18.81	……	……	……
FUS-MS	Ta	ppm	13.33	<0.1	0.04	……	0.5	0.5	0.00	0.3	0.5	-40.00	<0.1	0.098	……	……	……	……
FUS-MS	W	ppm	42.86	<1	0.07	……	<1	0.3	……	<1	1.3	……	<1	0.2	……	……	……	……
FUS-MS	Ti	ppm	49.58	<0.1	0.01	……	0.1	0.2	-50.00	……	……	……	<0.1	0.026	……	……	……	……
FUS-MS	Pb	ppm	9.91	<5	3	……	8	9.3	-13.98	27	15	80.00	7	6.3	11.11	……	……	……
FUS-MS	Bi	ppm	6951.47	3.9	0.02	19400	1.2	0.03	3900	……	……	……	0.9	0.02	4400.00	……	……	……
FUS-MS	Th	ppm	2.71	<0.1	0.03	……	2.2	2.4	-8.33	1.1	1.1	0.00	0.2	0.2	0.00	……	……	……
FUS-MS	U	ppm	1.84	<0.1	0.01	……	0.6	0.53	13.21	0.6	0.65	-7.69	<0.1	0.1	……	……	……	……
FUS-ICP	V	ppm	8.50	340	313	8.63	285	262	8.78	……	……	……	160	148	8.11	<5	5	……
FUS-ICP	Ba	ppm	8.70	10	7	42.86	178	182	-2.20	……	……	……	108	114	-5.26	503	506	-0.59
FUS-ICP	Sr	ppm	0.37	108	108	0.00	196	190	3.16	……	……	……	145	145	0.00	41	43	-4.65
FUS-ICP	Y	ppm	8.67	14	16	-12.50	21	24	-12.50	……	……	……	15	18	-16.67	46	43	6.98
FUS-ICP	Zr	ppm	9.93	12	16	-25.00	92	94	-2.13	……	……	……	34	41	-17.07	421	403	4.47

APPENDIX E

Mafic Comparison Geochemical Data

Sample	SiO_2	Al_2O_3	TiO_2	Fe_2O_3*	CaO	K_2O	P_2O_5	MnO	Na_2O	MgO	Total
				Lunar Crater: Stickney (2004)							
LC-01-05-01	46.07	14.48	2.45	12.80	9.94	1.87	0.79	0.20	3.64	9.18	101.42
LC-02-06-01	46.24	14.76	2.70	13.08	9.20	1.20	0.49	0.17	3.25	8.10	99.18
LC-03-06-01	45.74	15.13	2.30	11.81	9.19	2.02	0.81	0.20	4.48	6.99	98.67
LC-04-07-01	47.24	15.51	2.51	12.41	8.43	1.90	0.83	0.19	3.98	7.01	100.01
LC-05-07-01	46.18	14.98	2.71	12.30	9.66	1.61	0.62	0.17	3.32	8.42	99.95
LC-06-07-01	46.28	14.09	2.31	12.24	10.02	1.87	0.76	0.20	3.52	9.31	100.60
LC-07-07-01	47.54	15.58	2.49	12.57	8.49	1.96	0.83	0.19	4.00	7.12	100.75
LC-10-08-01	46.19	15.47	2.81	14.28	8.98	1.25	0.58	0.17	3.09	7.80	100.62
LC-13-08-01	46.99	15.35	2.56	13.73	9.29	1.04	0.41	0.17	3.04	9.01	101.60
LC-14-08-01	46.71	15.07	2.54	13.60	9.79	0.98	0.41	0.17	2.86	9.34	101.45
LC-20-08-01	46.34	15.22	2.63	12.36	9.60	1.78	0.54	0.17	3.52	8.71	100.87
LC-23-08-01	45.48	15.05	2.75	12.71	10.16	1.39	0.65	0.17	3.15	8.99	100.51
LC-28-08-01	46.18	13.29	2.41	14.39	8.58	0.80	0.50	0.18	2.28	11.29	99.90
LC-32-08-01	48.36	16.18	2.41	12.37	9.16	1.15	0.47	0.17	2.61	7.51	100.39
				Lunar Crater: Dickson (1997)							
LC11-96	43.50	13.50	2.70	15.40	9.40	0.71	0.40	0.18	2.70	10.40	98.89
LC16-96	48.50	15.80	2.60	13.30	8.60	1.15	0.50	0.17	3.40	5.60	99.62
LC17-96	48.10	14.30	1.90	12.80	8.90	1.04	0.40	0.17	2.90	8.90	99.41
LC18-96	45.30	14.60	2.70	13.10	9.80	1.24	0.60	0.17	2.80	8.80	99.11
LC31-96	54.90	16.90	1.60	9.40	7.90	1.57	0.40	0.13	3.00	4.10	99.90
LC34-96	47.30	14.70	2.40	13.50	8.80	1.01	0.40	0.17	3.10	8.30	99.68
LC38-96	50.60	15.30	2.30	12.40	8.50	1.06	0.40	0.16	3.40	6.30	100.42
LC45-96	46.90	15.00	2.50	13.30	9.20	1.17	0.50	0.17	3.50	8.40	100.64
				Death Valley: Tibbetts (2010)							
DV-08-30	49.43	16.32	2.27	11.45	8.10	2.25	0.72	0.16	3.76	5.05	99.51
DV-08-79	51.98	17.27	1.76	9.94	8.54	1.95	0.83	0.15	3.51	4.30	100.23
DV-08-87	49.80	16.99	1.85	10.45	8.69	1.84	0.85	0.16	4.10	5.08	99.81
DV-08-91	48.50	16.25	2.40	11.95	8.05	2.41	0.67	0.16	3.41	5.19	98.99
DV-08-118	51.07	17.07	1.56	9.91	8.00	1.56	0.77	0.16	3.44	5.47	99.01
DV-08-121	52.85	17.83	1.51	9.12	8.19	1.81	0.75	0.15	3.55	4.29	100.05
DV-08-125	50.73	16.60	1.41	9.26	10.14	0.72	0.24	0.15	3.14	7.30	99.69
DV-08-127	50.22	17.27	1.74	10.91	8.26	1.89	0.86	0.15	3.39	4.60	99.29
DV-08-130	51.43	17.50	1.68	9.24	8.41	1.60	0.58	0.15	3.92	5.34	99.85
DV-08-132A	51.86	16.74	1.55	9.30	8.50	1.33	0.45	0.15	3.45	6.54	99.87
DV-08-134	54.95	17.45	1.15	6.96	8.53	2.07	0.34	0.12	3.54	4.87	99.98
DV-08-138	49.25	18.09	1.43	8.96	10.76	1.00	0.39	0.15	3.27	6.53	99.83
DV-08-144	47.50	15.83	2.61	12.98	8.28	1.94	0.85	0.18	3.40	6.14	99.71
DV-08-149	50.34	16.99	1.86	10.70	9.01	1.88	0.83	0.16	3.62	5.04	100.42
DV-08-154	51.85	16.59	1.51	8.69	8.19	1.74	0.48	0.15	3.86	6.53	99.59
DV-07-15	51.04	17.10	1.59	10.70	8.34	1.64	0.83	0.16	3.39	5.26	100.05
DV-07-20	51.43	16.91	1.72	9.99	8.55	1.87	0.78	0.15	3.37	4.51	99.28
DV-08-27	48.26	15.88	2.61	13.37	8.42	1.92	0.87	0.18	3.32	5.86	100.69
DV-08-29	51.06	16.54	1.86	10.32	8.41	1.84	0.56	0.15	3.36	5.96	100.06
DV-08-34	49.83	16.24	2.03	11.41	8.17	1.93	0.93	0.16	3.62	5.28	99.60
DV-08-39	49.63	16.39	2.08	11.97	7.77	1.86	0.93	0.16	3.35	5.45	99.59
DV-08-42	46.47	15.74	2.73	13.54	8.33	2.12	0.69	0.17	3.15	6.42	99.36
DV-08-46	47.83	15.92	2.63	12.82	8.65	1.97	0.85	0.17	3.19	5.81	99.84
DV-08-56	51.64	16.41	1.77	9.80	8.45	1.74	0.52	0.15	3.49	6.27	100.24
DV-08-63	50.00	18.03	1.36	8.87	10.64	1.20	0.38	0.13	3.40	6.36	100.37
DV-08-69	49.59	17.04	1.52	8.98	9.83	1.10	0.48	0.15	3.69	7.78	100.16
DV-08-72	50.87	16.14	1.50	9.42	8.49	1.61	0.56	0.15	3.46	7.64	99.84
DV-08-86	49.42	16.59	1.89	11.25	9.28	1.82	0.81	0.16	3.39	5.37	99.98
DV-08-89	52.91	17.20	1.33	8.90	8.48	1.58	0.62	0.13	3.31	5.33	99.79
DV-08-92	53.32	17.03	1.29	8.39	7.99	1.80	0.59	0.13	3.41	5.48	99.43
DV-08-96	49.02	16.61	2.44	12.07	8.44	2.55	0.69	0.16	3.71	4.18	99.87
DV-08-102	47.78	17.61	1.87	10.44	9.79	0.73	0.71	0.17	3.92	7.11	100.14
DV-08-108	52.55	17.70	1.44	9.07	8.56	1.22	0.41	0.15	3.56	5.42	100.08
DV-08-110	48.07	15.97	2.49	12.82	8.78	1.94	0.90	0.18	3.16	5.07	99.38
				Southern Quinn Canyon Range: This Study							
Q1	59.58	16.41	0.99	6.90	6.48	3.00	0.34	0.11	3.00	3.16	99.97
Q2	47.87	15.54	2.42	11.85	6.98	2.13	0.71	0.17	4.03	4.15	95.84
Q90	49.75	15.21	2.21	11.06	6.54	2.46	0.70	0.16	4.02	3.60	95.71
Q91	48.01	16.89	2.89	12.21	7.88	1.75	0.56	0.16	3.77	4.66	98.77
				Crater Flat: Farmer et al., 1989							
CF-12-6-10	49.60	15.60	1.60	10.80	9.84	1.60	0.62	0.20	3.00	7.13	99.99
CF-11-7-1	49.00	16.80	1.80	10.90	8.89	1.80	1.10	0.20	3.50	5.96	99.95
FB78-5	51.20	17.20	1.50	9.94	8.73	1.60	1.10	0.20	3.40	5.22	100.09

Sample	SiO_2	Al_2O_3	TiO_2	Fe_2O_3*	CaO	K_2O	P_2O_5	MnO	Na_2O	MgO	Total
Crater Flat: Bradshaw and Smith (1994)											
C9-1-8	48.63	6.59	1.45	11.03	8.87	1.58	0.92	0.17	3.23	5.11	87.58
C9-1-9	48.89	16.76	1.45	11.22	8.39	1.62	0.91	0.18	3.26	5.19	97.87
C9-2-28	49.66	17.25	1.38	10.22	8.56	1.74	1.01	0.19	3.53	4.78	98.32
C9-2-30	49.00	16.93	1.45	10.44	8.50	1.75	1.45	0.18	3.40	4.75	97.85
C9-2-31	49.54	17.17	1.39	10.24	8.57	1.77	1.09	0.20	3.63	4.60	98.20
C9-2-34	50.33	17.29	1.48	10.69	8.85	1.76	1.20	0.18	3.48	5.13	100.39
C9-2-37	48.90	17.68	1.50	10.59	8.35	1.82	1.06	0.18	3.37	5.35	98.80
C9-2-41	49.38	17.15	1.53	10.80	8.49	2.00	1.08	0.21	3.34	5.02	99.00
C9-2-44	49.24	17.16	1.51	10.51	8.32	1.84	1.14	0.20	3.43	4.72	98.07
C9-2-46	49.68	17.02	1.40	10.37	8.78	1.68	1.17	0.19	3.55	5.09	98.93
Reveille Range Episode 1: Yogodzinski et al., 1996											
R9-1-48	47.50	16.89	2.53	9.55	9.40	1.10	0.39	0.14	3.35	6.08	96.93
R9-3-60	47.38	16.17	2.68	11.91	8.71	1.18	0.56	0.19	3.58	5.82	98.18
R9-4-61	47.54	15.80	2.82	12.27	8.57	1.33	0.56	0.20	3.55	5.75	98.39
R9-1-56	47.38	16.05	3.15	12.15	8.56	1.14	0.55	0.17	3.36	5.58	98.09
R8-1-29	47.47	16.13	2.81	11.89	8.44	1.36	0.62	0.17	3.70	4.54	97.13
R8-1-17	46.89	16.54	2.91	11.97	8.86	1.12	0.44	0.17	3.65	5.63	98.18
R8-1-7	46.11	16.34	2.70	11.18	9.13	1.63	0.36	0.17	3.43	5.09	96.14
R9-2-59	45.71	16.21	3.51	12.73	8.24	1.33	0.76	0.21	3.89	5.05	97.64
R0-1-77	46.49	15.69	3.37	13.26	8.23	1.34	0.48	0.18	3.09	4.65	96.78
Reveille Range Episode 1: Rash (1995)											
RR-46	48.90	16.31	2.57	11.96	8.58	1.59	0.53	0.17	3.18	5.31	99.10
Reveille Range Episode 2: Yogodzinski et al., 1996											
R8-1-18	45.82	15.54	3.47	13.71	7.55	1.41	0.67	0.20	4.07	4.53	96.97
R8-1-19	45.48	15.46	3.25	12.86	8.61	1.08	0.47	0.18	3.75	4.80	95.94
R8-1-22	44.30	15.38	2.94	10.78	9.48	1.80	0.63	0.17	3.42	8.32	97.22
R8-1-27	43.91	14.14	2.81	10.90	10.08	1.48	0.59	0.17	3.27	10.24	97.59
R9-1-46	46.31	15.80	3.47	11.53	7.36	1.48	0.75	0.16	4.12	6.01	96.99
R9-1-47	44.12	16.59	4.02	10.04	7.68	1.63	0.99	0.16	4.29	5.12	94.64
R9-1-55	46.95	17.17	3.57	10.49	6.85	2.63	0.84	0.17	4.43	3.86	96.96
Reveille Range Episode 2: Rash (1995)											
RR-28	48.03	17.02	2.93	11.26	7.25	2.65	0.63	0.18	3.66	4.32	97.93
Nevada Test Site: Farmer et al., 1989											
TS6-15-2	49.20	16.20	2.50	12.10	8.74	1.50	0.70	0.20	3.50	5.45	100.09
TS9-22-1	52.30	17.00	1.70	9.17	8.21	2.20	0.80	0.20	3.80	4.60	99.98
TS6-14-7A	48.00	16.30	2.00	9.35	9.36	1.10	0.50	0.20	3.40	9.75	99.96
CIMA Domes: Farmer et al., 1989											
PB-34	48.05	16.02	3.11	10.83	8.56	1.81	0.62	0.17	4.11	5.74	99.02
Reveille Range Tracy-Andesite: Yogodzinski et al., 1996											
R8-1-16	55.77	16.11	1.11	9.82	3.80	4.28	0.30	0.20	5.53	1.20	98.12
R9-1-43	58.92	16.94	0.47	6.74	3.62	5.58	0.11	0.17	6.25	0.52	99.32
R9-1-62	59.74	17.28	0.51	7.11	2.26	5.24	0.24	0.18	6.5	0.47	99.53
R8-1-42	60.14	17.23	0.51	7.2	2.04	5.68	0.18	0.18	6.58	0.38	100.12

Sample	Th	U	La	Ce	Sm	Eu	Tb	Yb	Lu	Pr	Nd	Gd	Dy	Ho	Er	Tm
Lunar Crater: Stickney (2004)																
LC-01-05-01	4.84	1.33	47.46	91.44	9.39	2.98	1.20	2.45	0.37	10.68	43.97	8.06	6.67	1.24	3.08	0.42
LC-02-06-01	2.64	0.75	26.57	52.11	6.85	2.32	1.04	2.29	0.34	6.19	27.08	6.73	6.03	1.16	2.80	0.39
LC-03-06-01	6.20	1.61	54.48	101.61	9.75	3.15	1.20	2.52	0.39	11.69	46.90	8.03	6.63	1.24	3.12	0.44
LC-04-07-01	5.00	1.29	46.93	87.83	8.84	2.90	1.19	2.55	0.39	9.96	40.44	7.96	6.67	1.25	3.18	0.44
LC-05-07-01	3.85	0.95	36.45	68.63	7.73	2.57	1.06	2.34	0.36	7.91	33.12	7.12	6.07	1.15	2.87	0.39
LC-06-07-01	4.69	1.23	46.01	88.45	9.23	2.89	1.17	2.47	0.37	10.37	42.58	8.04	6.57	1.22	3.03	0.42
LC-07-07-01	4.86	1.26	48.10	89.38	9.15	2.96	1.24	2.68	0.41	10.18	41.54	8.07	7.00	1.32	3.31	0.47
LC-10-08-01	2.83	0.47	30.75	60.24	7.41	2.60	1.11	2.30	0.35	7.19	31.14	7.06	6.19	1.15	2.97	0.39
LC-13-08-01	1.86	0.45	21.90	43.56	5.84	2.01	0.94	2.02	0.30	5.29	23.35	5.90	5.46	1.03	2.57	0.34
LC-14-08-01	1.83	0.48	20.98	41.94	5.71	2.02	0.90	1.99	0.30	5.10	22.54	5.77	5.24	0.98	2.47	0.34
LC-20-08-01	3.93	0.86	35.70	66.23	7.30	2.45	1.04	2.22	0.34	7.62	31.69	6.73	5.87	1.12	2.79	0.37
LC-23-08-01	2.81	0.76	30.26	60.36	7.46	2.49	1.06	2.18	0.32	7.30	31.74	6.89	5.99	1.11	2.72	0.37
LC-28-08-01	1.50	0.47	21.18	42.34	5.83	1.99	0.87	1.79	0.27	5.18	22.83	5.61	5.09	0.93	2.33	0.32
LC-32-08-01	2.84	0.75	25.96	49.43	6.34	2.16	0.98	2.18	0.33	5.87	25.16	6.18	5.65	1.08	2.70	0.36
Lunar Crater: Dickson (1997)																
LC11-96	1.00	0.00	17.00	34.00	5.00	1.90	0.80	1.80	0.30	4.00	21.72	5.00	5.00	1.00	2.00	0.30
LC16-96	2.00	1.00	25.00	50.00	7.00	2.40	1.10	2.60	0.40	6.00	23.61	7.00	7.00	1.00	3.00	0.40
LC17-96	2.00	1.00	22.00	43.00	6.00	1.90	0.90	2.20	0.40	5.00	23.15	5.00	5.00	1.00	3.00	0.40
LC18-96	3.00	1.00	31.00	61.00	7.00	2.40	1.10	2.30	0.30	7.00	26.40	7.00	6.00	1.00	3.00	0.40
LC31-96	5.00	1.00	36.00	71.00	8.00	2.10	1.00	2.60	0.40	9.00	36.35	7.00	6.00	1.00	3.00	0.40
LC34-96	2.00	0.00	22.00	43.00	6.00	2.10	0.90	2.00	0.30	5.00	25.91	6.00	6.00	1.00	3.00	0.30
LC38-96	2.00	1.00	22.00	44.00	6.00	2.10	1.10	2.40	0.40	5.00	25.81	6.00	6.00	1.00	3.00	0.40
LC45-96	2.00	1.00	26.00	50.00	7.00	2.30	1.00	2.30	0.40	6.00	23.10	6.00	6.00	1.00	3.00	0.40
Death Valley: Tibbetts (2010)																
DV-08-30	12.00	0.80	68.00	132.00	9.40	2.51	1.10	2.10	0.30	13.90	47.30	7.90	5.90	1.00	2.70	0.36
DV-08-79	16.00	1.90	89.00	169.00	10.40	2.77	1.10	2.60	0.38	19.50	59.20	7.70	5.80	1.10	3.00	0.43
DV-08-87	16.00	1.40	84.00	153.00	9.40	2.48	1.00	2.10	0.31	17.70	52.80	6.80	5.10	0.90	2.70	0.36
DV-08-91	11.00	1.10	67.00	131.00	10.00	2.68	1.10	2.40	0.32	16.10	52.20	7.90	6.00	1.10	3.10	0.41
DV-08-118	20.00	2.50	103.00	167.00	9.30	2.53	1.00	2.40	0.35	18.60	52.80	6.80	5.20	1.00	2.80	0.38
DV-08-121	18.00	2.40	89.00	163.00	9.40	2.48	1.00	2.50	0.38	18.10	54.60	7.10	5.50	1.00	3.00	0.44
DV-08-125	5.00	0.40	9.00	42.50	4.90	1.53	0.80	2.90	0.41	5.68	21.50	5.00	5.20	1.10	3.30	0.48
DV-08-127	22.00	3.00	128.00	206.00	10.90	2.83	1.00	2.20	0.32	22.80	65.30	7.50	5.30	1.00	2.70	0.37
DV-08-130	14.00	1.20	76.00	118.00	7.60	2.23	0.90	2.50	0.35	13.60	42.00	6.10	5.00	1.00	2.90	0.40
DV-08-132A	11.00	1.10	53.00	84.40	6.30	1.86	0.90	2.40	0.34	10.10	32.80	5.50	4.90	1.00	2.80	0.40
DV-08-134	8.00	0.90	24.00	59.20	4.80	1.48	0.70	2.10	0.29	7.23	24.50	4.20	3.90	0.80	2.30	0.34
DV-08-138	9.00	0.80	25.00	50.20	5.00	1.59	0.70	2.00	0.29	6.50	24.00	4.40	4.00	0.80	2.30	0.33
DV-08-144	11.00	0.70	60.00	124.00	10.00	2.71	1.10	2.50	0.37	15.70	53.20	7.90	5.90	1.10	3.10	0.43
DV-08-149	26.00	1.50	88.00	167.00	10.20	2.75	1.10	2.40	0.33	19.20	58.90	7.90	5.50	1.00	2.90	0.40
DV-08-154	12.00	1.00	53.00	84.00	6.50	1.92	0.90	2.50	0.37	10.40	34.90	5.70	5.00	1.00	2.90	0.42
DV-07-15	20.00	2.80	95.00	184.00	10.30	2.76	1.00	2.50	0.37	17.90	56.50	7.40	5.20	1.00	2.80	0.40
DV-07-20	17.00	2.00	84.00	161.00	9.80	2.66	1.00	2.40	0.36	16.20	53.30	7.10	5.10	0.90	2.70	0.39
DV-08-27	11.00	1.00	81.00	138.00	10.70	2.96	1.20	2.70	0.37	17.30	57.40	8.60	6.30	1.20	3.30	0.46
DV-08-29	8.00	0.80	31.00	95.70	7.80	2.17	0.90	2.50	0.37	10.30	37.20	6.40	5.00	0.90	2.80	0.41
DV-08-34	17.00	1.20	88.00	180.00	11.00	2.96	1.10	2.40	0.35	18.30	59.30	7.90	5.30	1.00	2.70	0.38
DV-08-39	16.00	1.10	99.00	178.00	11.10	2.99	1.00	2.50	0.35	18.10	59.70	8.00	5.40	1.00	2.80	0.39
DV-08-42	11.00	0.60	49.00	109.00	9.50	2.64	1.10	2.60	0.36	13.90	48.50	7.80	6.10	1.20	3.30	0.45
DV-08-46	9.00	0.60	73.00	97.60	7.80	2.14	0.90	2.00	0.28	12.30	41.00	6.20	4.60	0.90	2.50	0.34
DV-08-56	8.00	0.80	51.00	77.40	6.50	1.79	0.80	2.30	0.32	9.65	33.40	5.40	4.60	0.90	2.60	0.37
DV-08-63	9.00	0.60	39.00	67.90	5.20	1.58	0.70	1.80	0.25	8.10	26.90	4.60	3.80	0.70	2.20	0.30
DV-08-69	11.00	0.70	33.00	65.20	6.30	1.92	0.80	2.60	0.39	7.35	28.00	5.50	4.70	0.90	2.80	0.42
DV-08-72	14.00	1.00	67.00	128.00	7.80	2.14	0.90	2.50	0.38	12.80	43.50	5.90	4.80	0.90	2.70	0.40
DV-08-86	16.00	1.30	59.00	151.00	9.50	2.52	0.90	2.10	0.32	15.30	51.20	6.80	4.80	0.90	2.50	0.35
DV-08-89	13.00	1.10	64.00	128.00	7.60	2.08	0.80	2.10	0.31	12.60	42.50	5.60	4.10	0.80	2.30	0.33
DV-08-92	15.00	1.00	72.00	121.00	7.20	1.96	0.70	2.00	0.29	11.90	39.30	5.30	3.90	0.70	2.10	0.31
DV-08-96	11.00	1.50	63.00	129.00	9.90	2.64	1.00	2.30	0.33	13.70	47.40	7.20	5.50	1.00	2.80	0.38
DV-08-102	12.00	0.80	39.00	123.00	9.00	2.52	1.00	2.80	0.40	13.00	44.90	6.90	5.40	1.00	3.00	0.44
DV-08-108	9.00	0.70	42.00	78.00	6.00	1.71	0.80	2.60	0.39	8.09	28.80	5.20	4.60	0.90	2.80	0.41
DV-08-110	14.00	0.90	78.00	160.00	11.80	3.14	1.20	2.70	0.38	16.90	58.60	8.60	6.10	1.10	3.20	0.44
Southern Quinn Canyon Range: This Study																
Q1	12.10	2.20	52.70	107.00	8.10	1.91	0.90	2.90	0.42	12.50	41.00	6.40	5.00	1.00	3.00	0.46
Q2	3.10	1.40	44.80	88.70	9.00	2.87	1.30	3.20	0.46	10.10	38.30	8.50	7.10	1.40	3.90	0.53
Q90	4.00	1.60	47.10	91.90	9.30	2.87	1.30	3.30	0.49	10.40	40.00	8.60	7.30	1.40	4.00	0.55
Q91	2.60	1.00	33.00	65.70	7.60	2.60	1.10	2.60	0.35	7.65	30.40	7.40	6.00	1.10	3.20	0.43
Crater Flat: Farmer et al., 1989																
CF-12-6-10	6.20	1.20	72.00	132.00	8.30	2.40	1.90	3.60	0.75	……	53.00	……	……	……	……	……
CF-11-7-1	6.70	2.20	92.00	181.00	7.10	3.00	2.00	3.40	0.54	……	77.20	……	……	……	……	……
FB78-5	10.00	3.40	137.00	192.00	9.60	3.60	1.50	3.20	0.97	……	78.10	……	……	……	……	……

Sample	Th	U	La	Ce	Sm	Eu	Tb	Yb	Lu	Pr	Nd	Gd	Dy	Ho	Er	Tm
Crater Flat: Bradshaw and Smith (1994)																
C9-1-8	13.00	……	121.00	233.00	11.33*	2.74	……	2.69	0.34	……	75.00*	……	……	……	……	……
C9-1-9	12.40	……	118.00	219.00	11.74*	2.54	1.19	2.42	0.15	……	78.33*	……	……	……	……	……
C9-2-28	15.20	……	143.00	277.00	13.08*	3.13	1.61	1.72	0.38	……	89.98*	……	6.65	……	……	……
C9-2-30	12.90	……	128.00	243.00	12.34*	2.90	……	2.03	……	……	83.18*	……	6.39	……	……	……
C9-2-31	14.70	……	156.00	277.00	13.85*	2.85	1.09	3.13	……	……	96.18*	……	6.02	……	……	……
C9-2-34	13.80	……	141.00	268.00	13.24*	2.92	1.07	2.10	0.29	……	90.98*	……	6.18	……	……	……
C9-2-37	11.80	……	**120.00**	214.00	11.88*	2.61	1.83	2.49	0.33	……	78.38*	……	5.18	……	……	……
C9-2-41	11.60	……	122.00	209.00	12.19*	2.52	0.87	2.91	0.28	……	81.92*	……	6.46	……	……	……
C9-2-44	10.50	……	121.00	212.00	12.32*	2.43	……	3.31	……	……	82.54*	……	7.83	……	……	……
C9-2-46	15.60	……	154.00	295.00	13.55*	3.05	1.41	2.56	0.29	……	94.09*	……	5.74	……	……	……
Reveille Range Episode 1: Yogodzinski et al., 1996																
R9-1-48	1.96	……	21.00	41.90	4.70	1.64	0.66	1.71	0.28	……	21.55	……	……	……	……	……
R9-3-60	2.66	……	29.20	62.80	6.64	2.20	0.81	2.33	0.29	……	31.36	……	……	……	……	……
R9-4-61	2.66	……	29.20	59.10	6.47	1.99	1.03	2.32	0.39	……	30.33	……	……	……	……	……
R9-1-56	2.63	……	30.50	61.40	7.14	2.24	0.90	2.28	0.32	……	33.24	……	……	……	……	……
R8-1-29	2.92	……	31.80	63.90	7.31	2.28	0.96	2.14	0.29	……	34.60	……	……	……	……	……
R8-1-17	2.40	……	25.00	52.90	6.28	1.82	0.69	2.03	0.30	……	29.03	……	……	……	……	……
R8-1-7	2.41	……	24.70	51.70	5.49	1.98	0.82	2.04	0.27	……	25.25	……	……	……	……	……
R9-2-59	3.04	……	33.30	70.70	7.31	2.32	1.12	2.37	0.37	……	34.73	……	……	……	……	……
R0-1-77	1.98	……	27.20	55.40	6.56	2.15	0.87	2.14	0.26	……	30.07	……	……	……	……	……
Reveille Range Episode 1: Rash (1995)																
RR-46	2.76	0.79	34.90	72.10	6.87	2.36	1.31	2.46	0.30	……	32.20	……	……	……	……	……
Reveille Range Episode 2: Yogodzinski et al., 1996																
R8-1-18	3.33	……	35.00	69.00	9.77	3.25	1.37	2.97	0.47	……	42.06	……	……	……	……	……
R8-1-19	2.48	……	27.00	54.00	7.79	2.54	1.28	2.63	0.38	……	32.50	……	……	……	……	……
R8-1-22	4.53	……	44.00	84.00	8.15	2.38	1.00	2.30	0.37	……	41.56	……	……	……	……	……
R8-1-27	4.05	……	38.00	79.00	8.27	2.54	0.98	2.09	0.34	……	40.28	……	……	……	……	……
R9-1-46	3.88	……	36.00	78.00	8.96	2.64	1.24	2.45	0.38	……	40.59	……	……	……	……	……
R9-1-47	6.38	……	59.00	116.00	10.29	3.01	1.14	2.33	0.34	……	54.93	……	……	……	……	……
R9-1-55	5.31	……	55.00	106.00	8.88	2.76	1.36	2.45	0.34	……	48.21	……	……	……	……	……
Reveille Range Episode 2: Rash (1995)																
RR-28	4.94	1.21	56.20	109.00	7.96	2.90	0.99	2.23	0.27	……	43.15	……	……	……	……	……
Nevada Test Site: Farmer et al., 1989																
TS6-15-2	3.40	0.80	41.00	118.00	7.90	2.66	1.16	3.16	0.34	……	43.50	……	……	……	……	……
TS9-22-1	5.20	1.20	83.00	162.00	10.40	2.66	1.15	3.11	0.32	……	64.60	……	……	……	……	……
TS6-14-7A	3.60	0.80	28.00	71.00	5.40	1.73	0.91	2.11	0.33	……	24.60	……	……	……	……	……
CIMA Domes: Farmer et al., 1989																
PB-34	……	……	……	……	7.60	……	……	……	……	……	36.00	……	……	……	……	……
Reveille Range Tracy-Andesite: Yogodzinski et al., 1996																
R8-1-16	8.46	……	62.90	130.00	14.78	3.95	2.37	5.33	0.75	……	65.67	……	……	……	……	……
R9-1-43	9.77	……	73.00	137.00	13.73	2.30	2.03	5.11	0.68	……	65.64	……	……	……	……	……
R9-1-62	10.30	……	82.30	155.00	14.21	2.64	1.85	4.70	0.68	……	67.22	……	……	……	……	……
R8-1-42	……	……	……	……	13.67	……	……	……	……	……	65.36	……	……	……	……	……

Sample	{87}Sr/{86}Sr	{143}Nd/{144}Nd	EpNd	{206}Pb/{204}Pb	{207}Pb/{204}Pb	{208}Pb/{204}Pb	Sm	Nd	Rb	Sr
Lunar Crater: Stickney (2004)										
LC-01-05-01	0.703666	0.512914	5.38	19.23	15.637	38.703	9.391	43.968	42.90	910.00
LC-02-06-01	0.703332	0.512905	5.20	19.466	15.616	38.952	6.85	27.084	22.10	634.00
LC-03-06-01	0.703622	0.512903	5.17	19.309	15.702	38.846	9.754	46.904	51.60	1119.00
LC-04-07-01	0.703388	0.512911	5.32	19.387	15.59	38.845	8.843	40.44	41.00	931.00
LC-05-07-01	0.703438	0.512907	5.24	19.388	15.601	38.851	7.727	33.115	32.60	790.00
LC-06-07-01	0.703721	0.512893	4.97	19.212	15.627	38.668	9.228	42.576	43.90	888.00
LC-07-07-01	0.70338	0.512907	5.24	19.4	15.596	38.825	9.149	41.541	42.70	933.00
LC-10-08-01	0.703372	0.512893	4.97	19.449	15.584	38.866	7.411	31.14	22.00	773.00
LC-13-08-01	0.703274	0.512914	5.38	19.369	15.548	38.735	5.84	23.352	17.60	568.00
LC-14-08-01	0.703337	0.512912	5.34	0	0	0	5.709	22.541	16.10	569.00
LC-20-08-01	0.703355	0.512923	5.56	19.418	15.584	38.749	7.301	31.686	36.70	676.00
LC-23-08-01	0.703535	0.51292	5.50	19.171	15.58	38.543	7.46	31.74	24.70	717.00
LC-28-08-01	0.703374	0.51292	5.50	19.499	15.603	38.876	5.829	22.83	12.40	568.00
LC-32-08-01	0.703446	0.512902	5.15	19.458	15.607	38.925	6.339	25.162	21.20	608.00
Lunar Crater: Dickson (1997)										
LC11-96	0.7032	0.512905	5.20	19.482	15.634	38.948	5	21.7192	13.00	518.00
LC16-96	0.70365	0.512871	4.55	19.4	15.663	39.043	7	23.6129	23.00	505.00
LC17-96	0.704728	0.51281	3.35	19.375	15.653	39.005	6	23.1495	21.00	479.00
LC18-96	0.703253	0.512928	5.66	19.37	15.614	38.825	7	26.3975	28.00	669.00
LC31-96	0.70765	0.512247	-7.60	18.753	15.626	38.976	8	36.3462	43.00	659.00
LC34-96	0.703313	0.512919	5.49	19.431	15.621	38.938	6	25.9124	19.00	505.00
LC38-96	0.704802	0.512766	2.49	19.354	15.664	39.033	6	25.8101	17.00	448.00
LC45-96	0.703311	0.512933	5.76	19.428	15.609	38.857	7	23.0977	21.00	613.00
Death Valley: Tibbetts (2010)										
DV-08-30	0.707631	0.512063207	-11.21	18.10434212	15.58596451	38.83633128	9.40	47.30	27.00	866.00
DV-08-79	0.707487	0.51203788	-11.71	18.16507544	15.57553019	38.6784396	10.40	59.20	29.00	945.00
DV-08-87	0.707053	0.512096242	-10.57	18.21217884	15.60312094	38.73488688	9.40	52.80	22.00	994.00
DV-08-91	0.707973	0.512059019	-11.29	18.12588942	15.57726653	38.80534148	10.00	52.20	23.00	907.00
DV-08-118	0.706940	0.512100271	-10.49	18.22681096	15.58265362	38.5830216	9.30	52.80	24.00	929.00
DV-08-121	0.707161	0.512079367	-10.90	18.20636608	15.57011237	38.60973864	9.40	54.60	26.00	925.00
DV-08-125	0.709790	0.512305593	-6.48	18.20566454	15.60312094	40.53075408	4.90	21.50	13.00	461.00
DV-08-127	0.707399	0.511977463	-12.89	18.36120598	15.58817177	38.73227544	10.90	65.30	31.00	1086.00
DV-08-130	0.706501	0.512236389	-7.83	18.20857092	15.56910907	38.63133324	7.60	42.00	24.00	778.00
DV-08-132A	0.706402	0.512218574	-8.18	17.85589674	15.52834499	38.52898488	6.30	32.80	20.00	611.00
DV-08-134	0.706516	0.5123854	-4.93	18.42234018	15.59258629	38.8858482	4.80	24.50	38.00	633.00
DV-08-138	0.706113	0.512515859	-2.38	18.57267018	15.5962985	38.82648816	5.00	24.00	11.00	804.00
DV-08-144	0.707374	0.512040858	-11.65	18.00362102	15.55576518	38.71319184	10.00	53.20	19.00	791.00
DV-08-149	0.707108	0.512052507	-11.42	18.11737072	15.53650182	38.53601568	10.20	58.90	40.00	1605.00
DV-08-154	0.707285	0.512263197	-7.31	18.08930912	15.5651962	38.71530108	6.50	34.90	29.00	705.00
DV-07-15	0.707062	0.512114	-10.21	18.254	15.545	38.462	10.30	56.50	23.00	953.00
DV-07-20	0.707600	0.512093	-10.63	18.142	15.550	38.599	9.80	53.30	30.00	1000.00
DV-08-27	0.707400	0.512072	-11.05	17.942	15.550	38.692	10.70	57.40	21.00	803.00
DV-08-29	0.706789	0.512186	-8.82	17.822	15.519	38.854	7.80	37.20	31.00	633.00
DV-08-34	0.707490	0.512079	-10.90	18.059	15.545	38.497	11.00	59.30	26.00	1026.00
DV-08-39	0.707219	0.512083	-10.83	18.047	15.541	38.481	11.10	59.70	24.00	973.00
DV-08-42	0.707468	0.512103	-10.43	18.027	15.559	38.771	9.50	48.50	19.00	754.00
DV-08-46	0.707452	0.512076	-10.96	17.912	15.528	38.633	7.80	41.00	19.00	813.00
DV-08-56	0.706620	0.512203	-8.48	17.764	15.521	38.840	6.50	33.40	30.00	605.00
DV-08-63	0.706322	0.512187	-8.79	17.975	15.533	38.608	5.20	26.90	16.00	645.00
DV-08-69	0.706925	0.512471	-3.26	18.509	15.587	38.820	6.30	28.00	12.00	798.00
DV-08-72	0.707417	0.512081	-10.87	18.146	15.555	38.821	7.80	43.50	21.00	753.00
DV-08-86	0.707494	0.512083	-10.83	18.167	15.557	38.615	9.50	51.20	23.00	959.00
DV-08-89	0.707163	0.512075	-10.98	17.827	15.512	38.237	7.60	42.50	32.00	902.00
DV-08-92	0.707191	0.512114	-10.21	17.776	15.526	38.283	7.20	39.30	31.00	892.00
DV-08-96	0.707792	0.512073	-11.02	18.040	15.520	38.622	9.90	47.40	28.00	910.00
DV-08-102	0.706358	0.512181	-8.92	18.464	15.574	38.662	9.00	44.90	12.00	861.00
DV-08-108	0.707928	0.512182	-8.89	18.390	15.591	39.603	6.00	28.80	22.00	673.00
DV-08-110	0.707486	0.512029	-11.88	18.001	15.543	38.643	11.80	58.60	24.00	900.00
Southern Quinn Canyon Range: This Study										
Q1	0.708723	0.512178329	-8.97	19.08479438	15.67545887	39.11314392	5.330423	33.58523	90	797
Q2	0.704499	0.512773665	2.65	19.09952672	15.6374338	38.93526468	7.198169	34.2909	35	658
Q90	0.704585	0.512750685	2.20	19.12628546	15.62970839	38.97066978	7.655478	36.88507	43	622
Q91	0.704687	0.512830875	3.76	19.26659346	15.63552753	38.95334388	5.938793	26.81807	28	892
Crater Flat: Farmer et al., 1989										
CF-12-6-10	0.70747	0.511303	-10.41	. . . . .	. . . . .	. . . . .	11.9	53	26.1	878
CF-11-7-1	0.70704	0.511372	-9.06	. . . . .	. . . . .	. . . . .	12.3	77.2	19.9	1444
FB785	0.70701	0.511374	-9.02	. . . . .	. . . . .	. . . . .	12	78.1	22	1297

Sample	{87}Sr/{86}Sr	{143}Nd/{144}Nd	EpNd	{206}Pb/{204}Pb	{207}Pb/{204}Pb	{208}Pb/{204}Pb	Sm	Nd	Rb	Sr
Crater Flat: Bradshaw and Smith (1994)										
C9-1-8	0.70691	0.51214	-9.69	18.481	15.585	38.46	11.33	75	20	1276
C9-1-9	0.7069	0.512147	-9.55	18.494	15.586	38.461	11.74	78.33	20.4	1301
C9-2-28	0.70703	0.512195	-8.62	18.555	15.603	38.533	13.08	89.98	19.8	1769
C9-2-30	0.70696	0.512161	-9.28	18.498	15.586	38.48	12.34	83.18	18.9	1462
C9-2-31	0.70711	0.512196	-8.60	18.56	15.591	38.502	13.85	96.18	19.9	1848
C9-2-34	0.707	0.512169	-9.12	18.565	15.624	38.609	13.24	90.98	19.8	1641
C9-2-37	0.70691	0.512147	-9.55	18.446	15.575	38.421	11.88	78.38	22	1308
C9-2-41	0.70697	0.512159	-9.32	18.479	15.579	38.453	12.19	81.92	20	1363
C9-2-44	0.70691	0.512135	-9.79	18.491	15.586	38.496	12.32	82.54	19.3	1339
C9-2-46	0.70704	0.512185	-8.81	18.563	15.583	38.496	13.55	94.09	17.1	1771
Reveille Range Episode 1: Yogodzinski et al., 1996										
R9-1-48	0.70487	0.512799	3.17	19.075	15.642	38.74	4.7	21.55	21.8	616
R9-3-60	0.70586	0.512718	1.59	19.208	15.627	38.844	6.64	31.36	21	625
R9-4-61	0.70597	0.51268	0.85	18.957	15.634	38.661	6.47	30.33	25.4	619
R9-1-56	0.70611	0.512682	0.88	19.033	15.641	38.79	7.14	33.24	27.1	644
R8-1-29	0.70553	0.512757	2.35	19.18	15.695	38.828	7.31	34.6	29.3	608
R8-1-17	0.70429	0.512866	4.47	19.205	15.637	38.842	6.28	29.03	20.7	552
R8-1-7	0.70427	0.512816	3.50	18.964	15.625	38.603	5.49	25.25	21.7	595
R9-2-59	0.70423	0.512859	4.34	19.158	15.605	38.704	7.31	34.73	11.3	306
R0-1-77	0.70556	0.512742	2.06	18.987	15.659	38.688	6.56	30.07	20.5	703
Reveile Range Episode 2: Yogodzinski et al., 1996										
R8-1-18	0.70355	0.512869	4.53	19.331	15.627	38.932	9.77	42.06	25.3	569
R8-1-19	0.70347	0.512911	5.35	19.296	15.601	38.837	7.79	32.5	20.1	519
R8-1-22	0.70351	0.512869	4.53	19.232	15.661	38.92	8.15	41.56	49.7	793
R8-1-27	0.70339	0.512857	4.30	19.066	15.59	38.688	8.27	40.28	29.5	733
R9-1-46	0.70337	0.512822	3.62	19.13	15.593	38.727	8.96	40.59	28.9	728
R9-1-47	0.70346	0.512833	3.83	19.375	15.616	38.971	10.29	54.93	41.2	1070
R9-1-55	0.70359	0.512817	3.52	19.196	15.681	38.822	8.88	48.21	44.7	1034
Reveille Range Tracy-andesite: Yogodzinski et al., 1996										
R8-1-16	0.70368	0.512833	3.83	19.366	15.673	39.112	14.78	65.67	64.6	286
R8-1-42	0.70476	0.512804	3.26	19.489	15.705	39.256	13.67	65.36	94.6	87
R9-1-43	0.70635	0.512826	3.69	19.397	15.614	39.001	13.73	65.64	89.5	109
R9-1-62	0.70491	0.512804	3.26	19.419	15.64	39.061	14.21	67.22	95.2	79
Reveille Range: Rash (1995)										
RR-28	0.7036	0.512885	4.92	19.28	15.565	38.758	7.96	43.15	44.3	1087
RR-46	0.7055	0.512669	0.75	19.218	15.615	38.87	6.87	32.2	28.3	703
Nevada Test Site: Farmer et al., 1989										
TS6-15-2	0.70671	0.511772	-1.26	19.172	15.638	38.995	8.52	43.5	26.3	694
TS9-22-1	0.7072	0.511396	-8.61	18.359	15.598	38.737	8.75	64.6	32.1	805
TS6-14-7A	0.70387	0.511949	2.20	18.491	15.599	38.258		24.6	9.14	595
Cima Domes: Farmer et al., 1989										
PB-34	0.70303	0.512297	9.00	. . . . .	. . . . .	. . . . .	7.6	36	40.2	644

Sample	Sc	Cr	Co	Ni	Rb	Sr	V	Y	Zr	Nb	Cs	Ba	Hf	Ta	W	Pb
							Lunar Crater: Stickney (2004)									
LC-01-05-01	26.33	449.62	……	213.10	42.90	910.00	……	32.05	231.00	92.25	0.38	603.66	5.50	4.90	48.94	2.20
LC-02-06-01	28.32	198.97	……	177.42	22.10	634.00	……	29.37	168.00	51.66	0.35	352.63	4.29	2.73	41.55	1.61
LC-03-06-01	22.95	260.58	……	113.72	51.60	1119.00	……	32.76	261.00	103.91	0.52	784.63	5.85	5.63	50.28	2.91
LC-04-07-01	21.98	196.41	……	108.79	41.00	931.00	……	32.75	246.00	74.42	0.37	597.81	5.73	4.28	34.50	2.28
LC-05-07-01	29.15	233.00	……	148.09	32.60	790.00	……	29.95	194.00	65.94	0.24	572.53	4.68	3.57	31.94	2.03
LC-06-07-01	27.68	573.16	……	217.82	43.90	888.00	……	31.68	223.00	85.84	0.47	600.28	5.33	4.72	71.10	2.16
LC-07-07-01	23.21	219.27	……	194.21	42.70	933.00	……	34.45	251.00	85.92	0.49	639.92	5.89	4.35	52.67	2.69
LC-10-08-01	25.71	179.24	……	121.75	22.00	773.00	……	30.27	166.00	52.77	0.19	521.56	4.26	2.94	54.64	1.45
LC-13-08-01	28.20	276.35	……	177.08	17.60	568.00	……	26.42	128.00	40.93	0.13	338.61	3.40	2.14	37.32	1.06
LC-14-08-01	27.70	297.22	……	173.38	16.10	569.00	……	25.62	125.00	40.67	0.12	360.66	3.25	2.10	45.09	1.07
LC-20-08-01	30.00	296.20	……	153.91	36.70	676.00	……	28.51	204.00	71.70	0.32	510.08	4.98	3.60	34.12	1.90
LC-23-08-01	28.76	304.44	……	155.05	24.70	717.00	……	28.60	157.00	61.09	0.22	433.49	4.02	3.14	42.78	1.37
LC-28-08-01	22.87	259.04	……	339.86	12.40	568.00	……	24.33	116.00	35.59	0.08	341.92	3.07	1.90	36.77	0.85
LC-32-08-01	21.42	233.89	……	165.95	21.20	608.00	……	27.05	167.00	44.14	0.21	395.71	4.19	2.50	38.76	1.47
							Lunar Crater: Dickson (1997)									
LC11-96	27.00	249.00	……	261.00	13.00	518.00	……	24.00	124.00	25.00	0.00	227.00	2.80	1.90	……	1.00
LC16-96	24.00	98.00	……	75.00	23.00	505.00	……	34.00	193.00	30.00	0.00	307.00	5.10	2.30	……	1.66
LC17-96	26.00	244.00	……	179.00	21.00	479.00	……	27.00	163.00	25.00	0.00	300.00	4.10	1.90	……	1.60
LC18-96	26.00	185.00	……	135.00	28.00	669.00	……	28.00	180.00	44.00	0.00	411.00	4.30	3.30	……	1.25
LC31-96	24.00	38.00	……	48.00	43.00	659.00	……	31.00	233.00	13.00	1.00	718.00	5.80	1.20	……	6.76
LC34-96	24.00	194.00	……	134.00	19.00	505.00	……	27.00	149.00	29.00	0.00	358.00	3.70	2.20	……	1.31
LC38-96	23.00	133.00	……	82.00	17.00	448.00	……	32.00	182.00	22.00	0.00	359.00	4.70	1.90	……	2.23
LC45-96	26.00	182.00	……	140.00	21.00	613.00	……	29.00	160.00	38.00	0.00	385.00	4.00	2.60	……	1.39
							Death Valley: Tibbetts (2010)									
DV-08-30	26.00	30.00	55.00	29.00	27.00	866.00	293.00	19.00	297.00	20.00	< 0.5	1089.00	11.00	1.10	104.00	6.00
DV-08-79	26.00	40.00	32.00	26.00	29.00	945.00	254.00	20.00	382.00	24.00	1.00	1382.00	18.00	1.60	46.00	8.00
DV-08-87	24.00	50.00	161.00	41.00	22.00	994.00	262.00	18.00	343.00	26.00	0.60	1441.00	14.00	1.40	409.00	……
DV-08-91	27.00	30.00	43.00	27.00	23.00	907.00	352.00	19.00	289.00	19.00	< 0.5	1334.00	11.00	1.10	74.00	……
DV-08-118	23.00	90.00	41.00	47.00	24.00	929.00	219.00	18.00	375.00	24.00	1.20	1359.00	16.00	1.70	75.00	5.00
DV-08-121	24.00	< 20	107.00	16.00	26.00	925.00	198.00	19.00	379.00	25.00	0.80	1390.00	18.00	1.50	257.00	9.00
DV-08-125	35.00	200.00	135.00	80.00	13.00	461.00	226.00	18.00	194.00	4.00	< 0.5	376.00	4.00	0.30	283.00	1.00
DV-08-127	24.00	70.00	28.00	51.00	31.00	1086.00	239.00	18.00	428.00	32.00	3.00	1673.00	20.00	2.00	36.00	12.00
DV-08-130	24.00	90.00	32.00	57.00	24.00	778.00	274.00	18.00	317.00	20.00	< 0.5	905.00	9.00	1.40	40.00	5.00
DV-08-132A	29.00	150.00	127.00	75.00	20.00	611.00	230.00	17.00	244.00	17.00	1.10	855.00	4.00	1.10	316.00	1.00
DV-08-134	22.00	80.00	144.00	46.00	38.00	633.00	176.00	17.00	224.00	12.00	3.40	975.00	6.00	0.90	391.00	3.00
DV-08-138	32.00	140.00	106.00	53.00	11.00	804.00	247.00	14.00	179.00	10.00	< 0.5	595.00	5.00	0.80	230.00	1.00
DV-08-144	27.00	80.00	178.00	46.00	19.00	791.00	322.00	19.00	306.00	21.00	< 0.5	1048.00	10.00	1.30	421.00	1.00
DV-08-149	27.00	50.00	37.00	41.00	40.00	1605.00	250.00	39.00	505.00	41.00	0.60	1400.00	14.00	1.70	53.00	10.00
DV-08-154	26.00	170.00	35.00	93.00	29.00	705.00	210.00	22.00	250.00	13.00	< 0.5	908.00	10.00	1.10	68.00	5.00
DV-07-15	23.00	110.00	163.00	57.00	23.00	953.00	203.00	19.00	369.00	25.00	0.50	1350.00	13.00	1.50	387.00	0.00
DV-07-20	25.00	40.00	148.00	29.00	30.00	1000.00	276.00	23.00	346.00	22.00	0.70	1612.00	8.00	1.40	373.00	6.00
DV-08-27	29.00	70.00	165.00	39.00	21.00	803.00	333.00	19.00	327.00	24.00	0.50	1109.00	11.00	1.30	401.00	……
DV-08-29	26.00	110.00	124.00	60.00	31.00	633.00	268.00	19.00	236.00	16.00	< 0.5	814.00	7.00	1.10	289.00	5.00
DV-08-34	22.00	70.00	74.00	38.00	26.00	1026.00	276.00	19.00	381.00	26.00	0.80	1413.00	18.00	1.50	166.00	4.00
DV-08-39	23.00	70.00	76.00	39.00	24.00	973.00	242.00	19.00	377.00	27.00	0.70	1401.00	16.00	1.50	142.00	7.00
DV-08-42	26.00	100.00	112.00	48.00	19.00	754.00	342.00	19.00	285.00	19.00	< 0.5	930.00	10.00	1.10	212.00	1.00
DV-08-46	27.00	50.00	100.00	39.00	19.00	813.00	316.00	19.00	325.00	22.00	< 0.5	1082.00	11.00	1.00	213.00	1.00
DV-08-56	23.00	120.00	123.00	60.00	30.00	605.00	245.00	18.00	220.00	14.00	< 0.5	745.00	9.00	1.00	278.00	2.00
DV-08-63	31.00	140.00	140.00	66.00	16.00	645.00	223.00	15.00	198.00	11.00	< 0.5	672.00	6.00	0.70	295.00	2.00
DV-08-69	30.00	200.00	120.00	100.00	12.00	798.00	232.00	17.00	232.00	10.00	0.90	707.00	8.00	0.60	290.00	2.00
DV-08-72	24.00	250.00	141.00	134.00	21.00	753.00	213.00	18.00	305.00	17.00	< 0.5	1082.00	12.00	1.00	351.00	4.00
DV-08-86	27.00	90.00	119.00	62.00	23.00	959.00	293.00	17.00	325.00	25.00	0.50	1329.00	16.00	1.40	274.00	……
DV-08-89	23.00	200.00	182.00	51.00	32.00	902.00	206.00	17.00	288.00	17.00	0.80	1562.00	8.00	1.10	467.00	6.00
DV-08-92	23.00	90.00	180.00	60.00	31.00	892.00	214.00	17.00	281.00	16.00	0.50	1629.00	10.00	1.00	485.00	7.00
DV-08-96	28.00	20.00	86.00	23.00	28.00	910.00	332.00	19.00	291.00	19.00	< 0.5	1046.00	14.00	1.20	185.00	2.00
DV-08-102	28.00	80.00	142.00	49.00	12.00	861.00	256.00	18.00	313.00	20.00	0.50	844.00	11.00	1.30	347.00	……
DV-08-108	28.00	30.00	87.00	14.00	22.00	673.00	230.00	18.00	255.00	12.00	< 0.5	765.00	7.00	0.80	259.00	3.00
DV-08-110	26.00	50.00	77.00	32.00	24.00	900.00	291.00	20.00	356.00	25.00	0.50	1228.00	13.00	1.40	158.00	3.00
							Southern Quinn Canyon Range: This Study									
Q1	16.00	60.00	274	< 20	90.00	797.00	140	29.00	266.00	13.00	1.80	1070.00	6.80	1.10	714.00	12.00
Q2	15.00	30.00	221	< 20	35.00	658.00	151	33.00	122.00	39.00	< 0.5	628.00	3.80	3.20	465.00	< 5
Q90	14.00	40.00	43	< 20	43.00	622.00	152	34.00	237.00	45.00	< 0.5	664.00	6.80	3.80	103.00	< 5
Q91	16.00	20.00	50	< 20	28.00	892.00	197	28.00	110.00	35.00	< 0.5	420.00	3.30	3.10	85.00	< 5
							Crater Flat: Farmer et al., 1989									
CF-12-6-10	29.00	……	……	……	26.10	878.00	……	……	……	……	0.70	780.00	6.20	……	……	……
CF-11-7-1	19.00	……	……	……	19.90	1444.00	……	……	……	……	1.50	1330.00	8.00	……	……	……
FB78-5	22.00	……	……	……	22.00	1297.00	……	……	……	……	2.00	1140.00	8.50	……	……	……

Sample	Sc	Cr	Co	Ni	Rb	Sr	V	Y	Zr	Nb	Cs	Ba	Hf	Ta	W	Pb
Crater Flat: Bradshaw and Smith (1994)																
C9-1-8	19.10	110.10	27.90	44.20	20.00	1276.00	161.00	22.80	406.00	36.90	……	1740.00	8.01	1.82	……	13.61
C9-1-9	17.40	135.30	25.30	46.10	20.40	1301.00	176.00	23.30	420.00	35.80	……	1747.00	7.47	1.60	……	18.62
C9-2-28	17.80	48.00	23.80	39.20	19.80	1769.00	150.00	23.40	414.00	35.50	……	2006.00	7.42	1.19	……	16.44
C9-2-30	17.10	82.40	24.20	40.50	18.90	1462.00	155.00	23.40	435.00	37.60	……	1823.00	7.70	1.67	……	14.02
C9-2-31	16.40	95.60	23.10	45.70	19.90	1848.00	162.00	23.60	423.00	35.30	……	2030.00	6.32	1.41	……	15.86
C9-2-34	16.90	16.90	24.00	35.20	19.80	1641.00	158.00	23.40	424.00	36.50	……	1856.00	7.98	1.65	……	16.04
C9-2-37	17.70	17.70	25.20	48.10	22.00	1308.00	168.00	22.80	397.00	36.40	……	1698.00	7.38	1.59	……	14.89
C9-2-41	16.30	16.30	23.10	46.30	20.00	1363.00	171.00	23.00	406.00	33.20	……	1738.00	7.51	1.39	……	14.19
C9-2-44	14.60	14.60	21.10	42.70	19.30	1339.00	158.00	22.90	406.00	35.10	……	1687.00	6.65	1.45	……	13.86
C9-2-46	17.60	17.60	25.10	36.40	17.10	1771.00	167.00	22.80	415.00	33.90	……	1839.00	8.32	1.67	……	15.46
Reveille Range Episode 1: Yogodzinski et al., 1996																
R9-1-48	20.90	146.00	36.00	64.00	21.80	616.00	……	21.40	186.00	26.00	……	325.00	4.03	1.68	……	2.49
R9-3-60	19.60	81.00	42.00	51.00	21.00	625.00	……	24.80	239.00	35.00	……	406.00	5.67	2.33	……	3.20
R9-4-61	19.60	59.00	40.00	40.00	25.40	619.00	……	24.60	269.00	35.00	……	436.00	6.05	1.86	……	7.17
R9-1-56	20.10	81.00	40.00	37.00	27.10	644.00	……	25.00	258.00	35.00	……	379.00	5.80	2.25	……	3.79
R8-1-29	20.70	77.00	38.00	48.00	29.30	608.00	……	26.30	268.00	35.00	……	500.00	5.90	2.37	……	2.02
R8-1-17	22.00	75.00	42.00	……	20.70	552.00	……	……	……	32.00	……	387.00	5.38	2.30	……	2.26
R8-1-7	22.70	116.00	41.00	56.00	21.70	595.00	……	23.20	212.00	34.00	……	302.00	4.91	2.07	……	2.80
R9-2-59	20.60	32.00	38.00	……	11.30	306.00	……	……	……	51.00	……	583.00	5.38	2.70	……	3.03
R0-1-77	19.60	54.00	45.00	29.00	20.50	703.00	……	22.60	248.00	31.00	……	965.00	6.00	2.32	……	2.85
Reveille Range Episode 1: Rash (1995)																
RR-46	18.90	67.00	41.50	48.00	28.30	703.00		37.90	226.00	33.30	……	339.00	6.41	2.32	……	3.06
Reveille Range Episode 2: Yogodzinski et al., 1996																
R8-1-18	20.70	35.00	39.00	18.00	25.30	569.00	……	33.20	371.00	31.00	……	454.00	7.89	3.09	……	2.43
R8-1-19	21.40	97.00	39.00	46.00	20.10	519.00	……	27.60	298.00	37.00	……	409.00	6.56	2.39	……	1.90
R8-1-22	26.10	195.00	46.00	131.00	49.70	793.00	……	26.80	334.00	55.00	……	559.00	6.83	3.97	……	3.93
R8-1-27	30.00	348.00	53.00	193.00	29.50	733.00	……	24.20	316.00	49.00	……	557.00	6.81	3.53	……	3.24
R9-1-46	17.50	102.00	39.00	68.00	28.90	728.00	……	28.30	338.00	48.00	……	542.00	7.03	3.31	……	3.10
R9-1-47	16.50	38.00	31.00	23.00	41.20	1070.00	……	27.00	505.00	73.00	……	768.00	8.97	5.27	……	3.90
R9-1-55	11.70	14.00	25.00	9.00	44.70	1034.00	……	26.80	379.00	62.00	……	812.00	7.28	4.56	……	3.47
Reveille Range Episode 2: Rash (1995)																
RR-28	11.40	37.00	28.20	41.00	44.30	1087.00	……	32.80	304.00	67.60	……	445.00	7.25	4.55	……	3.14
Nevada Test Site: Farmer et al., 1989																
TS6-15-2	20.00	……	……	……	26.30	694.00	……	……	……	……	0.20	759.00	6.30	……	……	……
TS9-22-1	19.00	……	……	……	32.10	805.00	……	……	……	……	0.40	1515.00	8.90	……	……	……
TS6-14-7A	27.00	……	……	……	9.14	595.00	……	……	……	……	1.30	413.00	3.90	……	……	……
CIMA Domes: Farmer et al., 1989																
PB-34	……	……	……	……	40.20	644.00	……	……	……	……	……	……	……	……	……	……
Reveille Range Tracy-Andesite: Yogodzinski et al., 1996																
R8-1-16	12.40	19.00	9.00	1.00	64.60	286.00	……	51.90	879.00	64.00	……	849.00	16.70	4.85	……	5.77
R9-1-43	5.9	11	2	1	89.5	109	……	48	953	84	……	353	18.2	6.41	……	6.33
R9-1-62	6.5	3	2	1	95.20	79.00	……	48.5	947	88	……	364	18.8	6.46	……	4.99
R8-1-42	……	……	……	1.00	94.6	87.00	……	45.90	814.00	76.00	……	……	……	……	……	5.98

APPENDIX F

Southern Quinn Canyon Range Petrographic Descriptions

Correlated Unit	Sample Number	Textures	Minerology	Description
Andesite on west side	Q1	Phaneritic	50% pf, 40% cpx, 10% hb	fine-medium sized phenocrysts; microcrystalline matrix
younger east side basalt	Q2	Phaneritic	80% pf, 20% cpx	fine-medium sized phenocrysts; microcrystalline matrix; olivine in matrix; Iron oxides rims around cpx
not correlated	Q4	Phaneritic	45% pf, 35% b, 20% cpx, negligible amount of embayed q	medium-fine grained phenocrysts; fine-grained matrix with pf and cpx, cpx rims are oxidized, possilby two generations of pf
Pahranagat Tuff	Q6	Phaneritic	80% fiamme', 20% af	medium-fine grained phenocrysts; pumiceous matrix; matrix dominated;
Pahranagat Tuff	Q7	Phaneritic	80% fiamme', 20% af	fine grained phenocrysts; pumiceous matrix; matrix dominated;
Pahranagat Tuff	Q8	Phaneritic	30% b, 30% pf, 20% af, 10% q, 10% lithic fragments	medium-fine grained phenocryst dominated sample
Cow Canyon Tuff	Q9	Phaneritic	63% fiamme', 20% af, 15% lithic fragments, 2% b	fine-medium sized phenocrysts; pumiceous matrix dominated
Cow Canyon Tuff	Q10	Phaneritic	50% af, 40% q, 10% b	medium-fine grained phenocryst rich sample; sperulites present in
Clifford Spring Tuff	Q14	Aphanitic-Phaneritic	50% af, 30% pf, 20% q	matrix dominated; matrix aphanitic pumice and fine grained crystals
Pahranagat Tuff	Q18	Phaneritic	60% af, 20% q, 20% pf	medium-fine grained phenocrysts; devitrified pumiceous matrix;
Pahranagat Tuff	Q22	Phaneritic	50% pf, 40% cpx, 10% hb	glassy microcrystalline matrix; fine-medium sized phenocrysts
Pahranagat Tuff	Q23	Phaneritic	35% q, 30% pf, 30% af, 5% b	fine-medium grained phenocryst dominated sample; lithic and pumiceous rich matrix; spherulites abundant; highly devitrified; very
Pahranagat Tuff	Q24	Phaneritic	40% af, 30% pf, 20% b, 10% amphibole	medium-fine grained phenocryst rich sample
Pahranagat Tuff	Q25	Aphanitic-Phaneritic	40% af, 40% pumice fragments, 18% pf, 1% b, 1% q	fine grained phenocryst rich matrix dominated sample; matrix highly
Pahranagat Tuff	Q29	Phaneritic	70% pumice fragments, 20% af, 8% q, 2% b	pumiceous matrix dominated; fine grained phenocrysts
Pahranagat Tuff	Q30	Phaneritic	60% af, 40% pumice fragments, 10% q	medium-fine grained phenocrysts; pumiceous matrix
Pahranagat Tuff	Q34	Hypocrystalline	60% pumice fragments, 25% af, 10% lithic fragments, 5% b	vitric pumiceous matrix dominated with lithic fragments; fine grained
Pahranagat Tuff	Q38	Phaneritic	35% q, 30% pf, 30% af, 5% b	fine-medium grained phenocrysts; pumiceous matrix dominated; spherulites present; highly devitrified; very similar to sample Q23
Pahranagat Tuff	Q44	Porphyritic	35% af, 30% pf, 15% q, 10% b, 10% Fe-oxides	medium-fine grained phenocrysts; pumiceous matrix; spherolites
Pahranagat Tuff	Q46	Phaneritic	60% af, 20% q, 10% pf, 10% b	medium-fine grained phenocrysts; pumiceous matrix
Pahranagat Tuff	Q50	Aphanitic-Phaneritic	90% af, 10% pf	fine grained phenocrysts; pumiceous matrix dominated
Pahranagat Tuff	Q55	Phaneritic	80% fiamme', 10% af, 5% q, 5% lithic fragments	fine-medium grained phenocrysts; pumiceous matrix dominated
Cow Canyon Tuff	Q59	Phaneritic	90% af, 7% b, 3% q	pumiceous and lithic fragment dominated matrix; spherulites present
Clifford Spring Tuff	Q61	Phaneritic	60% af, 35% q, 5% b	medium-fine grained phenocrysts; devitrified pumiceous matrix
Cow Canyon Tuff	Q65	Hypocrystalline	100% af; phenocrysts are emplaced in fiamme' bands	pumiceous matrix dominated; highly devitrified, spherulites abundant
Pahranagat Tuff	Q68	Phaneritic	40% pf, 30% hb, 15% pyroxene, 15% amphibole	fine-medium grained phenocrysts; microcrystalline matrix
Clifford Spring Tuff	Q70	Phaneritic	60% af, 40% pumice fragments	medium to fine grained phenocrysts; pumiceous matrix dominated;
Pahranagat Tuff	Q75	Phaneritic	40% af, 30% b, 15% q, 10% hb, 5% pf	fine-medium grained phenocryst dominated sample; matrix is
younger east side andesite	Q82	Phaneritic	50% af, 30% b, 20% q	medium to fine grained phenocrysts; possibly two generations of afs; matrix is microcrystalline
Clifford Spring Tuff	Q83	Phaneritic	90% af, 10% b	fine-medium grained phenocrysts; pumiceous matrix dominated;
younger east side andesite	Q84	Phaneritic	50% pf, 20% hb, 20% b, 10% cpx	medium-fine grained phenocryst dominated sample; microcrystalline matrix
younger east side basalt	Q90	Phaneritic	90% pf, 10% olivine	fine grained phenocryst dominated sample; microcrystalline matrix
younger east side basalt	Q91	Phaneritic	70% pf, 25% cpx, 5% olivine	medium-fine grained phenocrysts; microcrystalline matrix
younger east side andesite	Q92	Phaneritic	70% pf, 20% amphibole, 10% hb	medium-fine grained phenocrysts; microcrystalline matrix
younger east side andesite	Q94	Phaneritic	30% pf, 30% hb, 20% b, 20% cpx	medium-fine grained phenocryst dominated sample; microcrystalline matrix
younger east side andesite	Q95	Phaneritic	50% pf, 30% cpx, 20% q	fine-medium grained phenocrysts; matrix is aphanitic; matrix dominated

APPENDIX G

Southern Quinn Canyon Range Sample Locations

SAMPLE NAME	LATITUDE	LONGITUDE
Q1	37.73741667	-115.8813667
Q2	37.897906613	-115.975458374
Q4	37.881674206	-115.938273903
Q6	37.834941328	-115.987041615
Q7	37.833791617	-115.968057753
Q8	37.833408485	-115.954124035
Q9	37.836708953	-115.914306296
Q10	37.83638333	-115.8575833
Q13	37.82938333	-115.8554667
Q14	37.80825	-115.86385
Q18	37.7434	-115.887583333
Q22	37.75688333	-115.8695
Q23	37.7736	-115.9153833
Q24	37.79423333	-115.9577833
Q25	37.82216667	-115.9539167
Q29	37.82216667	-115.9540667
Q30	37.82466667	-115.9552667
Q33	37.735733333	-115.8882
Q34	37.7588	-115.8718
Q38	37.774016667	-115.935033333
Q42	37.765216667	-115.9384
Q44	37.7614	-115.938333333
Q46	37.799966667	-115.9476
Q50	37.80515	-115.946616667
Q55	37.778843424	-115.932756442
Q56	37.80032672	-115.897005603
Q57	37.793226927	-115.894105482
Q59	37.795493544	-115.89378882
Q61	37.797743331	-115.905705824
Q65	37.784710778	-115.870238118
Q66	37.784527482	-115.867738049
Q68	37.804393034	-115.916072814
Q70	37.806576427	-115.907755934
Q75	37.807309714	-115.909855995
Q78	37.806859627	-115.917156192
Q82	37.847125926	-115.874321926
Q83	37.842276271	-115.857588105
Q84	37.833675722	-115.912106217
Q85	37.828475709	-115.92210646
Q90	37.916673301	-115.942490907
Q91	37.912606684	-115.945857642
Q92	37.942472838	-115.9317241
Q94	37.936122937	-115.935357496
Q95	37.932039741	-115.932707396

APPENDIX H

Pahranagat Tuff Data From Eric Christiansen

Sample Name	Latitude	Longitude	SiO2 %	Al2O3 %	Fe2O3(T) %	MnO %	MgO %	CaO %	Na2O %	K2O %	TiO2 %	P2O5 %	LOI %	Total %
QUINN-2AP	37.9478	-115.8056	77.1	12.6	0.84	0.05	0.19	0.47	2.22	6.42	0.11	0.01	2.76	99.91
QUINN-2BV	37.9478	-115.8056	77.78	12.35	0.79	0.06	0.31	0.67	3.38	4.54	0.12	0.01	1.18	100.35
QUINN-2BL	37.9478	-115.8056	77.91	12.35	0.91	0.08	0.3	0.54	3.02	4.76	0.12	0.01	0.42	99.69
QUINN-2BU1	37.9478	-115.8056	74.06	13.54	1.67	0.07	0.22	1.4	3.83	4.87	0.23	0.12	0.3	100.9
QUINN-2BU2	37.9478	-115.8056	74.81	13.58	1.75	0.07	0.44	1.29	3.16	4.62	0.23	0.06	ND	100.9
QUINN-2BUP	37.9478	-115.8056	77.9	12.46	0.82	0.13	0.16	0.49	3.48	4.44	0.1	0.01	ND	100.9

Sample Name	Latitude	Longitude	Yb ppm	Lu ppm	Hf ppm	Ta ppm	W ppm	Ti ppm	Pb ppm	Th ppm	U ppm	Sc ppm	V ppm	Cr ppm
QUINN-2AP	37.9478	-115.8056	ND	ND	ND	ND	ND	0.09	21	25	7.4	0.6	4.1	7.2
QUINN-2BV	37.9478	-115.8056	ND	ND	ND	ND	ND	0.11	24	27	5.6	3.3	4.4	5
QUINN-2BL	37.9478	-115.8056	ND	ND	ND	ND	ND	0.11	26	27	6	3	6.5	4.2
QUINN-2BU1	37.9478	-115.8056	ND	ND	ND	ND	ND	0.22	20	15	1.5	4	16.2	8.3
QUINN-2BU2	37.9478	-115.8056	ND	ND	ND	ND	ND	0.22	20	15	1.5	4	16.2	8.3
QUINN-2BUP	37.9478	-115.8056	1.78	0.27	4.3	2.3	260	0.1	25	35	1.8	3.5	5.5	3.9

Sample Name	Latitude	Longitude	Ni ppm	Cu ppm	Zn ppm	Ga ppm	Rb ppm	Sr ppm	Y ppm	Zr ppm	Nb ppm	Mo ppm	Sb ppm	Cs ppm
QUINN-2AP	37.9478	-115.8056	0.8	2.5	25	15.3	253	13	27	123	19.2	4	ND	ND
QUINN-2BV	37.9478	-115.8056	2.1	1.7	34	15.1	188	38	21	117	20.7	6	ND	ND
QUINN-2BL	37.9478	-115.8056	0.7	1.6	34	15.1	210	35	22	118	20	5	ND	ND
QUINN-2BU1	37.9478	-115.8056	2.9	3.3	38	14.5	136	241	15	173	10.9	1	ND	ND
QUINN-2BU2	37.9478	-115.8056	2.9	3.3	38	14.5	136	241	15	173	10.9	1	ND	ND
QUINN-2BUP	37.9478	-115.8056	3.9	2.5	29	15.8	268	19	23	136	26.9	3	0.8	5.5

Sample Name	Latitude	Longitude	Ba ppm	La ppm	Ce ppm	Nd ppm	Sm ppm	Eu ppm	Tb ppm
QUINN-2AP	37.9478	-115.8056	38	37	81	28	7.1	ND	ND
QUINN-2BV	37.9478	-115.8056	96	31	67	26	7.1	ND	ND
QUINN-2BL	37.9478	-115.8056	107	38	82	31	8.1	ND	ND
QUINN-2BU1	37.9478	-115.8056	691	41	97	27	6.8	ND	ND
QUINN-2BU2	37.9478	-115.8056	691	41	97	27	6.8	ND	ND
QUINN-2BUP	37.9478	-115.8056	126	31	92	31	7.1	0.48	0.5

*ND = No Data

APPENDIX I

Battleship Butte

Battleship Butte, an alluvial section containing volcanic clasts, was an independent study that is useful for displaying the capability of correlating ash-flow tuff units by major and trace element geochemistry. Located east of the Arrow Canyon Range and south of the Meadow Valley Mountains, Battleship Butte is comprised of two alluvial units; a lower unit with Paleozoic clasts and about 5 % of Tertiary volcanic clasts unconformably overlain by an upper unit with only Paleozoic clasts (Figures 36, 37 and Appendix L). Geochemical analysis of eleven volcanic clasts collected from the lower alluvium at Battleship Butte were used to determine provenance. Possible source areas are: the Kane Springs Wash Caldera, the Caliente Caldera Complex, or both. In addition to testing the ability to correlate ash-flow tuffs, identifying the source of the volcanic clasts provides insight into basin deposition and formation of the lower alluvium unit.

In much of southeastern Nevada, Paleozoic rocks are overlain unconformably by mid-Teriary ash-flow tuffs and lava flows that are related to episodic Cenozoic extensional tectonism that produced a southward sweeping magmatic-volcanic belt in the eastern Basin and Range during Oligocene-Miocene time (Bartley et al., 1988). The 23-13 Ma Caliente and 16-14 Ma Kane Springs Wash Caldera Complexes are the youngest of silicic volcanic centers in this belt and each has a characteristic geochemical signature (Scott et al., 1996).

Ash-flow tuffs of the Caliente Caldera Complex are calc-alkaline with metaluminous, peraluminous, and peralkaline affinities. The Tuff of Etna (14 Ma), a peralkaline tuff, erupted from a caldera within the Caliente Caldera Complex (Nealey et al., 1992). Eruptions from the Kane Springs Wash Caldera Complex volcanic began about 16 Ma with tuffs now preserved north of the caldera. Caldera collapse was related to the eruption of the peralkaline Kane Wash Tuff (14-14.6 Ma), which contains two members, the Gregerson Basin Member and Delamar Tuff (Novak, 1984). After formation of a resurgent dome, eruptions were concentrated within the caldera. These intracladera tuffs are metaluminous. Local metaluminous basalt and andesite flows covered intracaldera and outflow sheets between 12.7-11.5 Ma (Novak, 1984).

Geochemical analysis data using ICP-MS techniques at Activation Laboratories of eleven volcanic clasts from the upper alluvial unit at Battleship Butte were compared to known major and trace element geochemical data from the Caliente Caldera Complex (Nealey et al., 1984) and the Kane Springs Caldera (Novak, 1984). Figures 28, 29, and 30 plot major and trace element geochemical data from Battleship Butte, Caliente Caldera Complex and Kane Springs Caldera on the LeBas et al. (1986) classification diagram in order to show the array of compositions from each area. Because a distinctive trait of ash-flow tuffs from both calderas is their alkaline affinities, samples from Battleship Butte, Caliente Caldera Complex, and Kane Springs Caldera were compared by using the Shand's Index diagram (Maniar and Piccoli, 1989). Battleship Butte and Kane Springs Caldera rhyolite samples plotted as peralkaline (Figure 31 and 32), while Caliente Caldera Complex rhyolite samples plotted as peralkaline, metaluminous, and peraluminous (Figure 33). Comparing rhyolitic ash flow tuffs using Sun and McDonough (1989) primitive mantle normalized spider diagrams, Battleship Butte samples BB1 and BB11 correlate to the Tuff of Etna from the Caliente Caldera Complex (Figure 34), while, BB10 correlates to the Gregerson Basin Member of the Kane Wash

Tuff from the Kane Springs Wash Caldera (Figure 35) by following the same trace element geochemical trends.

Basin sedimentation was contemporaneous with Cenozoic extension in the White River and Meadow Valley Wash basins (DiGuisseppi, 1991). The White River and Meadow Valley Wash basins initially had internal drainage but are now externally drained due to the capture of these basins by the Colorado River system. Increased incision of the captured basins resulted from a tectonically lowered Colorado River system base level (DiGuisseppi, 1991; Bohannon, 1984). Battleship Butte is located to the south of the Meadow Valley Mountains in the White River drainage basin. The White River drainage basin includes the Kane Springs Wash Caldera Complex and the western part of the Meadow Valley Mountains. The Meadow Valley Wash drainage basin includes the Caliente Caldera Complex and the eastern part of the Meadow Valley Mountains.

Since Caliente Caldera Complex and Kane Springs Caldera ash flow tuffs are present in the lower alluvial section of Battleship Butte and the Battleship Butte alluvial units are incised by the current Quaternary drainage system, this suggests that the unconformity between the upper and lower alluvial sections indicates a change of provenance from a mixture of Paleozoic and Tertiary volcanic clasts to only Paleozoic rocks. A possible source for both of these clast types is Paleozoic and Tertiary sections in the Meadow Valley Mountains. Another source for Paleozoic rocks is the Arrow Canyon Range to the east of Battleship Butte. Overall, Battleship Butte provides evidence for the Southern White River and Meadow Valley Wash flow systems transition from internally drained to externally drained basins and subsequent capture by the Colorado River system.

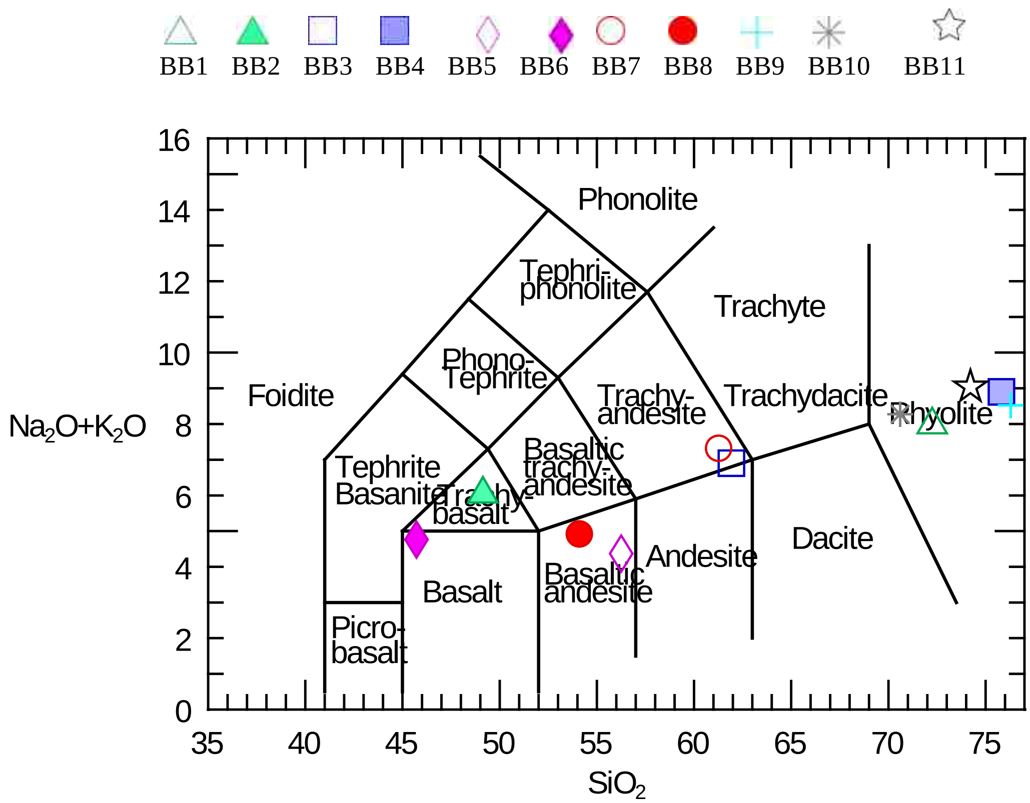

Figure 28: Battleship Butte samples display a wide range of compositions.

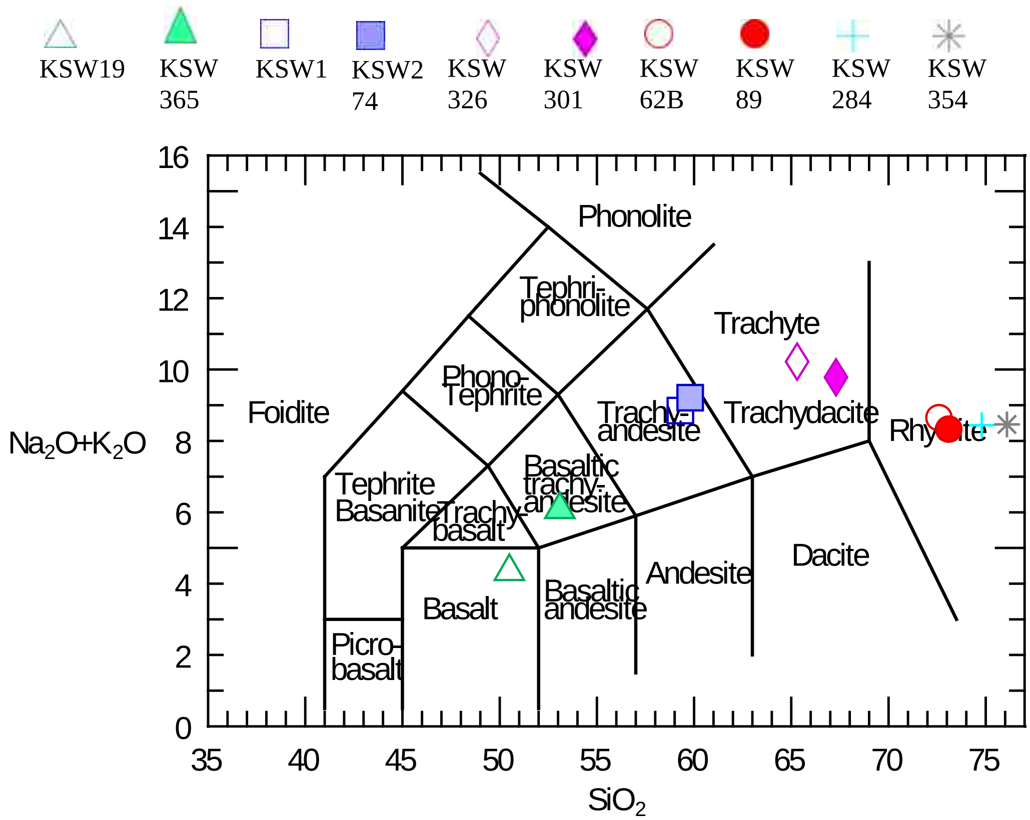

Figure 29: Kane Springs Wash Caldera samples (Novak, 1984) display a wide range of compositions similar to Battleship Butte.

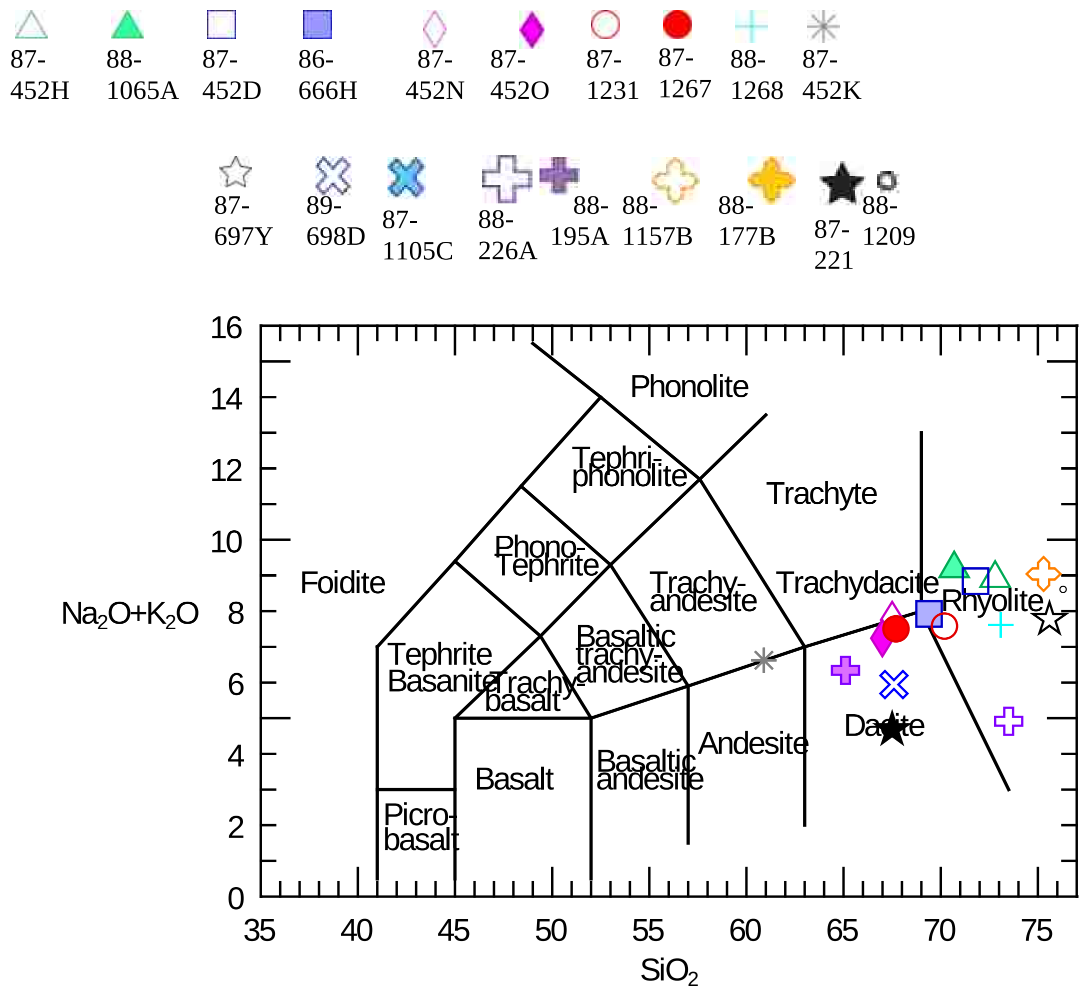

Figure 30: Caliente Caldera Complex samples (Nealey, 1992) display a more concentrated range of compositions.

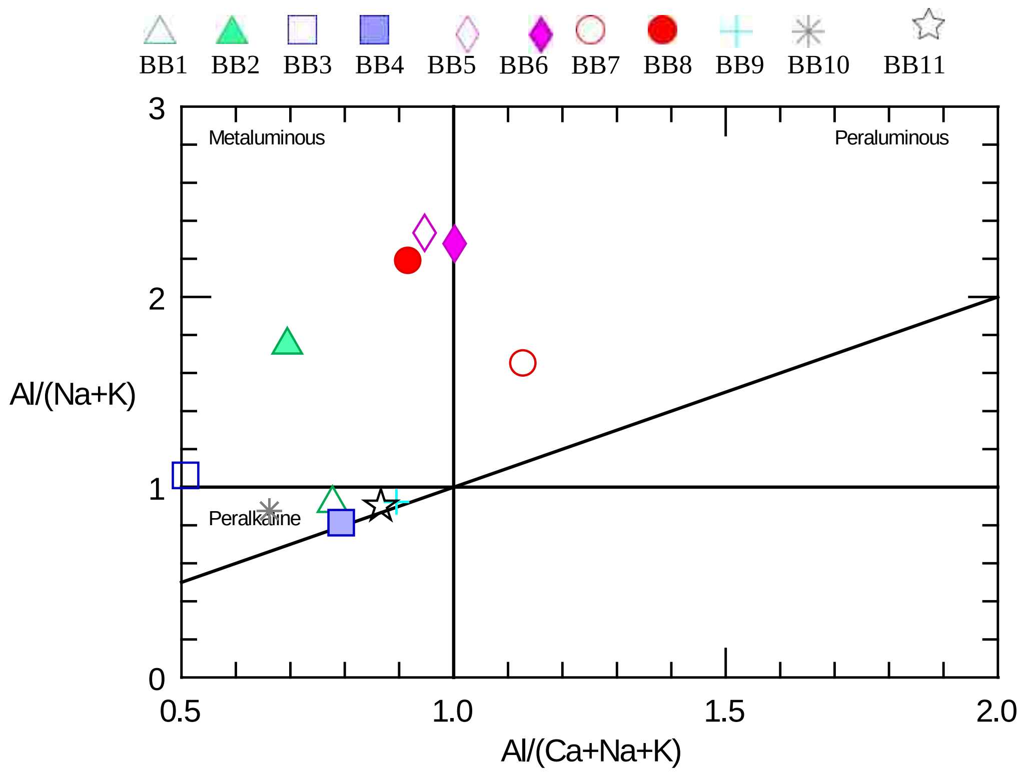

Figure 31: Battleship Butte samples plotted show that rhyolite samples are peralkaline.

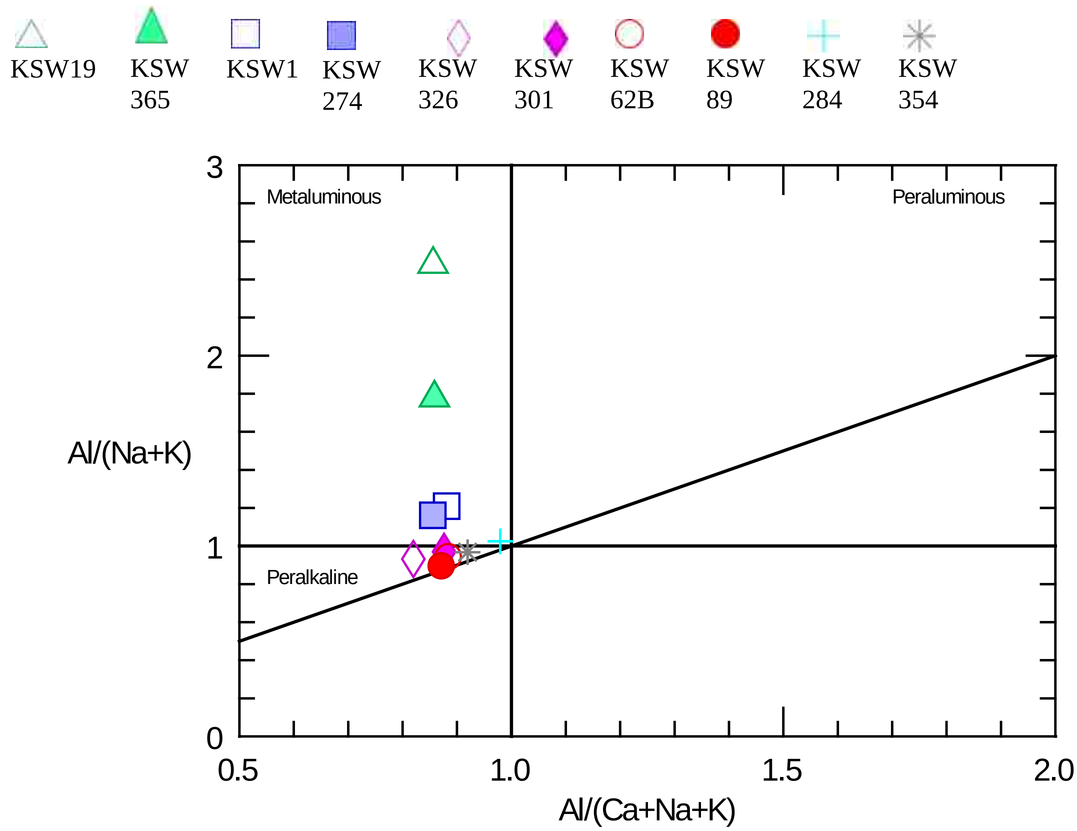

Figure 32: Kane Springs Wash Caldera samples (Novak, 1984) show that all rhyolite samples are peralkaline and have a similar trend to Battleship Butte samples.

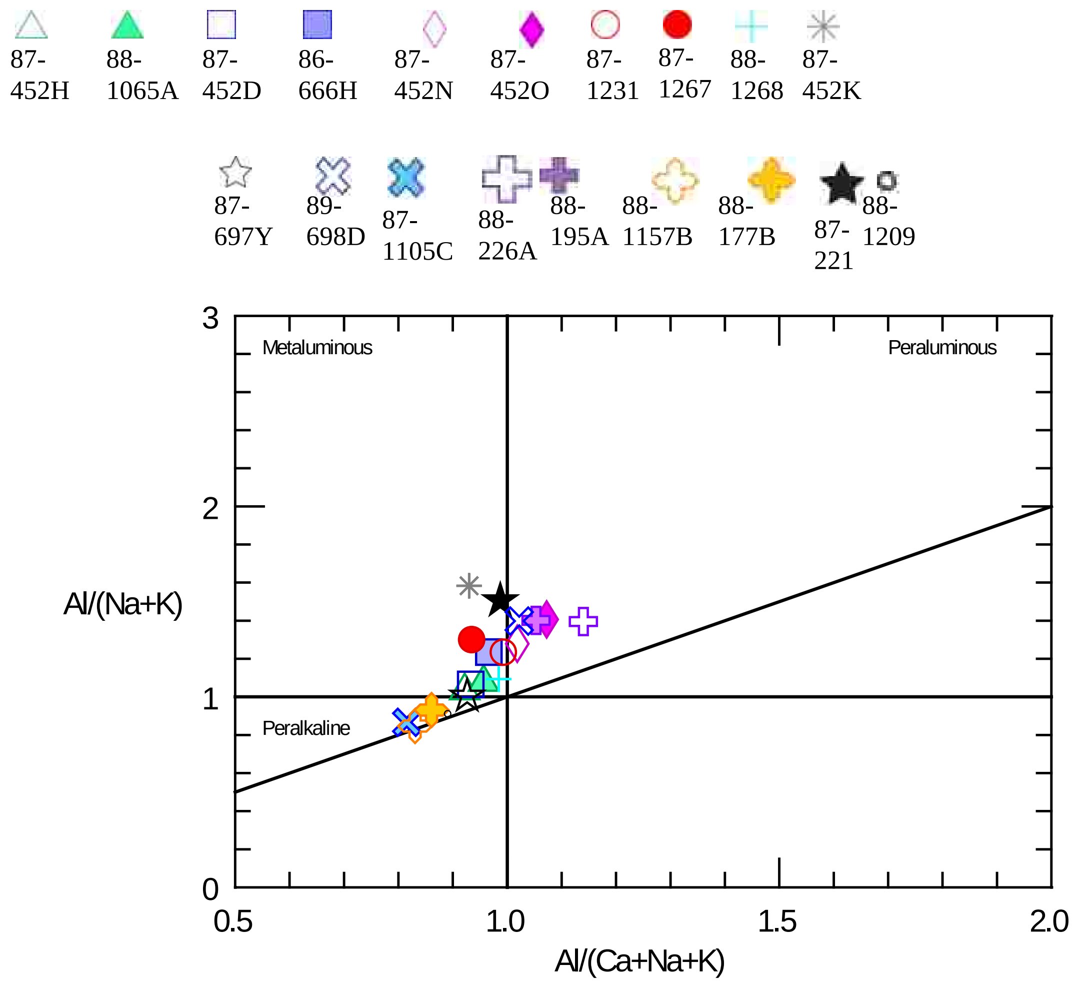

Figure 33: Caliente Caldera Complex samples (Nealey, 1992) show rhyolite samples are peralkaline, metaluminous, and peraluminous.

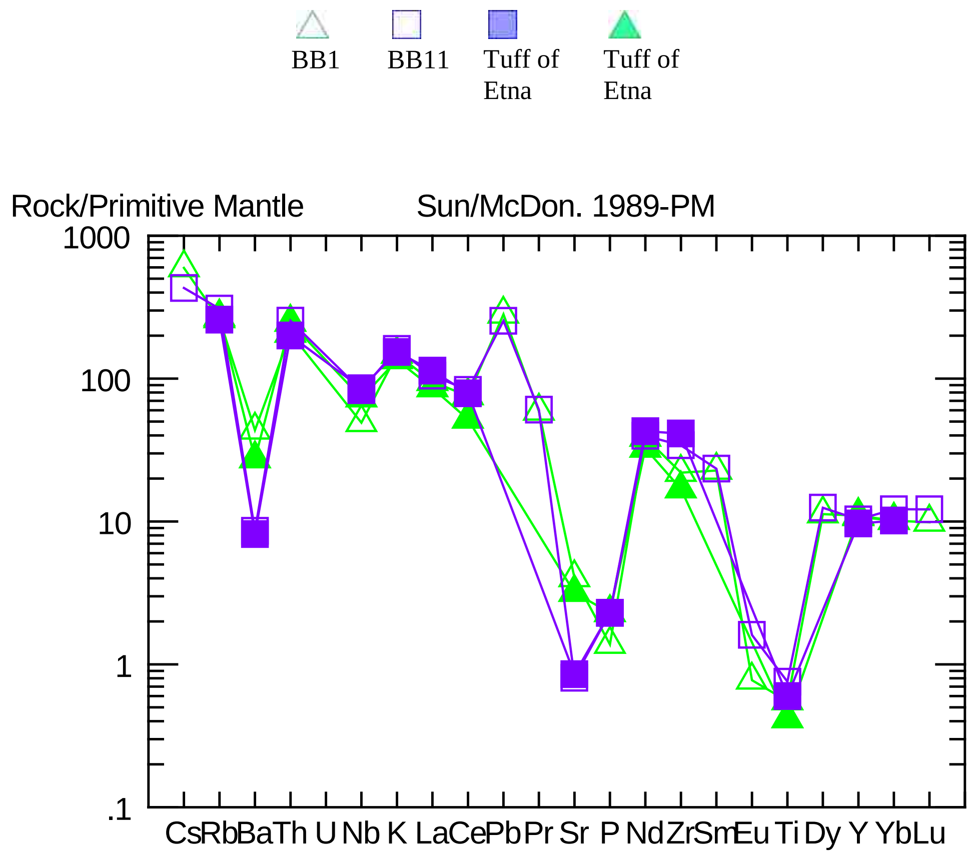

Figure 34: Samples BB1 and BB11 from Battleship Butte plotted with the Tuff of Etna from the Caliente Caldera Complex show correlation to the Tuff of Etna.

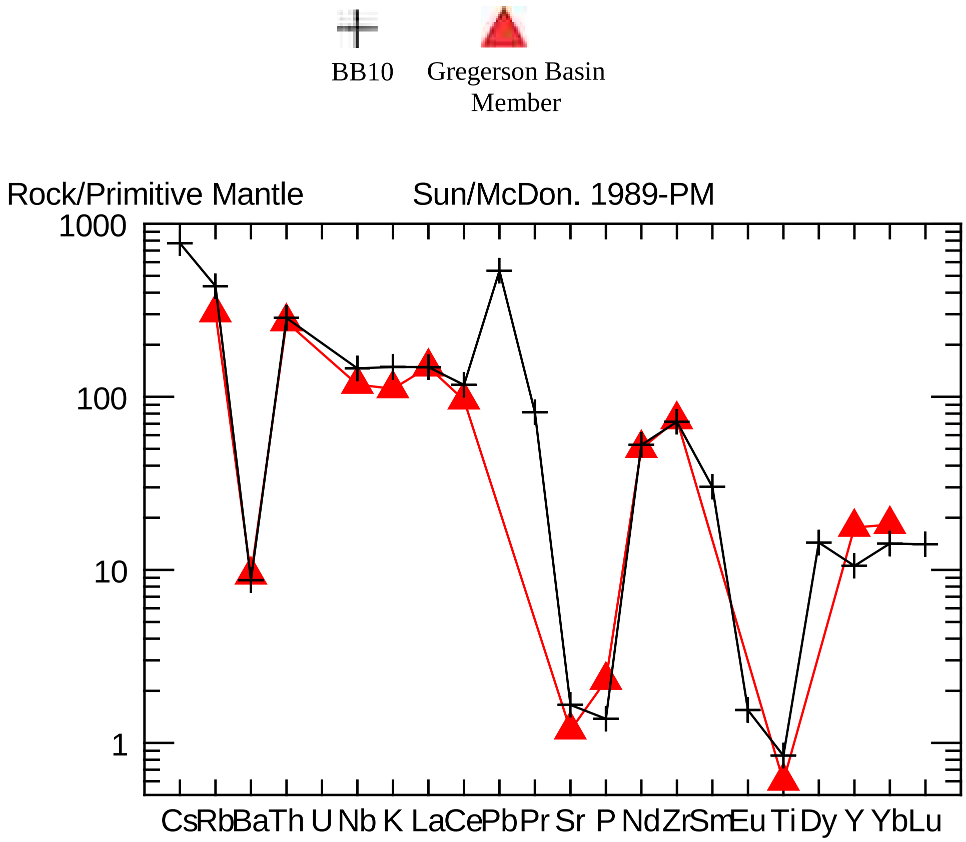

Figure 35: Sample BB10 from Battleship Butte plotted with the Gregerson Basin Member of the Kane Wash Tuff shows correlation to Gregerson Basin Member.

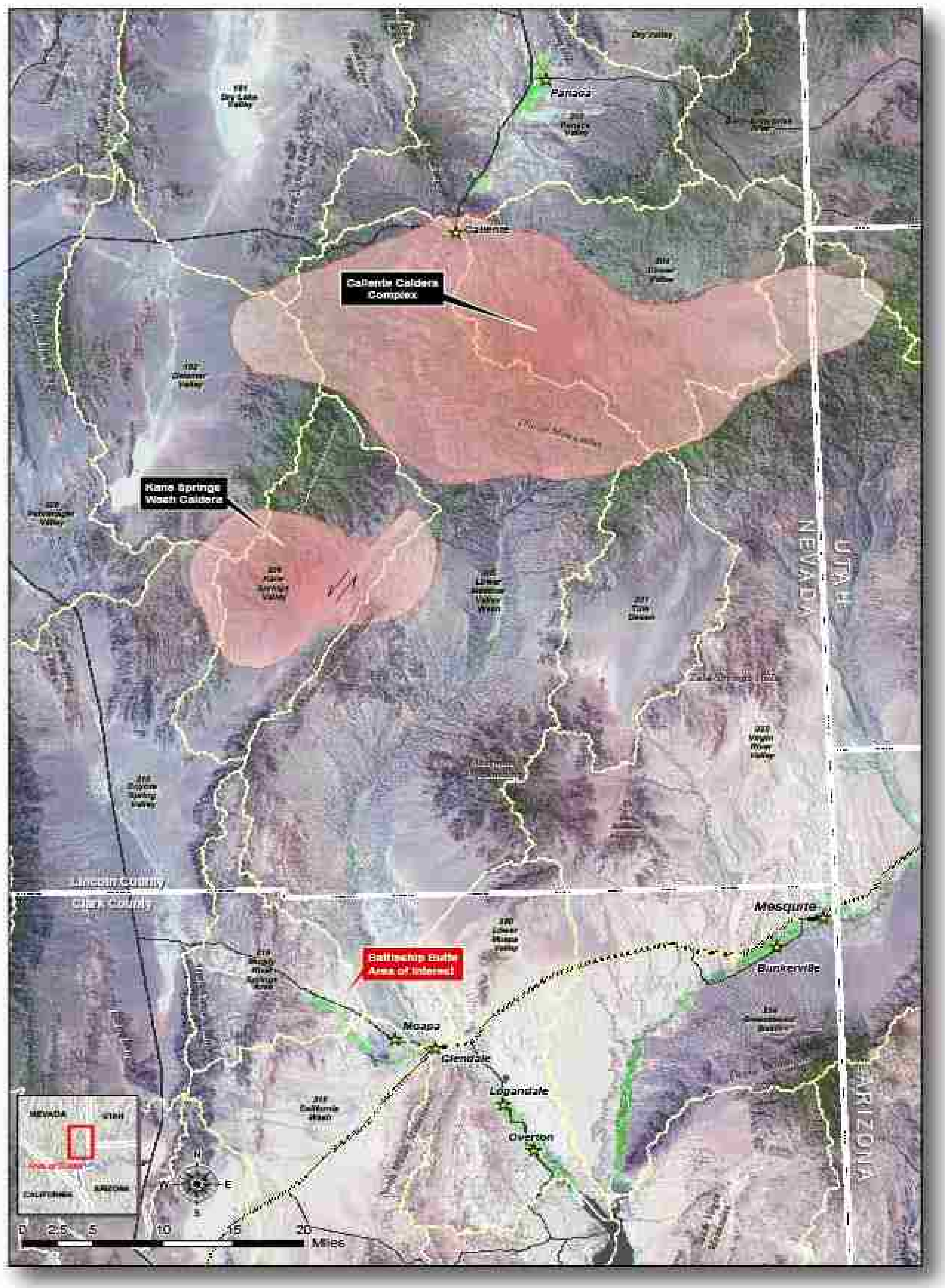

Figure 36: Overview map with imagery taken from 2002 LANDSAT 30 meter imagery. Approximate caldera locations taken from Unruh et al., (1995) BARCO Study.

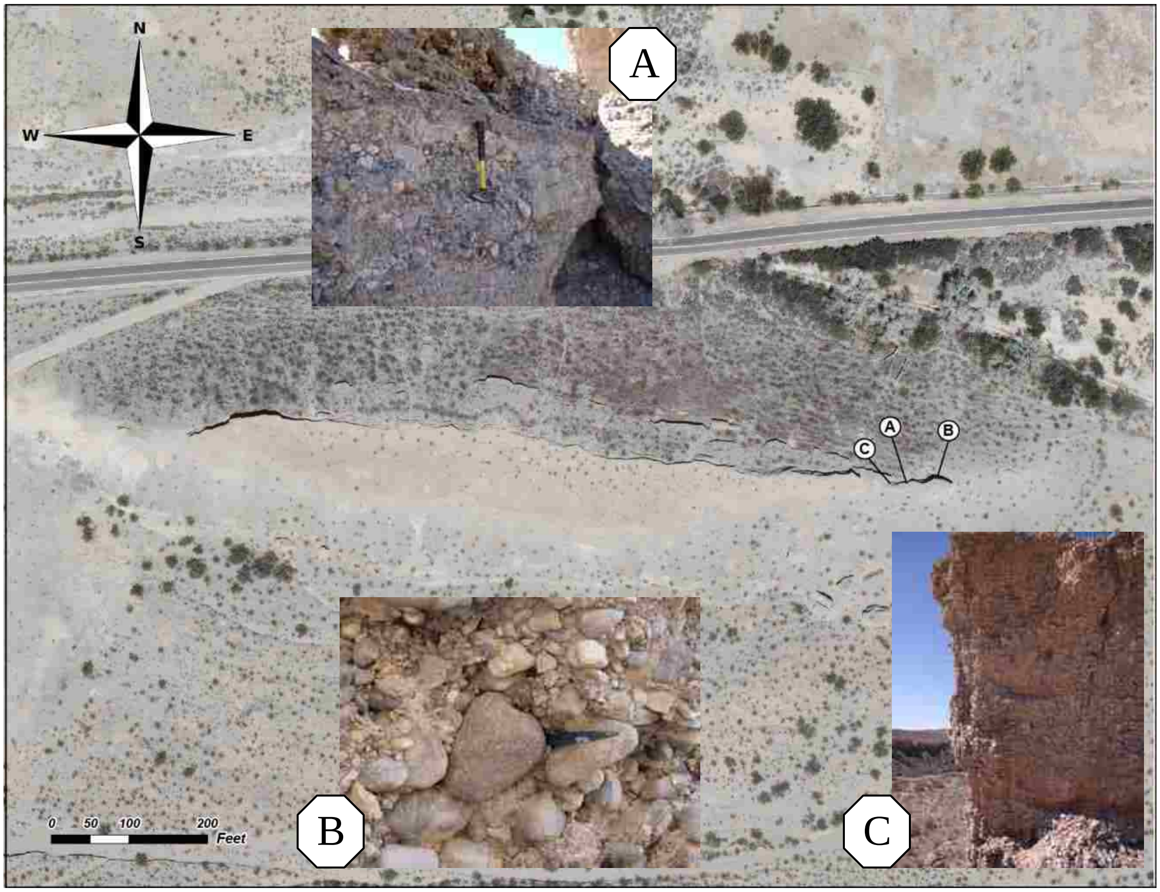

Figure 37: Battleship Butte Study Area.

APPENDIX J

Southern Quinn Canyon Range Geologic Map

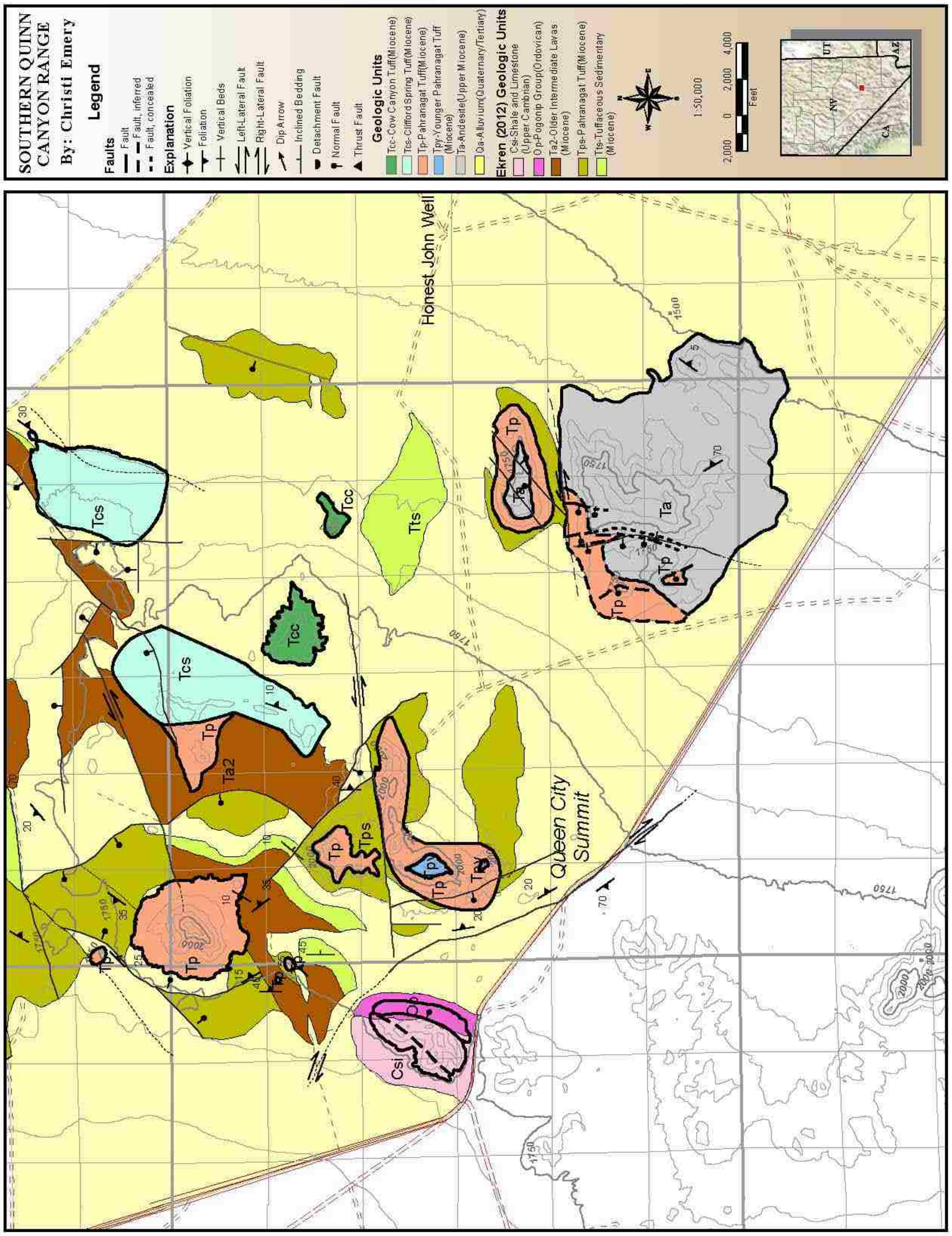

APPENDIX K

Southern Quinn Canyon Range Sample Location Map

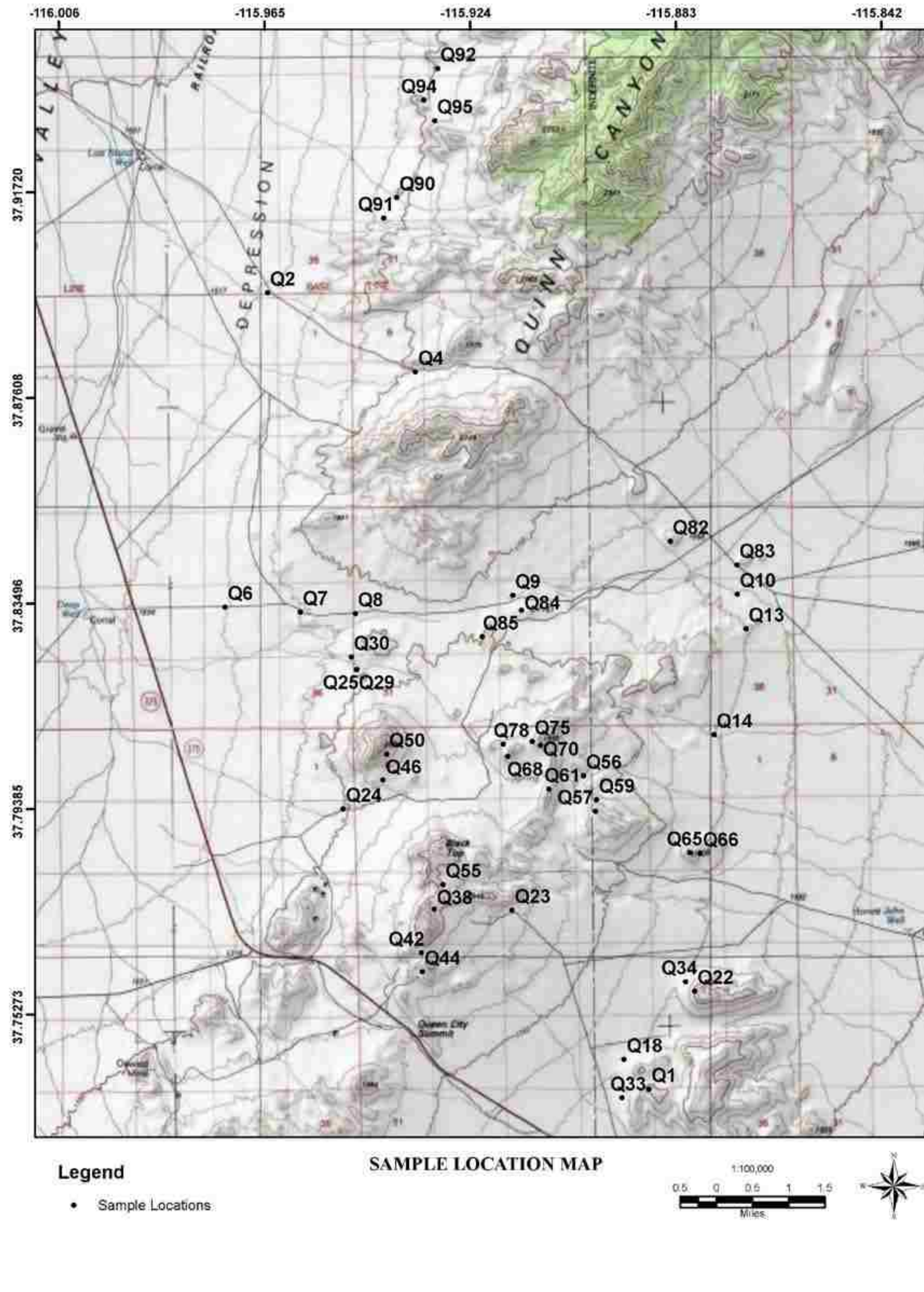

APPENDIX L

Battleship Butte Study Area Map

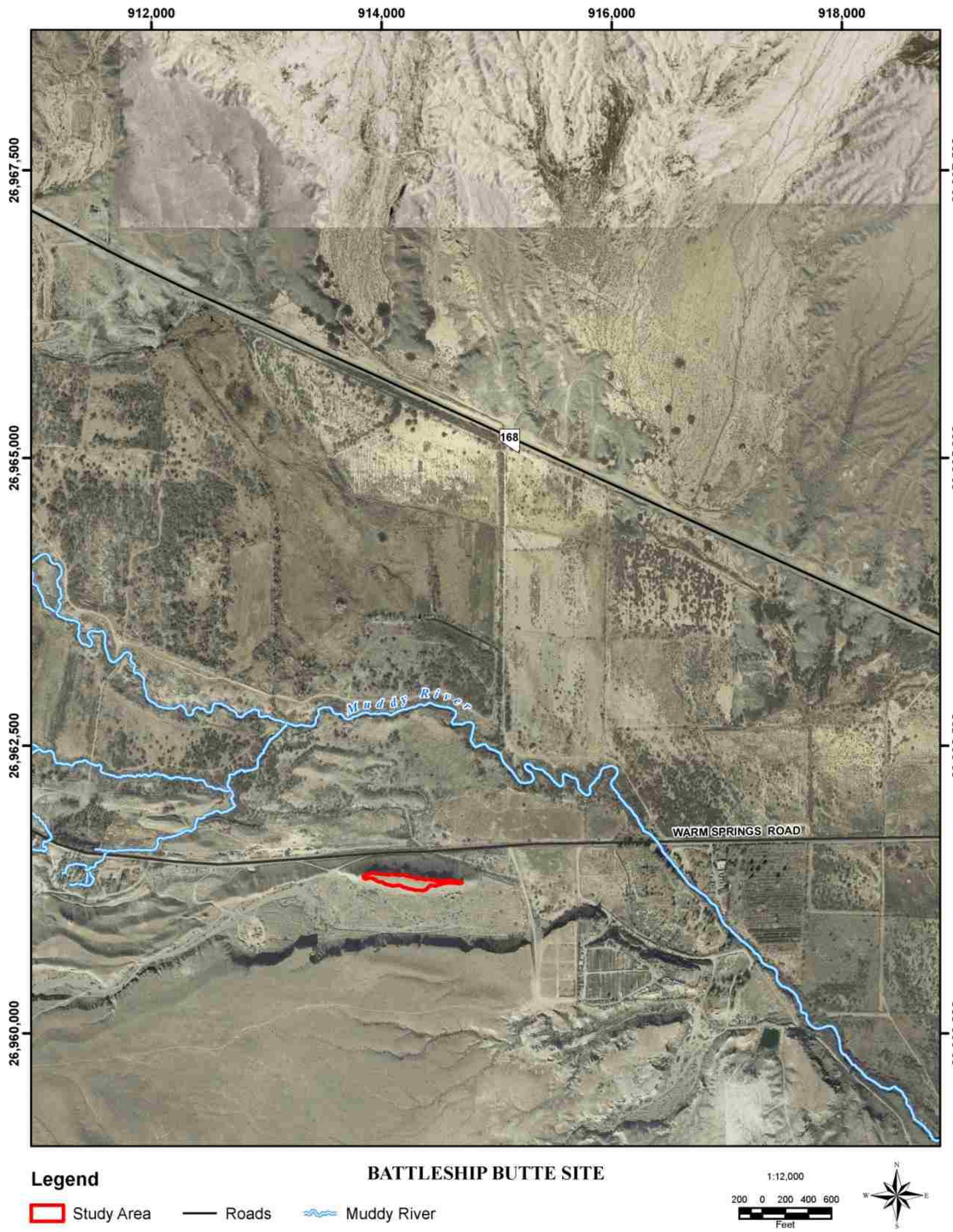

REFERENCES

Axen, G.J., Taylor, W.J., and Bartley, J.M., 1993. Space-time patterns and Tectonic controls of the Tertiary extension and magmatism in the Great Basin of the western United States: Geological Society of America Bulletin, v. 105, p. 56-76.

Bartley, J.M., Axen, G.J., Taylor, W.J., and Fryxell, J.E. (1988). Cenozoic tectonics of a transect through eastern Nevada near 38˚ north latitude. This extended land: Geologic Journeys in the southern Basin and Range, Geological Society of America, Cordilleran section, Field trip guidebook. p. 1-20.

Best, M.G., Christiansen, E.H., Deino, A.L., Gromme, C.S, McKee, E,H., and Noble, D.C., 1989. Excursion 3A: Eocene through Miocene volcanism in the Great Basin of the western United States: New Mexico Bureau of Mines and Mineral Resources Memoir 47, p. 91- 133.

Best, M.G., and Christiansen, E.H., 1991. Limited Extension During Peak Tertiary Volcanism, Great Basin of Nevada and Utah: Journal of Geophysical Research, v. 96, no. B8, p. 13509-13528.

Best, M.G., Christiansen, E.H., Deino, A.L., Gromme, C.S., and Tingey, D.G., 1995. : Correlation and emplacement of a large, zoned, discontinuously exposed ash flow sheet; the $^{40}Ar/^{39}Ar$ chronology, paleomagnetism, and petrology of the Pahranagat Formation, Nevada: Journal of Geophysical Research, v. 100, no. B12, p. 24,593-24,609.

Best, M.G., and Hamblin, W.K., 1978. Origin of the northern Basin and Range province: Implications from the geology of its eastern boundary: Geological Society of America Memoir, 152, p. 313-400.

Bohannon, R. G., 1984, Nonmarine Sedimentary rocks of Tertiary age in the Lake Mead region, southeastern Nevada and northwestern Arizona: U.S. Geological Survey Professional Paper 1259, 72 p.

Bradshaw, T.K. and Smith, E.I., 1994. Polygenetic Quaternary volcanism at Crater Flat, Nevada. Journal of Volcanology and Geothermal Research, v.63, p. 165-182.

Conrad, C.P., B. Wu, E.I. Smith, T.A. Bianco, A. Tibbetts, 2010. Shear-driven upwelling induced by latereal viscosity variations and asthenospheric shear: A mechanism for intraplate volcanism, Physics of the Earth and Planetary Interiors, v. 178, p. 162-175.

Cornwall, H.R., 1972. Geology and mineral resources of southern Nye County, Nevada: Nevada Bureau of Mines and Geology Bulletin 77, 49p.

Cross, T.A., and Pilger, R.H., Jr., 1978. Constraints on absolute motion and plate interaction inferred from Cenozoic igneous activity in the western United States: American Journal of Science, v. 278, p. 865-902.

DiGuiseppi, W.H. and Bartley, J.M. (1991). Stratigraphic effects of change from internal to external drainage in an extending basin, southeastern Nevada. Geological Society of America Bulletin, v. 103, p. 48-55.

Dickson, Loretta D., 1997. Volcanology and Geochemistry of Pliocene and Quaternary Basalts on Citadel Mountain, Lunar Crater Volcanic Field, Pancake Range, Nevada. [M.Sc. thesis]: University of Nevada, Las Vegas, 146 pp.

Druitt, T. H., and Sparks, R.S.J., 1984. On the formation of calderas during ignimbrite eruptions: Nature, v. 310, p. 679-681.

Ekren, E.B., Anderson, R.E., Rogers, C.L., and Noble, D. C., 1971. Geology of the northern Nellis Air Force Bases Bombing and Gunnery Range, Nye County, Nevada: US Geological Survey Professional paper 651, p. 91.

Ekren, E.B., Rogers, C.L., and Dixon, G.L., 1973, Geologic Bouger Gravity map of the Reveille Range quadrangle, Nye County, Nevada: United States Geological Survery Miscellaneous Geologic Investigations Map I-806.

Ekren, E.B., Rowley, Peter D., Dixon, G.L., Page, W.R., Kleinhampl, F.J., Ziony, J.I., Brandt, J.M., and Patrick, B.G. (2012). Geology of the Quinn Canyon Range and Vicinity, Nye and Lincoln Counties, Nevada. Southern Nevada Water Authority Doc. No. HAM-ED-0004.

Farmer, G.L., Perry, F.V., Semken, S., Crowe, B., Curtis, D., and Paolo, D.J., 1989. Isotopic evidence on the structure and origin of subcontinental lithosphere mantle in southern Nevada: Journal of Geophysical Research, v. 94, p. 7885-7898.

Foland, K.A., and Bergman, S.C., 1992. Temporal and spatial distribution of basaltic volcanism in the Pancake and Reveille Ranges north of Yucca Mountain: Paper presented at Third International Conference on High Level Radioactive Waste Management, American Nuclear Society, LaGrange Park, Ill., p. 2366-2371.

Honn, D.K., 2005. Nested Calderas of the Northern Kawich Range, Central Nevada. [M.Sc. thesis]: University of Nevada, Las Vegas, 93 pp.

Irvine, T.N., and Baragar, W.R.A., 1971. A guide to the chemical classification of the common volcanic rocks: Canadian Journal of Earth Science, v. 8, p. 523-548.

Kleinhampl, F.J., and Ziony, J.I., 1985. Geology of northern Nye County, Nevada: Nevada Bureau of Mines and Geology Bulletin 99A, 172 p.

Krogh, T. E., 1973. A low contamination method for hydrothermal decomposition of zircon and extraction of U and Pb for isotopic age determinations. Geochim. Cosmochim. Acta, v. 37, p. 485-494.

Krogh, T.E., 1982. Improved accuracy of U-Pb ages by the creation of more concordant systems using an air abrasion technique. Geochimica et Cosmochimica Acta, v. 46, p. 637-649.

LeBas, M.J., LeMaitre, R.W., Strekeisen, A., and Zanettin, B., 1986. A chemical classification of volcanic rocks on the total alkali-silica diagram: Journal of Petrology, v. 27, p. 745-750.

Lee, Cin-Ty A., Luffi, P., Plank, T., Dalton, H., and William, L.P., 2009. Constraints on the depths and temperatures of basaltic magma generations on Earth and other terrestrial planets using new thermobarometers for mafic magmas, Earth and Planetary Science Letters, 279, p. 20-33.

Li, X., Yuan, X., Kind, R., 2007. The lithosphere-asthenosphere boundary beneath the western United States: Geophysical Journal International, v. 170, p. 700-710.

Lipman, Peter, 1997. Subsidence of ash-flow tuff calderas: relation to caldera size and magma-chamber geometry: Bulletin of Volcanology, v.59, p. 198-218.

Lovering, T.G., 1962. The Origin of Jasperoid In Limestone: Economic Geology Bulletin 57, p. 861-888.

Maniar P.D. and Piccoli, P.M. 1989. Tectonic discrimination of granitoids. Geological Society of America Bulletin, v. 101, p. 635-643.

Martin, M.W., and Naumann, T.R., 1995. Tertiary geology of the Reveille Quadrangle, Nye County, Nevada: Text to accompany NBMG Map 104. p. 1-6.

McKee, E.H., and Noble, D.C., 1986. Tectonic and magmatic development of the Great Basin of western United States during late Cenozoic time: Modern Geology, v. 10, p. 39-49.

McKee, E.H., and John, D.A., 1987. Sample locality map and potassium-argon ages and data for Cenozoic igneous rocks in the Tonopah 1° X 2° quadrangle, central Nevada: U.S. Geological Survey Miscellaneous Field Studies Map MF-1877-I.

McKee, E.H., Noble, D.C., and Silberman, M.L., 1970. Middle Miocene hiatus in volcanic activity in the Great Basin area of the western United States: Earth and Planetary Sciences Letters, v.8, p. 93-96.

McKee, E.H., and Silberman, M.L., 1975. Cenozoic igneous history of the southern Cordillera south of 42 degrees North: Geological Society of America, Abstracts with Programs, v. 7, p.1196-1197.

McKelvey, M., 2008. Geology of the southern Reveille Range, Nye County, Nevada. [M.Sc. thesis]: University of Nevada, Las Vegas, 102 pp.

Naumann, T.R., Smith, E.I., Shafiqullah, M., and Damon, P.E., 1991. New K-Ar ages for mafic to intermediate volcanic rocks in the Reveille Range, Nevada: Isochron West, p. 12-16.

Nealey, L. David, Rowley, Peter D., Unruh, Daniel M., Budahn, James R., Snee, Lawrence W., Mehnert, Harald H., and Anderson, R. Ernest, 1992. Preliminary Geochemistry of Miocene Ash-Flow Tuffs in and near the Caliente Caldera Complex, Southeastern Nevada and Southwestern Utah Barco Study Unit, p. 91-109.

Novak, Steven W. Eruptive History of the Rhyolitic Kane Springs Wash Volcanic Center, Nevada (1984). Journal of Geophysical Research, vol. 89, no. B10, p. 8603-8615.

Parish, R.R., 1987. An improved micro-capsule for zircon dissolution in U-Pb geochronology. Isotope Geoscience, v. 66, p. 99-102.

Patchett, P.J., and Ruiz, J., 1987. Nd isotopic ages of crust formation and metamorphism in the Precambrian of eastern and southern Mexico. Contributions to Mineralogy and Petrology, v. 96, p. 523-528.

Putirka, Keith D. 2008. Thermometers and Barometers for Volcanic Systems. Reviews in Mineralogy and Geochemistry, Vol. 69, p. 61-120.

Rash, K.B., 1995. Geology and Geochemistry of Tertiary Volcanic Rocks in the Northern Reveille Range and Southern Pancake Ranges, Nye County, Nevada [M.Sc. thesis]: University of Nevada, Las Vegas, 191pp.

Richard, P., Shimizu, N., and Allegre, C.J., 1976. 143Nd/146Nd, a natural tracer: an application to oceanic basalts. Earth and Planetary Science Letters, v. 31, p. 269-278.

Rytuba, J.J. and Heropoulus, Chris, 1992. Mercury in Epithermal gold systems-an important by-product: U.S. Geological Survey Bulletin 1877, p. D1-D8.

Scott, R.B., Grommé, C.S., Best, M.G., Rosenbaum, J.G., and Hudson, M.R., 1992. Stratigraphic Relationships of Tertiary Volcanic Rocks in Central Lincoln County, Southeastern Nevada, in Geologic Studies in the Basin and Range-Colorado Plateau Transition in Southeastern Nevada, Southwestern Utah, and Northwestern Arizona: BARCO study, U.S. Geological Survey Bulletin, 2056, p. 7-41.

Scott, Robert S., Rowley, Peter D., Snee, Lawrence W., Anderson, R. Ernest, Harding, Anne E., Unruh, Daniel M., Nealey, L. David, Hudson, Mark R., Swadley, W.C., and Ferreis, Dawna E., 1996. Synchronous Oligocene and Miocene Extension and Magmatism in the Vicinity of Caldera Complexes in Southeastern Nevada. Open File Report 96-4 Field Trip No. 7. Colorado Geological Society p. 1-36.

Sherlock, Maureen G., Cox, Dennis, P., and Huber, Donald F., 1996. Chapter 10: Known Mineral Deposits and Occurances in Nevada: An Analysis of Nevada's Metal-Bearing Mineral Resources: Nevada Bureau of Mines and Geology Open File Report 96-2, p.10-1-10-38.

Silberman, M.L., Bonham, H.F. Jr., Garside, L.J., Ashley, R.P. 1978. Radiometric ages of volcanic and plutonic rocks and hydrothermal alteration-mineralization in the Tonopah mining district and vicinity, Nye and Esmeralda counties, Nevada. Open File Report-USGS. 41p.

Stickney, Elizabeth K., 2004. The Volcanology and Petrogenesis of the Northern Lunar Crater Volcanic Field, Nye County Nevada. [M.Sc. thesis]: University of Nevada, Las Vegas, 93pp.

Sun, S.S., and McDonough, W.F., 1989. Chemical and isotopic systematics of Ocean basalts; implications for mantle composition and processes: Magmatism is the Ocean Basin, Geologic Society of London, p. 313-345.

Tibbetts, Ashley K., 2010. Petrogenesis of the Greenwater Range: Comparison to the Crater Flat Volcanic Field and Implications for Hazard Assessment. [M.Sc. thesis]: University of Nevada, Las Vegas, 141pp.

Tingley, Joseph V., 1991. Mineral Resources of the Timpahute Range 30' By 60' Quadrangle: Nevada Bureau of Mines and Geology Report 46, 40p.

Unruh, D.M, Nealey, L.D., Rowley, P.D., Snee, L.W., Mehnert, H.H., Anderson, R.E. 1995. Strontium and Neodymium Isotopic Survey of Ash-Flow Tuffs and Related Rocks from the Caliente Caldera Complex, Southeastern Nevada and Southwestern Utah, in Geologic Studies in the Basin and Range- Colorado Plateau Transition in Southeastern Nevada, Southwestern Utah, and Northwestern Arizona: BARCO study, U.S. Geological Survey Bulletin, 2056, p. 111-128.

Wang, K., Plank, T., Walker, J.D., Smith, E.I., 2002. A mantle melting profile across the Basin and Range, SW USA. Journal of Geophysical Research v. 107, 21.

Wendt, I and Carl, C. 1991. The statistical distribution of the mean squared weighted deviation. Chemical Geology: Isotope Geoscience Section, vol. 86, no. 4, pp. 275-278.

Wernicke, B., Spencer, J., 1999. Basin and Range extension. Geological Society of America Special Paper 338, p. 341-356.

West, M., Ni, J., Baldridge, W.S., Wilson, D., Aster, R., Gao, W., Grand, S. 2004. Crust and upper mantle shear wave structure of the southwest United States: implications for rifting and support for high elevation. J. Geophys. Res. 109 doi: 10.1029/2003JB002575.

Yogodzinski, G.M., Naumann, T.R., Smith, E.I., and Bradshaw, T.K., 1996. Evolution of a mafic volcanic field in the central Great Basin, south central Nevada: Journal of Geophysical Research, v. 101, no. B8, p. 17,425-17,445.

CV

Christi Emery

9473 Sandy Reef Ave. Unit A, Las Vegas, NV, 89147, (702) 280-2816,
christirocks@yahoo.com

Education

University of Tennessee at Chattanooga – Chattanooga, TN
Bachelor of Science in Geology, May 2005

Professional Experience

Southern Nevada Water Authority, Las Vegas, NV, April 2007-Present

Geoscience Consultants, LLC, Las Vegas, NV, January 2008-March 2008

GeoTek, Las Vegas, NV, February 2006-April 2007

S&ME, Chattanooga, TN, December 2003-January 2006

Publications

- Emery, Christi A., 2010. Groundwater and Surface Water Monitoring at the Muddy River Springs Area. Nevada Water Resources Association Annual Conference Poster Presentation. NWRA. Las Vegas, NV.
- Emery, Christi A., 2009. Using Igneous Geochemistry for Insight Into Surface Water Flow Paths, Battleship Butte Alluvial Deposits, Near Moapa, NV, Also Introducing the Volcanic Evolution of the southern Quinn Canyon Range: Implications for Regional Correlation of Volcanic Units. Rocky Mountain Section Geological Society of America Annual Meeting Poster Presentation. GSA. Orem, UT.
- Emery, Christi A., 2008. Barometric and Earth Tide Corrections to Garnet Valley, Muddy Springs Area, and Coyote Spring Valley Water Levels. Nevada Water Resources Association Annual Conference Poster Presentation. NWRA. Mesquite, NV.